ALGINATE BASED CELL SEEDED HYDROGEL SCAFFOLD FOR MENISCAL REPAIR: DEVELOPMENT AND EVALUATION

TABLE OF CONTENTS

Table of Figure Captions

Table Captions

CHAPTER 1

1. INTRODUCTION

Menisci, two C-shaped discs of fibrocartilagenous tissues present in the medial and lateral sides of each knee joint between the tibia and femur are more prone to injuries like meniscal tears. These types of injuries are common among athletes and people who are involved in labor-intensive occupations. Medial meniscal tears occur more frequently than lateral meniscal tears (Campbell et al., 2001). Meniscal tear occurring at the avascular zone is more difficult to heal. The primary method of diagnosing meniscal pathology is Magnetic Resonance Imaging (MRI). The mean annual incidence of meniscus tears among 10,000 populations was 9.0 in males and 4.2 in females (Hede et al., 1990).

Meniscectomy, either complete or partial, was considered to be the treatment strategy for any type of meniscal injury. The success of transplantation depends on many factors including proper tissue preservation, transplant integrity, and fixation method (Jackson et al., 1992; Rodeo et al., 2000a). Removal of this anatomical structure will lead to degenerative changes of articular cartilage and its related symptoms like osteoarthritis (Chatain et al., 2003; Cole et al., 2003; Fairbank, 1948). After meniscectomy cartilage volume loss was 4 % per year from the lateral compartment (Verdonk and Kohn, 1999). This gives way to the concept of arthroscopic partial meniscectomy (APM) which is now a commonly preferred orthopaedic surgical procedure (Abram et al., 2020). But partial meniscectomy even causes defects depending on the site of lesions within the meniscus.

The amount of excise tissue was inversely proportional to the function of the knee (Hede et al., 1992).

Allograft transplantation (Wirth et al., 2002), and meniscal substitutes (Goble et al., 1999) were used as an alternative approach to meniscal repair. But the methods have disadvantages like immunogenic reactions (Tucker et al., 2012) in the case of allograft transplantation, failure of conversion of the graft into fibrochondrocytes (Goble et al., 1999) in substitutes.

Tissue engineering can be used as an alternative and promising method for meniscal defect repair using a tissue-engineered construct. This can be done either by using scaffolds, which can be natural or synthetic, or by delivering the cells like fibrochondrocytes or stem cells directly to the defective sites (Arnoczky et al., 1988; Izuta et al., 2005; Peretti et al., 2004). Currently, there are several limitations in the development of an appropriate scaffold. The main problem is the requirement of invasive surgery, which involves the risk of healing and infection. Another problem is the shape of the material to fit the defect site. Poor-fitting of scaffold to the defect site will result in dead space which results in fluid accumulation and inflammation. It will also affect the stability of the implant (Temenoff and Mikos, 2000). To address these issues new scaffolds have been developed in injectable form. This is based on the injection of a monomer or polymer that can form a gel at the site of implantation in response to stimuli. This has the advantage of delivering molecules into the small surgical incision. It also helps in the proper integration of scaffolds with the surrounding tissues (Gao et al., 2020).

The present investigation focuses on the preparation of an in-situ forming injectable hydrogel matrix from Alginate dialdehyde (ADA) and gelatin without the use of any such toxic cross-linking agents. Here, ADA was prepared by the oxidation of sodium alginate with meta periodate. The aldehyde groups in ADA would crosslink with the amino groups in proteins such as gelatin through Schiff's base. The aldehyde groups in ADA also form hemiacetal linkages with the adjacent hydroxyl groups within the molecule. This would lead to a reduction in the number of aldehyde groups available for reaction with amino groups of gelatin. It was found that the addition of Sodium tetraborate (Borax) can solve this issue of hemiacetal formation. Borax has a long history of medical use and the acute adult quantitative dose-response in humans ranged from 1.4 to 70 mg/kg body weight (Kot, 2015). Gelation time could be tailored by varying the concentrations of the reactants employed for reaction.

This thesis has been divided into 5 chapters. Chapter 2 is Literature review and it provides a detailed description of the meniscus, its development, Extra Cellular Matrix (ECM) components, mechanism of injury, current treatment options and its drawbacks. The importance of tissue engineering in the field of meniscal injury has been explained in detail. Different types of polymers used for meniscal tissue engineering and the importance of injectable hydrogels in this field were also described. The existing literature on various polymers used for preparing injectable hydrogels for meniscal tear was presented. The importance of alginate, the need for its modification, types of modifications were highlighted. Among the different modification procedures, the importance of the oxidation method has been reviewed. The oxidation product, alginate

dialdehyde (ADA), and its applications in tissue engineering have been presented. The role of gelatin in hydrogel synthesis has been explained. Various applications of hydrogel, made from ADA and gelatin (ADAG), in the field of tissue engineering has been reviewed by selecting the articles published during the period 2016-2020. The use of Platelet Rich Plasma (PRP) in the treatment of meniscal injury has been reviewed and discussed. The lacunae in the current field of meniscal tissue engineering and the current objectives of the study were also presented in chapter 2.

Chapter 3 deals with the materials, methods and protocols, etc. used in the work. This chapter starts with the characterization of raw materials used for hydrogel preparation. Synthesis of ADA and its characterization. Stability studies of ADA at different storage temperatures for different time periods and its characterization methods. Preparation of ADAG hydrogel with and without PRP and its characterization methods were explained. Spectroscopic characterization using UV-Visible, Fourier Transform Infrared (FTIR), Raman and NMR were described. Mechanical testing was done with Universal Testing Machin (UTM). Porosity and surface evaluation was done with micro-CT and Scanning Electron Microscopy (SEM). The procedure for sample preparation and analysis was given. *In vitro* evaluation of hydrogel was done using fibrochondrocytes cells isolated from rabbit meniscus. A detailed procedure for the isolation was described. Hydrogels with and without PRP were cultured in the presence of fibrochondrocytes and their cytocompatibility was analyzed by direct contact assay, MTT assay and live dead staining. The proliferation of cells in the presence of hydrogel by alamar blue assay was also described. The biochemical analysis of cell seeded hydrogel was described using

Glycosaminoglycan (GAG), DNA and collagen estimation. A detailed *in vivo* procedure for the evaluation of hydrogel in a rabbit meniscal tear model was given. The histopathological evaluation of explanted tissue after the respective time period was also explained.

Chapter 4 presents the results obtained from the experiments conducted and discusses these results with the help of scientific data already published.

Chapter 5 summarizes the salient findings in this work and concludes the thesis.

CHAPTER 2

2. REVIEW OF LITERATURE

2.1. Anatomy of meniscus

The word *meniscus* comes from the Greek word *me-niskos*, meaning “crescent”. Menisci are two wedge-shaped semi lunar C-shaped discs of fibrocartilaginous tissues present in medial and lateral sides of each knee joint between the tibial and femoral bearing surfaces (Figure 1) (Buma et al., 2004). The outer portion of the meniscus is convex, thick and attached to the knee joint capsule but the inner portion is concave, thin and free (Cooper et al., 1991). They are approximately 35 mm in diameter and 110 mm in length (Kohn and Moreno, 1995). There are usually two types of menisci, namely, medial and lateral meniscus.

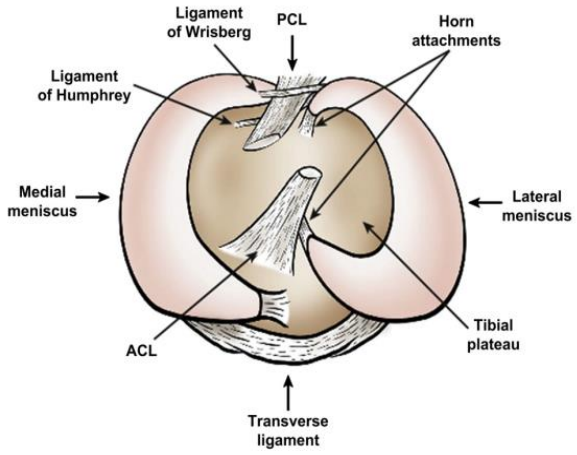

Figure 1. Anatomy of the meniscus: superior view of the tibial plateau (Makris et al., 2011).

2.1.1. Medial meniscus

The medial meniscus is semilunar in sh ape. A study conducted by McDermott et al. (2004) in adult human meniscus showed that the approximate size of the medial meniscus was

45.7 ± 5.0 mm long and 27.4 ± 2.5 mm wide. The anterior horn of the medial meniscus was attached anteriorly to the tibial attachment of the anterior cruciate ligament (ACL) whereas the posterior horn was attached firmly to the tibial posterior intercondylar fossa between the posterior root of the lateral meniscus and the posterior cruciate ligament (PCL) (Fox et al., 2012).

2.1.2. Lateral meniscus

Lateral menisci are more circular compared to medial menisci. McDermott et al., (2004) showed that the lateral meniscus was 35.7 ± 3.7 mm in length and 29.3 ± 3.0 mm wide. The area occupied by the lateral meniscus in the tibial plateau was higher compared to the medial meniscus (Thompson et al., 1991). The anterior and posterior horns of the lateral menisci are attached to the tibia. The anterior horn lies anterior to the intercondylar eminence and adjacent to the attachment site of ACL. The posterior horn is attached to the lateral tibial spine and anterior to the insertional site of the posterior horn of the medial meniscus (Johnson et al., 1995).

2.2. Embryology

The first anatomical description of the meniscus as disk-shaped semilunar cartilage was done by Young in 1889 (Fisher, 1936). Menisci arise from the mesenchymal tissue differentiation within the limb bud (Andrish, 1996). The development of menisci was indicated by the triangular formation of increased cellular density at 6.5 weeks old embryos (Uhthoff and Kumagai, 1992). They were easily identifiable by 7.5 weeks after ovulation

and by 8 weeks they were clearly defined as more cellular and the cells were clearly recognizable (Figure 2 A & B) (Gardner and O'Rahilly, 1968).

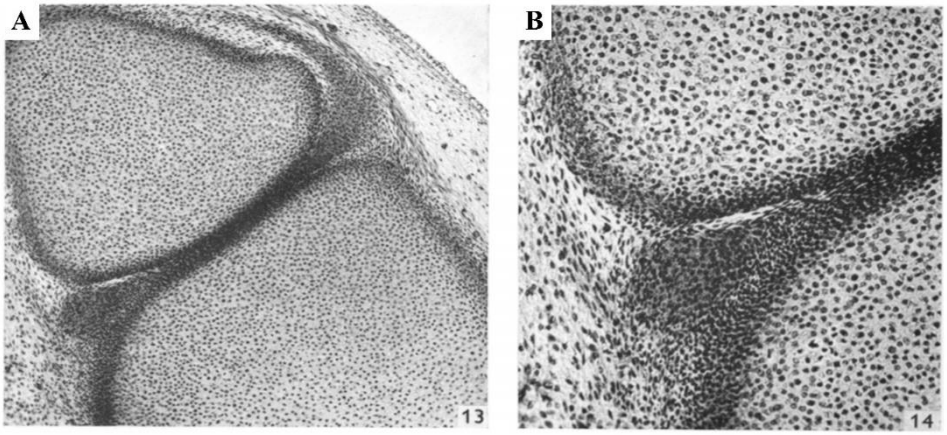

Figure 2. Histology of Menisci, 8 weeks postovulatory, at different magnifications: A) 100x; B) 200x (Gardner and O'Rahilly, 1968).

Blood vessels penetrate the peripheral one-third of the menisci by 12 weeks. By 18-20 weeks blood vessels reached the tip of the lateral menisci. Spindle-shaped cells were identified relatively parallel in the lateral meniscus and random in the medial meniscus at 14 weeks (Figure 3 A & B). Collagen bundles could be identified by 17 weeks of gestation only. The arrangement of collagen bundles was different in both menisci till complete development. By 25 weeks parallelly oriented collagen fibers formed thick bundles in the lateral meniscus whereas the arrangements were not clearly defined in the medial meniscus (Figure 3 C & D). The development of lateral menisci occurs earlier than medial menisci because of the adaptation against possible overloads given to lateral menisci soon after birth.

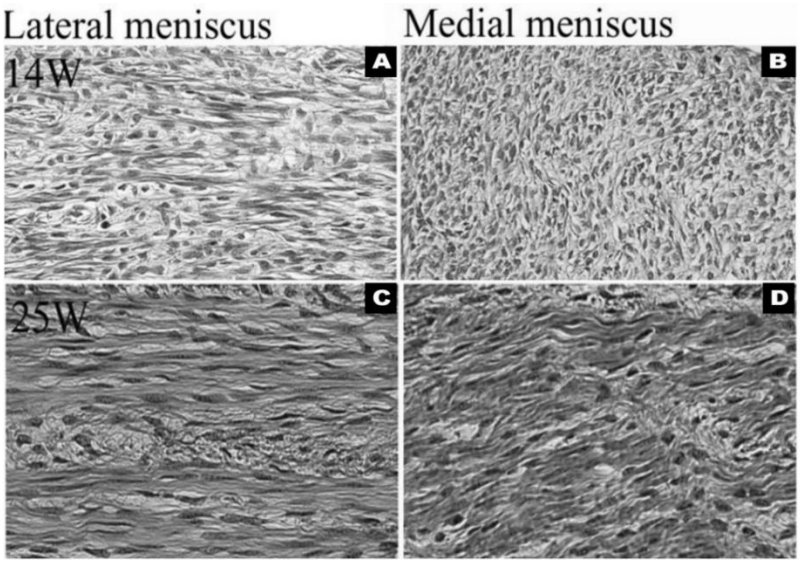

Figure 3. Histology of human foetus menisci: A & B - Cellular arrangements; C & D - Collagen fiber arrangement (Fukazawa et al., 2009).

2.3. Composition of meniscus

Meniscus consists of an extracellular matrix component and cellular components (Figure 4). A detailed description of its components is given below.

2.3.1. Extracellular matrix

Biochemical analysis, according to Guo et al. (2015), showed that meniscal tissue contained 72% water, 22% collagen, 0.8% glycosaminoglycans (GAG) with chondroitin-6-sulphate as the major GAG constituent (Figure 4); the rest is made up of DNA and adhesion molecules and these numbers vary with age, species, and location (Ghadially et al., 1983).

2.3.2. Water

According to Adams et al. (1983), the average water content of the medial and lateral menisci was 66.65 ± 1.64 % and 65.09 ± 1.52 %, respectively. The water content of the

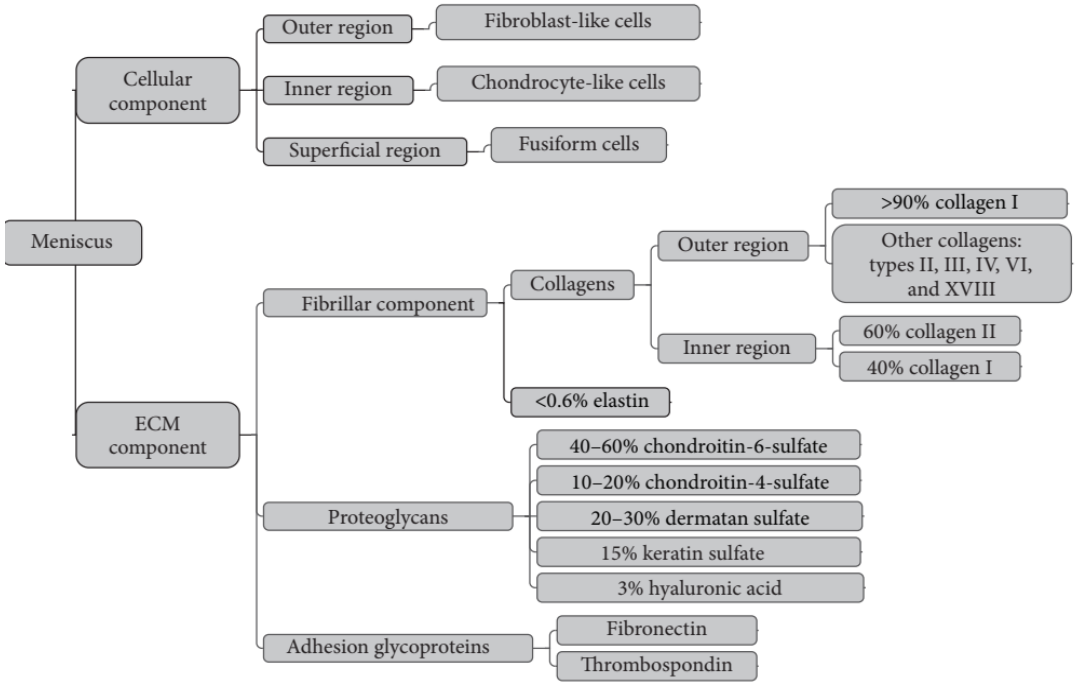

Figure 4. The composition of the meniscal cellular and extracellular matrix (ECM) components (Guo et al., 2015).

meniscus changed depending on the location of the meniscus and also with the increase in the pathological grade (Proctor et al., 1989). The posterior part of the meniscus has higher water content. Tissues from the superficial, middle and deep layers showed similar water content. The viscoelastic properties of the meniscus are due to the interaction between water and extracellular matrix molecules.

2.3.3. The fibrillar collagen

During postnatal development, the orientation of collagen fibers in the tissues determines the tensile stress to which the meniscus is subjected. MacCONAILL (1951) summarized the function of collagen fibers as: “the law of collagenisation is: as iron filings are to a magnetic field so are collagen fibers to a tension field”. Collagen accounts for 60-70% of the dry weight in menisci. Type I accounts for 90% of collagen within the meniscal tissue.

The surface of the meniscus is covered by a delicate fibrillar network of 10 µm width and 30 nm in diameter (Petersen and Tillmann, 1998). In the meniscal body Collagen 1 fibers are arranged in the circumferential orientation. Radial fibers are less in number, but they act as “tie” holding the circumferential fibers together (Figure 5) (Bracht et al., 2007).

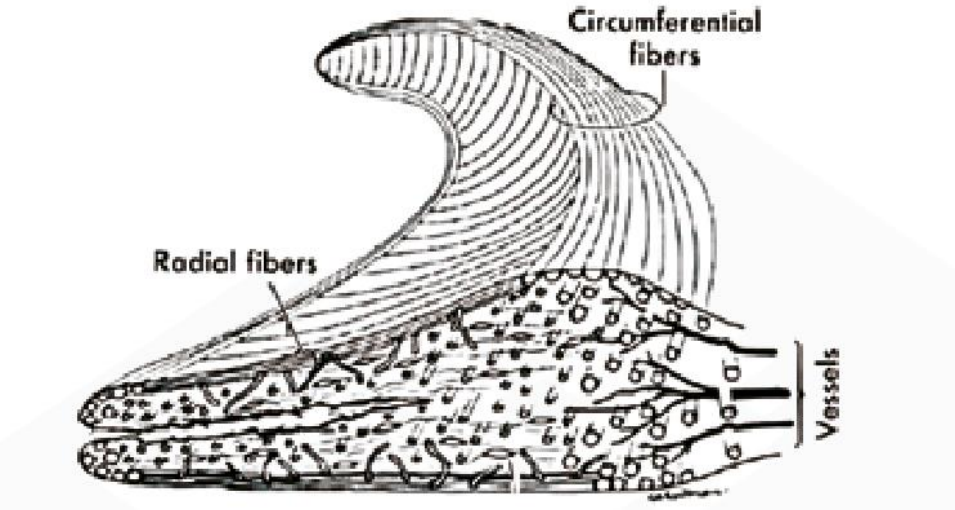

Figure 5. Orientation of collagen fibres in meniscus (Bracht et al., 2007).

2.3.4. Proteoglycans

Proteoglycans are negatively charged hydrophilic molecules, formed by a core protein with one or more covalently attached glycosaminoglycan chains. They contribute to 1 % to 2 % of the dry weight of the meniscus. The normal adult human meniscus consists of 40 % chondroitin-6-sulfate, 20 % chondroitin-4-sulfate, 20 % dermatan sulfate, and 15 % of keratin sulfate (Herwig et al., 1984). Higher concentrations of glycosaminoglycan are found in the inner half of the menisci, especially in the primary weight-bearing areas (Ghosh and Taylor, 1987). Aggrecan is the major proteoglycan responsible for the viscoelastic compressive properties of the meniscus (Nakano et al., 1997).

2.4. Vascular anatomy

The lateral and medial menisci receive their blood supply from the lateral medial genicular arteries. Embryology of meniscus revealed that in the early development there was blood supply throughout the meniscus. But in the later developmental stage, due to weight-bearing and knee movement, the inner portion of the menisci becomes avascular. The peripheral border of the medial and lateral meniscus is relatively well-vascularized, which has important implications for meniscus healing (Arnoczky and Warren, 1982). The avascular part of each meniscus receives nourishment from synovial fluid via diffusion (Espino et al., 2014). Based on the vascularity the meniscus is divided into different zones (Figure 6), namely, the outer, vascular/neural region (red-red zone), the inner, completely avascular/aneural region (white-white zone) and the red-white region, which presents attributes from both the red-red and white-white regions (Arnoczky and Warren, 1982).

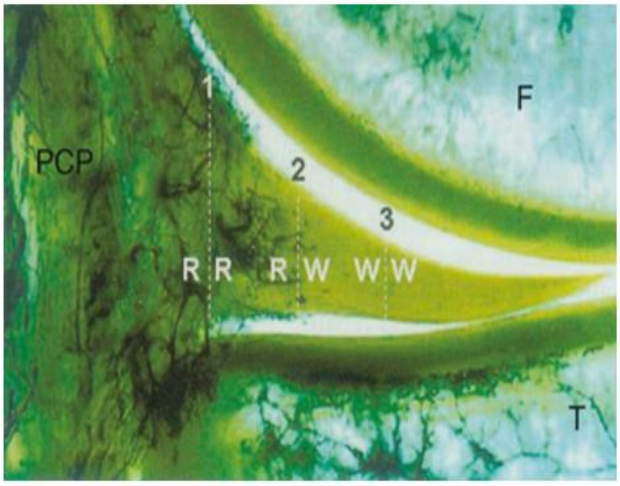

Figure 6. Three zones of meniscus: (1) RR = red-red area, (2) RW = red-white area, (3) WW = white-white area (Chahla et al., 2017).

2.5. The meniscus cells

During the early stages of development, all the cells in the meniscus have the same cellular morphology in terms of size and shape with no regional variations. However, in the later

stages of development, the cells become discrete in terms of morphology and phenotype. The cells also varied in terms of number and topographic localization (Makris et al., 2011). Human meniscus tissue is mainly populated by round or oval cells, comparable to the chondrocytes in the articular cartilage and fibroblast-like cells (Ghadially et al., 1983). The round or oval cells in the inner zone of the meniscus produce more type I collagen than the type II collagen of articular chondrocytes.

So, this meniscus cell was termed as fibrochondrocytes based on the difference in expression of collagen types (Mcdevitt and Webber, 1990). Another cell population recognized in the superficial zone of the meniscus was flattened, fusiform morphology without cell extensions (Figure 7). It has been suggested that these cells are specific progenitor cells with therapeutic and regenerative capabilities (Bracht et al., 2007). The cell phenotype and extracellular matrix composition render the outer portion of the meniscus similar to fibrocartilage, while the inner portion possesses similar but not identical features to articular cartilage.

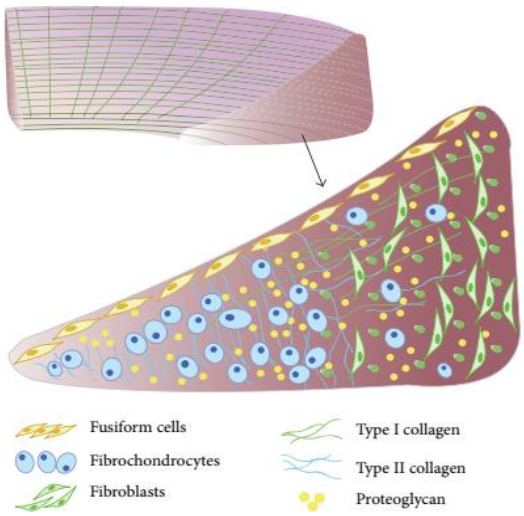

Figure 7. Schematic diagram of meniscus internal ultrastructure (Niu et al., 2016).

2.6. Meniscal biomechanics

Menisci are an important multifunctional component of the knee with a complex biomechanical system. The main function of menisci is load transmission, shock absorption, proprioception, joint stabilization and lubrication. During the loading of the knee, the menisci transmit 70 % of its load in the lateral compartment and 50 % in the medial compartment. During extension and 90° flexion, they transmit about 50 % and 85 % of the loads through posterior horns of the meniscus, respectively, to protect the articular cartilage against compressive stresses. Vertical compressive stress applied to the meniscus is converted to hoop stress and prevents its extrusion with the help of circumferential collagen fibers and the insertion ligaments of the anterior and posterior horns as shown in figure 8 (Biçer et al., 2016).

The tensile properties of the menisci facilitate load bearing and shock absorption functions. It has been reported that the tensile strength of the menisci was approximately

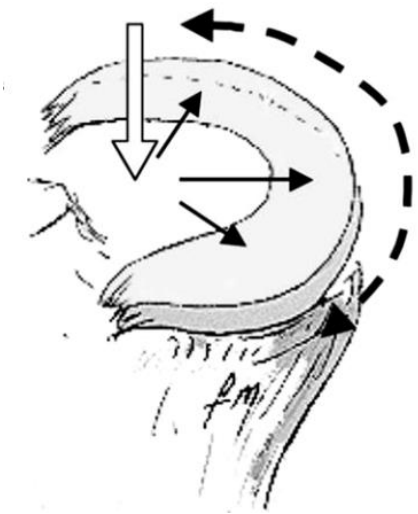

Figure 8. Meniscal biomechanics: Compressive force (white arrow) is converted to radially directed force (black arrows), which is then converted as hoop stresses (dashed arrow) within the meniscus (Boyd and Myers, 2003).

ten times greater compared to the articular cartilage (Proctor et al., 1989). The viscoelastic properties of the meniscus are due to its water content which in turn helps in withstanding shear forces and distributing tensile and compressive loads.

2.7. Pathogenesis

Meniscal tears are the most common type of knee joint injury. Meniscal injuries may be acute or degenerative due to repetitive wear and tear commonly encountered in middle-aged and older patients. Acute tears occur due to the combinatorial effect of compressive shear and rotational forces across the meniscus from the femoral condyles onto the tibial plateau. Degenerative meniscal lesions occur gradually over time and are usually associated with osteoarthritis (OA) (Bhattacharyya et al., 2003). Since the posterior horn of the medial meniscus absorbs most of the weight of the medial compartment, it is the most frequent area that a meniscus tear can occur (Englund et al., 2012). Meniscal tears can be classified based on patterns and location. Typical tear patterns are shown in figure 9. They include vertical, longitudinal, oblique, transverse (radial), horizontal, meniscal root, bucket-handle, and complex (Howell et al., 2014). The most common meniscal tears

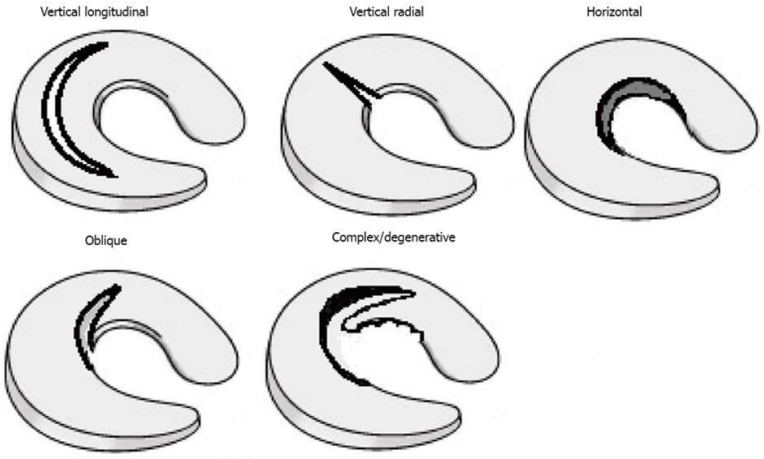

Figure 9. Types of meniscal tear (Gu and Wang, 2010).

among active young people and in the elderly are longitudinal-vertical and degenerative tears, respectively (Metcalf and Barrett, 2004). The healing potential of a meniscal tear is dependent on tear location. Tears involving the inner zone (white-white) have the least healing potential due to a lack of blood supply.

2.8. Mechanism of injury and epidemiology

Generally, meniscal tears occur due to sporting activity (e.g., soccer, rugby football), or a nonsporting activity like squatting, or nonactivity. In athletes, meniscal tears may result from excessive application of force onto the meniscus. But in older people, the degeneration of the meniscus makes it susceptible to injury. The mechanism of injury typically involves a twisting or shearing motion. In non-contact-related injuries, cutting, decelerating, or landing from a jump result in a meniscal tear.

Age has been considered a risk factor for both medial and lateral meniscal injury. A study conducted by (Ridley et al., 2017) showed that a population with more than 30 years of age is more prone to medial meniscal injury while the age group below 20 is more susceptible to lateral meniscal injury (Figure 10). As the age progresses the elasticity of the meniscus decreases leading to meniscal injury. Apart from age, another suggested risk

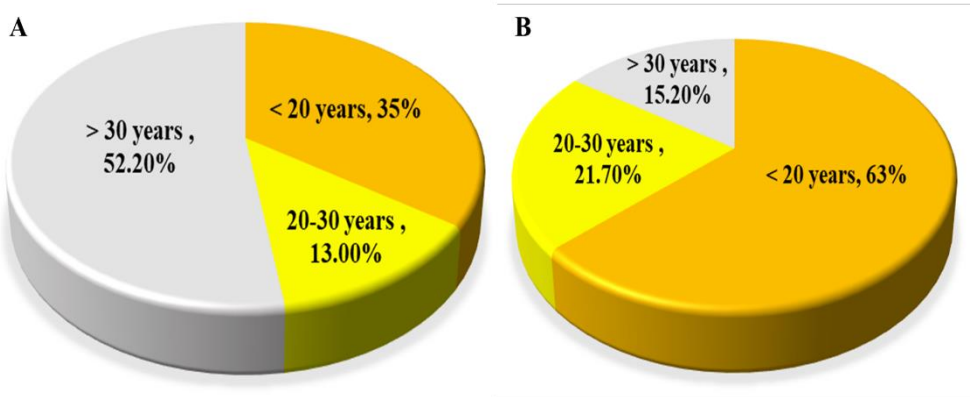

Figure 10. Meniscal injuries by age group: A) Medial; B) Lateral menisci.

factor for meniscal injury is gender. Studies have reported that males are more prone to meniscal injury compared to females. The male-to-female ratio for meniscal injury is 2.5:1. Among these males had more lateral meniscal tears than females (Kluczynski et al., 2015). In India, only limited epidemiology studies were reported. A recent cross-sectional, observational study conducted among 76 kabaddi players was reported by Dhillon et al., (2017). They observed meniscus tears in 68.42 % of the players. Among these 32 were medial meniscus tears and 20 were lateral meniscus tears. Another cross-sectional study conducted by John et al. (2016) revealed that out of 465 athletes, 284 were had meniscal tears.

2.9. Treatment strategies for meniscal tears

Given the function of the meniscus and the development of osteoarthritis after its removal make orthopaedic surgeons consider the protection of the meniscus by repair or reconstruction following injury. Meniscal injury can be managed by non-operative and operative procedures. The surgeon's decision on the management of meniscal tear is influenced by the patient's conditions such as age, lifestyle, health, location of the tear, quality of tissue and grade of the tear (Di Matteo et al., 2016).

2.9.1. Non-operative management

Non-operative management is useful for longitudinal partial-thickness tears through the posterior horn of the lateral meniscus associated with an ACL tear, full-thickness peripheral tears and radial tears less than 5 mm in length (Saidoff and McDonough, 2004). Previously, the 'PRICE' (protection, rest, ice, compression, elevation) protocol was used widely for non-operative management (Bleakley et al., 2007). But now anti-inflammatory

and analgesic medications, quadriceps strengthening, unloader bracing and intra-articular injections are used for 3 to 6 months (Mordecai et al., 2014). If the patient's symptoms persist even after these treatments surgical procedure is considered.

2.9.2. Operative management

Operative management of meniscal tears are of three types: meniscectomy, meniscal repair and meniscal reconstruction.

2.9.2.1. Meniscectomy

Meniscectomy can be performed totally or partially by open or arthroscopic procedure. In the current treatment strategy, total meniscectomy is not recommended as a primary procedure in meniscal lesions. Complete removal of this anatomical structure will lead to degenerative changes in articular cartilage and its related symptoms like osteoarthritis. According to Fox et al. (2012), the cartilage volume loss after meniscectomy was 4 % per year from the lateral compartment. Their study indicated that the resection of 15 - 34 % of the meniscus increases the contact pressure by more than 300 %. There were also evidences that total meniscectomy would lead to degeneration of the joint. This gave way to partial meniscectomy which can be performed in an open or arthroscopic fashion. This is recommended in patients with a radial tear in the white-white zone and degenerative meniscal tears which cannot be managed by non-operative treatment for 3-6 months (Doral et al., 2018). An arthroscopic partial meniscectomy (APM) is the most frequently used surgical procedure for the treatment of meniscal tears. APM is widely used because of low morbidity, good short-term results and the speed of procedure (Beaufils et al., 2015). Even though short-term results following partial meniscectomy were encouraging, long-term

studies showed that partial meniscectomy only delay the degeneration of cartilage but does not prevent it (Faunø and Nielsen, 1992).

2.9.2.2. Meniscal repair

In order to preserve the important functions of the meniscus and to minimize the long-term complications associated with meniscectomy, surgeons consider repair of the meniscal injury as extensively as possible. Meniscal repairs can be done by open and arthroscopic procedures. Several methods are available for meniscal repair (Figure 11). The selection of these methods depends on tear patterns, the surgeon's experience, and the availability of resources (Cengiz et al., 2017).

To enhance healing after meniscal repair, especially in the avascular area (white-white zone) a variety of augmentation techniques and biological products are introduced. They are trephination, needling, platelet-rich plasma (PRP), bone marrow aspirate, fibrin clot and growth factors (Anz et al., 2014; Fox et al., 1993; Kamimura and Kimura, 2014; Pujol et al., 2015). Even though biological augmentation has a significant effect in meniscal

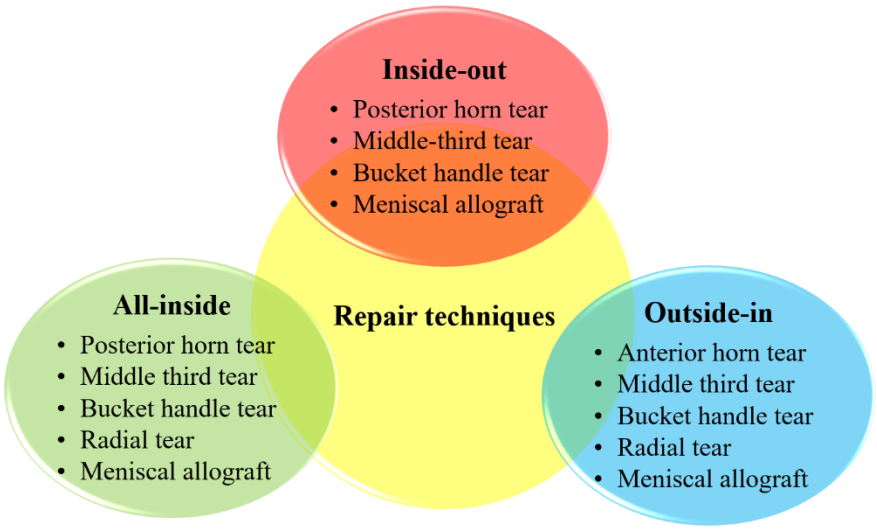

Figure 11. Meniscal injury patterns and appropriate repair techniques.

surgery there are still relatively few clinical studies available to support this evidence (Moran et al., 2015).

2.9.3. Allografts and meniscal substitutes

2.9.3.1. Meniscal Allograft Transplantation

Meniscal allograft transplantations (MAT) have been widely recommended considering the meniscal loss after total or nearly total meniscectomy. Currently, there are several processes to obtain graft for MAT - fresh, frozen and freeze-dried (Figueroa et al., 2019). MAT can be used for patients with a stable knee joint, for good alignment of the joint, and for early osteoarthritis of the knee. Literature shows that MAT appears to provide good results only in short-term follow-up but on long-term follow-up narrowing of joint spacing is observed (Rosso et al., 2015; Vundelinckx et al., 2014). Other drawbacks of MAT are immunological reaction at the implanted site, potential disease transmission, size-matching of the graft to the donor site, need of having appropriate preservation techniques and limited donor availability (Rodeo et al., 2000b; Rosso et al., 2015).

2.9.3.2. Meniscal substitutes

Two implant devices have been made available for clinical practice, one is a collagen meniscus implant (CMI® or Menaflex™), and the other is a polyurethane implant (Actifit®) (Figure 12 A & B). CMI® was reported to be made from type I collagen matrix which is resorbable and biocompatible. It consists of a porous cross-linked matrix that allows the ingrowth and regeneration of new meniscal tissue (Figure 12 C) (Marcacci et al., 2015). Actifit® is a synthetic polymer composed of polyester (poly-ε caprolactone acid) and polyurethane. This device has a highly interconnected pore structure that

encourages tissue regeneration by the growth and proliferation of cells from the meniscal wall (Figure 12 D) (Baynat et al., 2014).

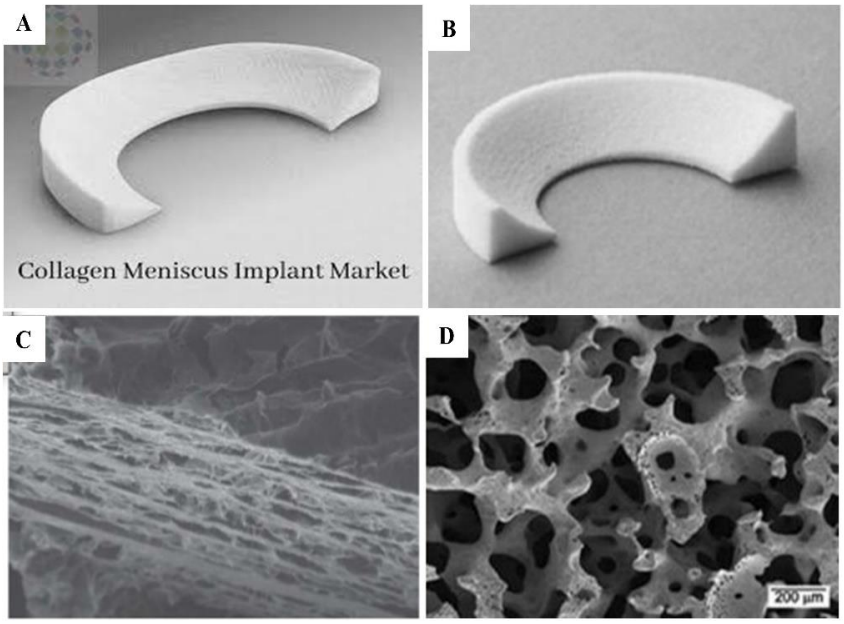

Figure 12. A) Collagen Meniscal Implant (CMI®); B) polyurethane implant (Actifit®); SEM images of: C) CMI®; D) Actifit (Baynat et al., 2014; RAJAT JANGIR, 18:02:09 UTC).

These two implants have been recommended for patients with an intact peripheral meniscal rim and limited cartilage damage after meniscectomy. Literature shows that these two substitutes have provided a positive clinical outcome in terms of knee function and pain reduction for treating partial medial and lateral meniscus tears (Monllau, 2013; Verdonk, 2013) but the regenerated tissue collected after the evaluation period is different from the native meniscus in terms of tissue organization, mechanical properties and extracellular matrix composition (Pereira et al., 2011). Moreover, the reduction in the area of damage to the articular cartilage is very critical for the meniscal implants to avoid the consequences of meniscectomy. To overcome the limitations with allografts and commercially available acellular meniscal substitutes, there is a great expectation from tissue engineering under

the broad umbrella of regenerative medicine for the development of superior strategies using scaffold, cells and bioactive agents.

2.10. Meniscal Tissue Engineering

Tissue engineering combines the principles of both biology and engineering for the development of functional substitutes that can restore, maintain and improve the function of damaged tissue (Furth and Atala, 2014). Scaffolds for tissue engineering the meniscus may be categorized into three broad classes: synthetic polymers, hydrogels and tissue-derived materials (Makris et al., 2011).

For the selection of an ideal scaffold for meniscal regeneration, it is important to know the properties of each material to be used for scaffold preparation. Bioabsorbable polymers, either synthetic or natural, are used for preparing meniscal scaffolds. Synthetic polymers used are polyurethane (PU), polyglycolic acid (PGA), polylactic acid, and poly (-caprolactone) (PCL), etc. (Esposito et al., 2013; Kang et al., 2006; Mulder et al., 2013). The advantages of these polymers are their good biomechanical and versatile properties. But their disadvantages are hydrophobicity, lack of bioactivity, aseptic inflammation and immune response at the area of implantation (Guo et al., 2015). Natural polymers used are collagen, hyaluronan, silk, bacterial cellulose, etc. (Chiari et al., 2008; Kaplan and Mandal, 2013; Martínez et al., 2012; Zaleskas et al., 2001).

Among the different biomaterials discussed above, polymeric hydrogels have gained much importance as they exhibit good biocompatibility, tunable, have the ability to encapsulate cells and deliver bioactive molecules (Slaughter et al., 2009; Zhu and Marchant, 2011). Hydrogels have networks of three-dimensional crosslinked polymeric chains. The intrinsic

hydrophilic nature provides them with the capabilities of being swollen and hydrated. However, it is important for the hydrogels to have adequate mechanical and lubricating features appropriate for the target tissue application.

2.11. Hydrogel as a platform for meniscal tissue engineering

Hydrogel systems are found to be interesting for use in tissue engineering because they can be prepared in situ by physical or chemical stimuli, have high water content, the ability to encapsulate cells homogenously, efficient mass transfer, tunable physical properties and minimally invasive delivery (Zorzi et al., 2016). The injectable hydrogels are attractive because they can fill and assume the size and shape of the defect that requires repair. Highly hydrated hydrogels can mimic the ECM and therefore are ideal for cell proliferation and differentiation. Most importantly, injectable hydrogels potentially avoid an open surgery procedure and avoid the need for patient-specific scaffold prefabrication, enhancing the physicomechanical properties of the injured site by delivering a variety of bio-actives, drug molecules, and growth factors (Kretlow et al., 2007) (Figure 13).

The choice of biomaterials and appropriate fabrication methods play a crucial role in developing an ideal injectable hydrogel that can function as scaffolds for meniscal tissue engineering. Hydrogels can be prepared from polymers obtained from both natural and synthetic sources. A review of the limited literature available on injectable hydrogels for meniscal tear showed that most of them described the use of natural polymers. The upcoming sections will give an overview of different injectable formulations used for meniscal tear repair.

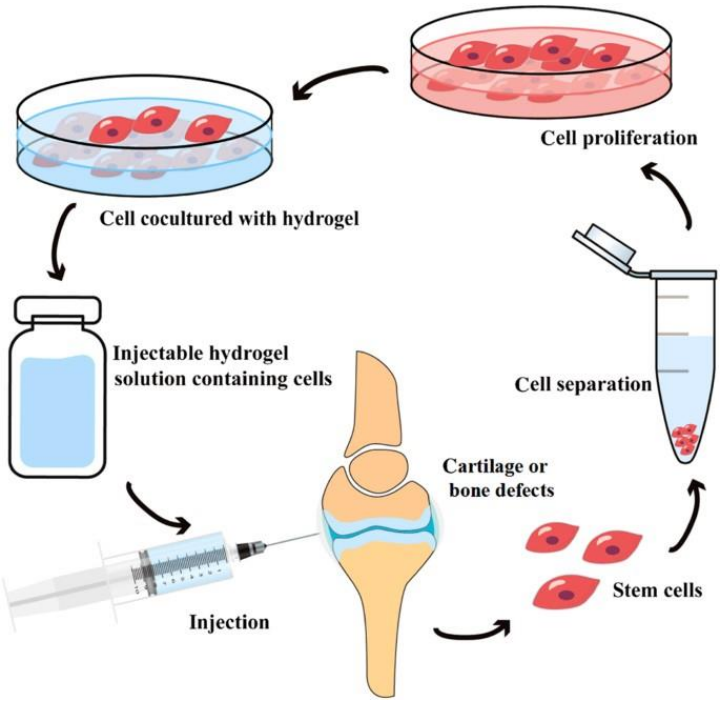

Figure 13. Schematic representation of making injectable hydrogel and their applications.

A tissue-derived injectable Extra Cellular Matrix (ECM) hydrogel for meniscal repair and regeneration was reported by (Wu et al., 2015). The ECM hydrogel was prepared from the porcine meniscus. The injectability of hydrogel was tested by subcutaneous injection in mouse tissue. The chondrocytes and mouse 3T3 fibroblasts encapsulated in the hydrogel for 2 weeks showed good cellular compatibility. They also observed good cell infiltration both *in vitro* and *in vivo*.

Zorzi et al. (2016) reported a clinical study on fifty patients using an injectable hydrogel prepared from hyaluronic acid derivative (HYADD4®). An outcome of the study was that the patients got better results in terms of pain reduction, improvement of knee functionality and reduction in length & depth of the meniscal lesion.

In another work, an enzyme-based approach was used to prepare injectable hydrogels (Kim et al., 2018). Here hydrogel was formulated using Tyramine (TA)- Hyaluronic acid (HA) and gelatin in the presence of tyrosinase (TYR) mediated cross-linking. The TYR-mediated crosslinking exhibited tissue-adhesive properties. Furthermore, fibrochondrocytes encapsulated TYR crosslinked hydrogels demonstrated good biocompatibility and resulted in enhanced ECM synthesis and expression of Collagen type I, II and aggrecan. Histological analysis confirmed the uniform distribution of fibrochondrocytes in the hydrogel.

In another work, injectable hydrogel of methacrylated gelatin (mGL) loaded with adipose stem cells (ASC) and TGF-b3 was used for in vitro repair of meniscal tear (Sasaki et al., 2018). They created an *in vitro* radial bovine meniscal tear model and injected the hydrogel into the tear and covered by an aligned electrospun poly-E-caprolactone nanofibrous scaffold (NFS) to ensure retention of the hydrogel at the tear site. The study showed that mGL hydrogels preloaded with TGF-b3 induced chondrogenic differentiation of ASCs and promoted meniscal healing in an *in vitro* radial meniscal tear model. The mechanical properties of repaired meniscal explants were also higher in the ASC TGF-b3 loaded hydrogel.

Berton et al. (2020) carried out a study to evaluate the clinical efficacy and healing effects of injectable hyaluronic acid (HA) hydrogel, Hymovis®, for the conservative management of degenerative meniscal lesions (DMLs). All 40 patients enrolled in the study underwent magnetic resonance imaging (MRI) and T2 mapping after 60 days of treatment. The results after MRI showed that treatment of DMLs with HA hydrogel supports the conservative

management of DMLs by enhancing the meniscal healing. One-year follow-up study of these patients showed that the need for arthroscopic partial meniscectomy (APM) was less.

2.12. Alginate as a biomaterial for meniscal tissue engineering

Alginate is a naturally occurring anionic and hydrophilic polysaccharide obtained from brown algae cell walls and bacteria (Szekalska et al., 2016). Alginate has been extensively used for many biomedical applications, due to its biocompatibility, low toxicity, low cost, and mild gelation by the addition of divalent cations such as Ca^{2+} (Tariverdian et al., 2019).

2.12.1. Structure of alginate

Alginate is an anionic linear polysaccharide that contains blocks of (1–4)-linked β-D-mannuronic acid (M) and α-L-guluronic acid (G) monomers in varying proportions (Sun and Tan, 2013). The blocks in alginate chains are composed of three different forms of polymer segments: homogenous G residues, homogenous M residues and heterogenous MG residues (Figure 14) (Sachan et al., 2009). Depending on the source material the G and M residues in commercially available alginate may vary. The G-units of alginate are believed to participate in intermolecular cross-linking with divalent cations to form hydrogels. The M/G ratio, length of G unit and molecular weight are critical factors affecting the physical properties of alginate and its ability to form hydrogels (George and Abraham, 2006).

2.12.2. Solubility and molecular weight

Alginic acid is slightly soluble in water. Depending on the molecular weight, the sodium salt of alginate is quite soluble in water at concentrations ranging from 3 to 10 % at room temperature and at pH range 5.5 to 8.5 (Solandt, 1941). The molecular weight of

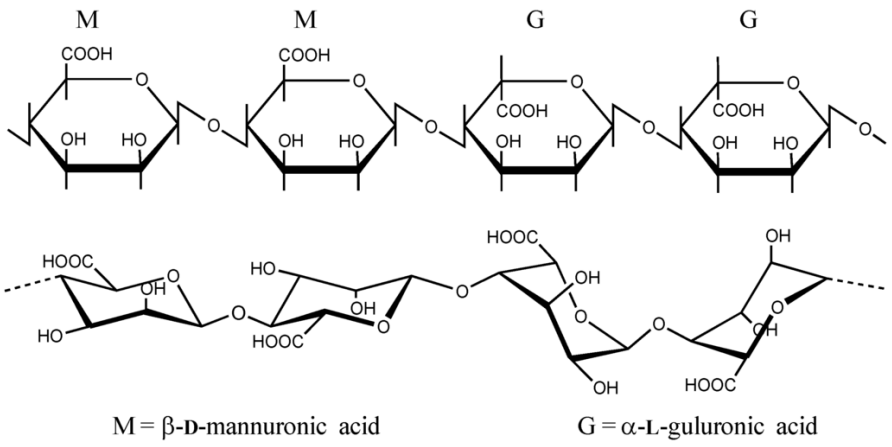

Figure 14. Structure of Alginate (Andersen et al., 2015).

commercially available sodium alginates ranges from 32,000 to 400,000 g/mol (Lee and Mooney, 2012).

2.12.3. Degradation in Organisms

Alginate is non-degradable in mammals because mammals lack alginase enzymes in their body. However, in the case of divalent cation crosslinked alginate hydrogels, the divalent cations could be replaced gradually by monovalent cations (for example, Na+) from the surrounding media and dissolve the hydrogel in the medium (Sahoo and Biswal, 2021). There are reports in the literature focussing on the degradation of alginate crosslinked by different crosslinking agents. Shahriari et al. (2016) described the degradation of calcium crosslinked alginate hydrogels used for spinal cord repair both *in vitro* and *in vivo*. *In vitro* degradation studies using rheology showed that the shear modulus of hydrogel decreased by 97 % within 2 days, but even after 28 days there was no change in the superficial geometry of the hydrogel. *In vivo* evaluation indicates that the alginate hydrogel was not present/functional after two weeks post-implantation. Another study by Kurowiak et al. (2020) reported the use of alginate gels crosslinked by calcium chloride, barium chloride

and a combination of both for the treatment of urethral injuries. It was found that material crosslinked with Ca^{2+} ions alone showed slower degradation compared to one with a combination of Ca^{2+}/Ba^{2+} ions.

2.12.4. Modification of alginate

The alginate chains have several free carboxyl and hydroxyl groups. These groups can be used for the chemical modification of alginate. By chemically modifying the alginate its properties such as solubility, hydrophobicity, degradation and biological characteristics can also be modified (J.-S. Yang et al., 2011). The upcoming section will describe the chemical modification of hydroxyl and carboxyl groups present in alginate.

2.12.5. Chemical modification of carboxyl groups

2.12.5.1. Esterification

The esterification reaction is a type of nucleophilic acyl substitution. Here the most reactive nucleophile in alginate is the C6 carboxylate group. This carboxylate can react with an organic molecule "R" to yield the corresponding esters as shown in figure 15. This reaction is carried out in nonaqueous media to prevent undesired reactions with water. The alginate esters thus formed can be used for the synthesis of microspheres (Leonard et al., 2004), self-assembled nanoparticles that will be stable in aqueous media (Li et al., 2011) and also for preparing amorphous solid dispersions for the controlled release of poorly water-soluble drugs (Pawar and Edgar, 2013).

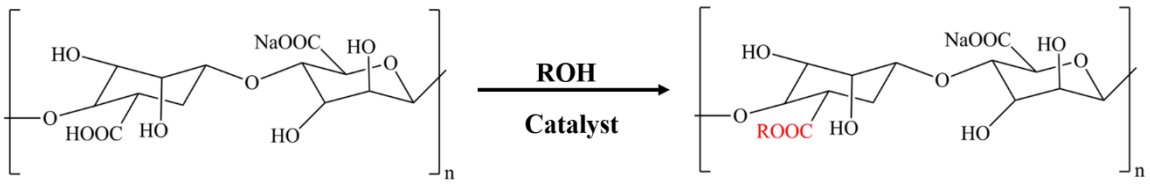

Figure 15. Scheme of esterification of alginate (Yang et al., 2011).

2.12.5.2. Amidation

Amidation reaction in alginate is a two-step procedure. This includes the esterification of carboxyl groups with methanol as described in section 2.12.5.1 and further aminolysis of the obtained methyl ester with seven selected primary amines, hydrazine and hydroxylamine (Taubner et al., 2013). Yang et al. (2011) used 1-ethyl-3-(3-dimethyl aminopropyl) carbodiimide hydrochloride (EDC-HCl) to covalently couple 1-Octyl amine to sodium alginate. The modified alginate named as octyl-grafted amphiphilic alginate-amide derivative (OAAD) as shown in figure 16 was further used for λ-cyhalothrin (LCH) microcapsule application. This microcapsule helped in the controlled release of LCH. Banks et al. (2019) also used EDC-HCl to form amide linkages with carboxylate groups in alginate (Figure 16). The hydrogel formed by modified alginate can be used for pH dependant drug delivery release system in the gastrointestinal tract.

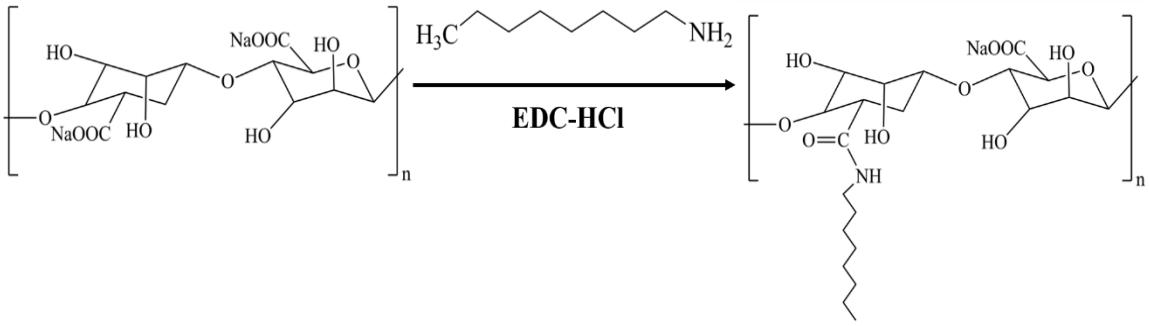

Figure 16. Amidation reaction of Alginate with EDC.

2.12.6. Chemical modification of hydroxyl groups

2.12.6.1. Acetylation

Acetylation of alginate can occur naturally and synthetically. Recently Chanasit et al. (2020) and Franklin et al. (2004) reported the analysis of O-acetylation of human pathogen *Pseudomonas aeruginosa.* They found that three proteins, namely, AlgI, AlgJ

and AlgF have been implicated to form a complex and act together with AlgX for the O-acetylation of alginate at the C2 and C3 hydroxyl groups of the mannuronic acid (Figure 17). The O-acetylation of alginate in *P. aeruginosa* is an important factor contributing to its pathogenicity which will prevent them from recognition and clearance by the host immune system (Pier et al., 2001). The very first report describing the chemical acetylation of alginates was published in 1946. The acetylating reagent used here is acetic acid (Chamberlain et al., 1946).

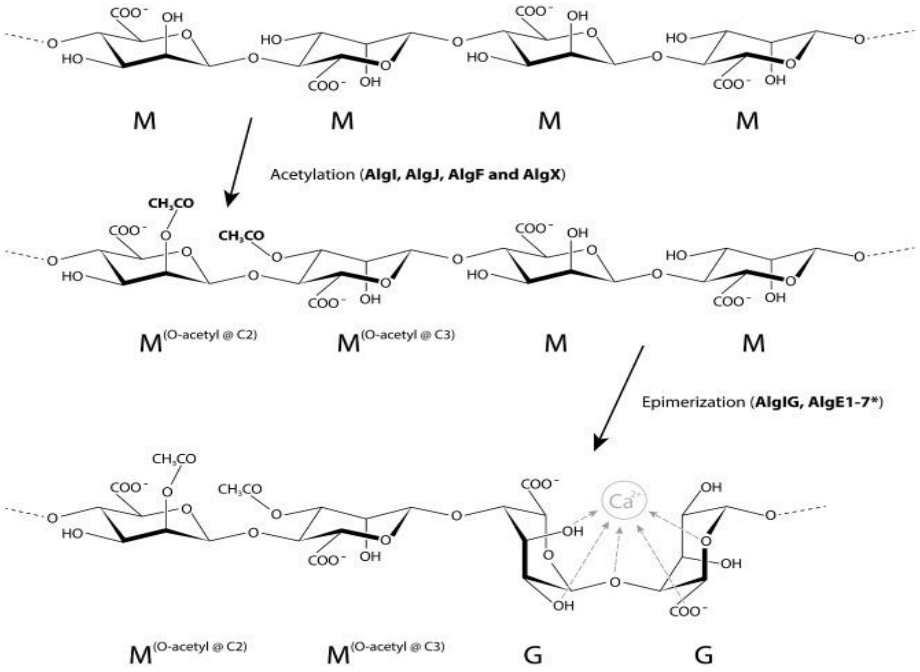

Figure 17. Acetylation of Alginate (Hay et al., 2013).

2.12.6.2. Sulfation

Sulfated alginate has high blood compatibility, structural similarity with heparin which gives them anticoagulant activity (Alban et al., 2002). Ma et al. (2016) reported the preparation of sodium alginate sulfates (SASs) using H_2SO_4 and N, N'-Dicyclocarbodiimide (DCC) as the sulfating agents. Later SASs was conjugated with

dopamine to obtain mussel inspired adhesive heparin-mimetic macromolecules (DA-g-SASs). Another method for the preparation of alginate sulfate was reported by Mhanna et al. (2017). They synthesized alginate sulfates in a two-step procedure (Figure 18). In the first step, they converted sodium alginate into its tetra butyl ammonium salt to improve the material solubility in the reaction condition. In the second step, alginate tetra butyl ammonium salt was mixed with DMF and an excess of SO_3/pyridine was added to induce the sulfation of free hydroxyl groups. The highly sulfated alginates synthesized were found to maintain the stemness of the adipose derived stem cells.

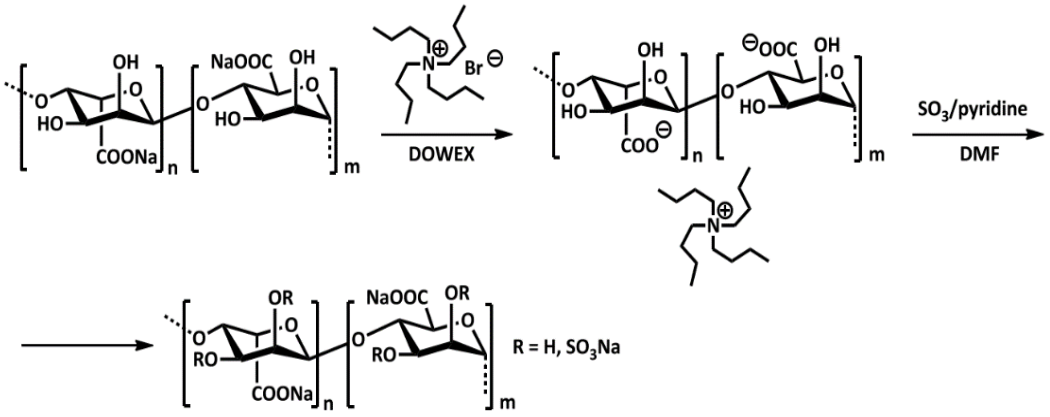

Figure 18. Sulfation Reaction (Mhanna et al. 2017).

2.12.6.3. Oxidation

Oxidation of alginate has gained much attention compared to other modification procedures. Oxidation reactions are carried out on the hydroxyl groups at C-2 and C-3 positions of the uronic units of sodium alginate with the help of sodium periodate. This leads to the opening of the sugar ring by rupturing of carbon-carbon bonds resulting in the formation of two aldehyde groups in each oxidized monomeric unit (Figure 19). The reaction needs to be carried out in dark to prevent side reactions. The number of aldehyde

groups can be limited by controlling the oxidation reaction (Gomez et al., 2007). The upcoming sections will give a detailed update on oxidized alginate, also called alginate dialdehyde.

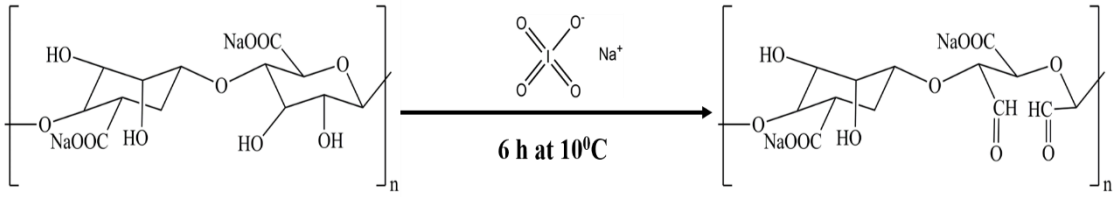

Figure 19. Oxidation of Alginate (Gomez et al., 2007).

2.13. Oxidized alginate (OA) / Alginate dialdehyde (ADA) for tissue engineering

Due to their similarity with the extracellular matrix of tissues alginate-based hydrogels have been used widely in various tissue engineering applications. A major limitation of alginate-based hydrogels is their rather low *in vivo* degradation happening unpredictably by releasing high and low molecular weight alginate chains. Low molecular weight (<50 KDa) alginate chains can be cleared through the kidney. Apart from this, alginate also exhibits poor cell adhesion and migration due to the lack of cell-surface receptors, and protein adsorption onto alginate (Bai et al., 2013). Literature shows that the chemical modification of alginate by oxidation using sodium meta periodate as a catalyst can overcome all these limitations in contrast to other modification procedures (Bouhadir et al., 2001).

2.13.1. Synthesis of oxidized alginate

Oxidized alginate (OA), also known as alginate dialdehyde (ADA), was synthesized via periodate oxidation of sodium alginate. The oxidation procedure of alginate was introduced in 1928 by Malaprade (Jejurikar et al., 2012). ADA has gained much attention in tissue

engineering because of the presence of more reactive groups and better degradation compared to alginate. A common method for introducing aldehyde groups into polysaccharides or glycoproteins is oxidation with periodate. Even though periodate can oxidize both M and G units in alginate, the initial rate of oxidation was 50% faster for G units compared to M units (Kristiansen et al., 2010). Sodium meta periodate can oxidize the -OH groups at the second and third carbon positions (C-2 and C-3) of the alginate chain as shown in Figure 19 in section 2.12.6.3. This results in the breakage of the carbon-carbon bond leading to the formation of two aldehyde functional groups. A study conducted by Painter (1988) showed that alginate has an oxidation limit closer to 50%. This oxidation limit corresponds to the formation of six-membered hemiacetal linkage between the aldehyde residues and the closest adjacent hydroxyl groups of the unoxidized residues (Painter and Larsen, 1973). Usually, the periodate oxidation will be carried out in dark to prevent side reactions and to keep the periodate stable (Head, 1950).

Alginate oxidation can be carried out in both aqueous and ethanol-water mediums. But in an aqueous medium, only low concentrations of alginate can be oxidized. In an aqueous medium, the yield of the reaction was 25-30% but in an ethanol-water mixture, the yield increased to 50-60% (Reakasame and Boccaccini, 2018). In order to obtain pure ADA, the reaction mixture needs to be dialyzed in distilled water to remove unreacted components and further lyophilized to obtain the final product. ADA thus synthesized has been used in various tissue engineering applications after crosslinking.

2.13.2. Crosslinking of ADA

ADA contains numerous aldehyde pendent groups in its polymer chain. The carbon of the aldehyde group possesses a sp^2 hybrid orbit which gives its positive charge. It also contains carbonyl oxygen which possesses a negative charge (Wang et al., 2010). These aldehyde groups can form covalent bonds with other materials. Literature reveals that ADA can form crosslinks with chitosan, gelatin, casein, collagen, etc. The following literature would give a brief overview on different ADA based hydrogels developed for various tissue engineering applications.

Bajpai et al. (2016) prepared hydrogel films by crosslinking casein with ADA. ADA with a degree of oxidation 57.7 % was used for preparing films. Aldehyde groups in ADA reacted with amino groups of casein formed Schiff's base crosslinks. The films showed good water absorption capacity and exhibited high Water Vapour Transmission Rate, which was the requirement of a good wound dressing material.

In a study conducted by Baniasadi et al. (2016) the authors evaluated the role of self-crosslinking oxidized alginate gelatin (OA-GEL) hydrogels for muscle tissue engineering. They used OA with different degrees of oxidation (10, 30 and 50%) for their work. Authors found that the properties of hydrogel could be tuned by varying the degrees of oxidation OA and OA to GEL ratio. The hydrogels prepared with degrees of oxidation 30 % and 50 % were found to be suitable for muscle tissue engineering. The hydrogel developed was found to be cytocompatible with Warton Jelly-derived Umbilical Cord-Mesenchymal Stem Cells. Klontzas et al. (2019) prepared hydrogels using ADA, gelatin and glycine-histidine-lysine (ADA-Gel-GHK). The ADA they used had a degree of oxidation of 33%. They

encapsulated umbilical cord blood mesenchymal stem cells (UCB MSCs) in these hydrogels and prepared beads by crosslinking with calcium chloride. The cells embedded in the hydrogels were able to differentiate into the osteogenic lineage and authors proposed to use the system in bone tissue engineering applications.

Ma et al. (2020) reported a self-healing injectable OA hydrogel in combination with hydroxyapatite (HA) and carboxymethyl chitosan (CMCS). Initially, they prepared a hybrid of alginate (Alg) and HA. Later the alginate in Alg/HA was oxidized to form an oxidized HA/Alg hybrid (OHAH). This hybrid was used for preparing injectable hydrogel with CMCS. The amino groups in CMCS form Schiff's base with the aldehyde groups in OHAH. The injectable hydrogel was found to be cytocompatible with L929 cells.

2.14. Gelatin for tissue engineering

Gelatin is prepared by partial acid hydrolysis (Gelatin Type A) or by alkaline hydrolysis (Gelatin Type B) of a principal protein of connective tissues in animals, namely, collagen (Hoque et al., 2015). The physical properties and heterogeneity of gelatin depended on the source of collagen and its preparation techniques (Djagny et al., 2001). Gelatin has been used widely for various medical applications due to its ready availability at low cost, low antigenicity, biodegradable & biocompatible nature and the presence of RGD peptide sequence that promote cell adhesion.

Gelatin is made up of 19 amino acids linked together in a partially ordered fashion (Schrieber and Gareis, 2007). The amino acid that is not present in gelatin is tryptophan and it has low contents of methionine, cystine and tyrosine (Jamilah and Harvinder, 2002). Even though the amino acid composition of gelatin differs depending on the sources, it

always contains a large amount of glycine, proline and hydroxyproline with a typical sequence Gly-X-Y where glycine is most abundantly present in gelatin; X and Y are mostly proline and hydroxyproline, respectively (Figure 20) (Gilsenan and Ross-Murphy, 2000).

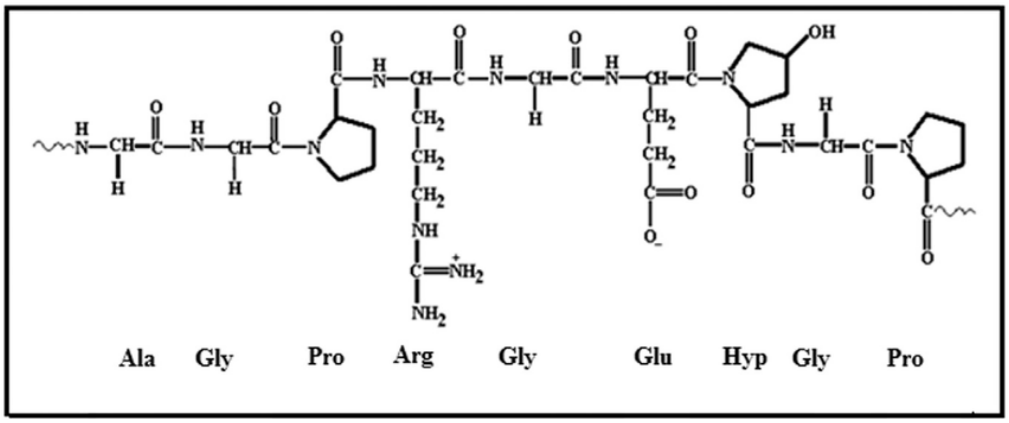

Figure 20. Structure of Gelatin (Devi et al., 2016).

Dissolution of gelatin is practically more convenient than commercially available collagen, especially when it requires at higher concentrations. Gelatin can be easily dissolved at temperatures between 40 to 50 ^{0}C. The solubility of gelatin at this temperature depends on the concentration (up to 40 %) and viscosity of the solution (Kramer, 2001). One of the important properties of gelatin is the ability to form temperature reversible gels. When a gelatin solution is cooled below 40°C, the viscosity of the solution started to increase slowly. But as the gel point is reached there would be a sudden increase in viscosity. At the initial stage of gelation, there would be steric rearrangement in gelatin molecules leading to the formation of an ordered helical configuration. In the second stage, helical regions from different gelatin molecules form a 3D network. Finally, the 3D network will be stabilized by hydrogen bonding. But when gelatin is heated in an aqueous medium, the

hydrogen bond will break, thereby weakening the 3D network leading to its dissolution (Djabourov et al., 1988).

2.14.1. Crosslinking of Gelatin

Gelatin has a number of pendant reactive sites in its molecular structure. They include amino groups, carboxylic acid groups and hydroxyl groups. These pendant groups provide ample scope for chemical modifications or crosslinking. Glutaraldehyde is one of the most widely used crosslinking agents because it can effectively stabilize collagen or its derivatives. However, the literature showed that glutaraldehyde is cytotoxic (Poursamar et al., 2016). Glutaraldehyde can react with the free amino groups of lysine or hydroxylysine in gelatin forming imine linkage (Yang et al., 2018). Genipin is another crosslinker that has lower toxicity compared to glutaraldehyde. Literature shows that genipin can crosslink with epsilon amino groups of lysine and hydroxylysine residues in gelatin (Kirchmajer et al., 2012). 1-Ethyl-3-(3-dimethyl aminopropyl) carbodiimide (EDC) is a zero-length crosslinker of polysaccharides and proteins. EDC can react with carboxyl amino acid residues such as Asp, Glu, or the C-terminal carboxyl group of the protein to form an unstable reactive acylisourea ester. This intermediate ester can interact with a primary amine (Lys or protein N-terminal amine) to form a peptidyl bond with the elimination of a water molecule (Chen et al., 2005). EDC will not incorporate into the reaction and can be easily removed (Figure 21). The upcoming section will give a brief idea about gelatin hydrogels used for tissue engineering applications.

Tormos et al. (2015) prepared injectable hydrogels of chitosan - gelatin (CG) loaded with doxycycline (DOX) and transglutaminase (TG). DOX prevented the premature

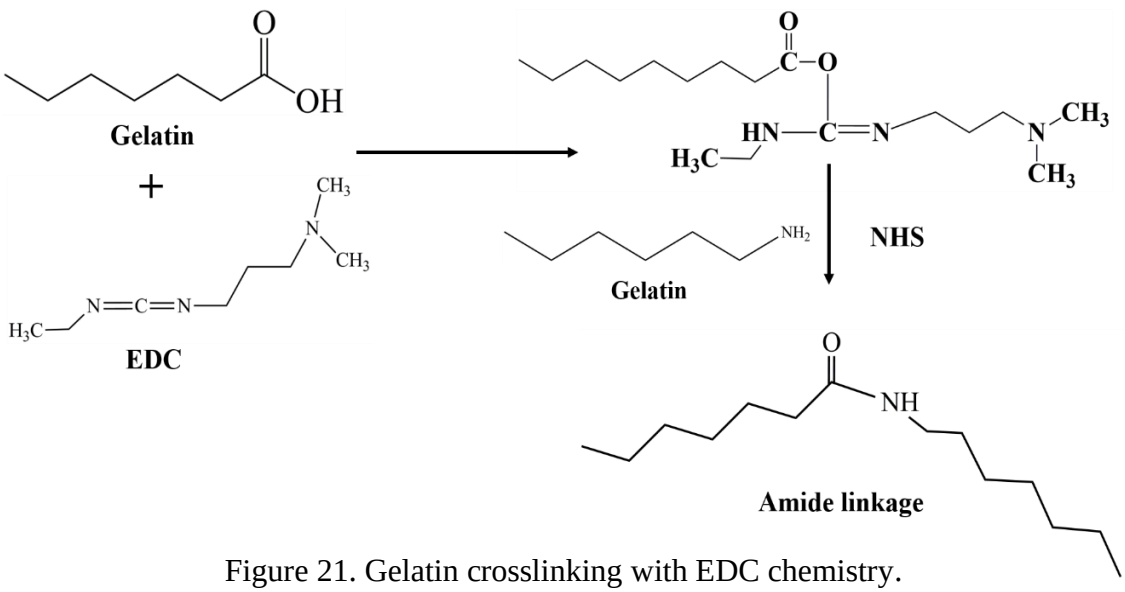

Figure 21. Gelatin crosslinking with EDC chemistry.

degradation of CG hydrogels by inhibiting the gelatinases (MMP-2/9) activity and TG acted as a crosslinker. CG hydrogels crosslinked with TG had enhanced mechanical stability, controlled release of DOX and helped in the retention of human foreskin fibroblasts (hFF-1).

Padhi et al. (2016) developed Gelatin/i-Carrageenan hydrogels using glutaraldehyde as a chemical crosslinker for the release of broad-spectrum antibiotics ciprofloxacin. Here amino groups of gelatin and sulfate groups in i-carrageenan interacted forming ionic bonds. By adding glutaraldehyde additional covalent crosslink could be achieved with the free amino groups of gelatin thereby providing more flexibility as well as mechanical strength to the hydrogel. The prepared hydrogel formulations could offer controlled release of ciprofloxacin drug for a longer period. The hydrogel showed good mucoadhesive behaviour and has been proposed as a good material for applications such as wound dressing and dermal patches.

Kessler et al. (2017) prepared hydrogels using methacrylated gelatin (GelMA) and hyaluronan (HyaMA) with Adipose-derived stem cells (ASCs) for soft tissue engineering applications. The hydrogels were prepared by adding Lithium phenyl-2,4,6-trimethylbenzoylphosphinate (LAP) as a photo-crosslinker. The combined form of GelMA/HyaMA hydrogels promoted adipogenic differentiation and viability compared to GelMA hydrogels.

Wang et al. (2018) prepared bacterial cellulose (BC) - gelatin hydrogels for tumor cell culture. The hydrogel was prepared using natural crosslinker procyanidin (PA). The chemical structure, morphology, mechanical properties, porosity, and wettability of the hydrogels were evaluated. *In vitro* evaluation using a human breast cancer cell line (MDA-MD-23) showed that cancer cells seeded on hydrogels maintained their normal morphology and could proliferate and migrate into the hydrogel matrix. The cells migrated into the hydrogel matrices were found to be viable. The BC/gelatin hydrogels were proposed to be used as a feasible and cost-effective candidate for *in vitro* cancer biology studies.

There are reports on the preparation of sodium alginate (SA)-gelatin (GL) hydrogels for 3D printing of co-cultures of non-small cell lung cancer (NSCLC) patient derived xenograft (PDX) cells and lung Cancer Associated Fibroblasts (CAFs) cells. Hydrogels prepared with SA and GL showed good printability and cell viability. Live dead assay showed that PDX cells were viable even after 4 days of culture in the printed scaffold. Co-culturing of PDX and CAF cells showed the formation of small spheroids inside the cell-seeded printed scaffolds. The printed PDX and CAF spheroids suggested the crosstalk

between these cells which promotes Epithelial-Mesenchymal Transitions. Thus 3D printed Alg-GL hydrogel seeded with PDX and CAF cells allow to study the tumor stroma interactions to mimic *in vivo* tumor microenvironments (Mondal et al., 2019).

(Wei et al., 2020) reported their work on photo crosslinked gelatin molecules reinforced by collagen fibrils and bioactive glass (MBG) for tissue adhesive applications. The tissue adhesive developed had adhesive strength superior to fibrin glue and the composition was cytocompatible with L929 cells.

(Chun et al., 2021) prepared positive charge tuned gelatin hydrogel for siRNA anti-scarring therapy. Here gelatin (Gtn) was conjugated with a phenol molecule, tyramine (Tyr) using the carbodiimide crosslinking reaction to form a Gtn-Tyr precursor. Tyr 'annihilated' the free negatively charged COOH groups on the gelatin to create a positively charged environment for the gelatin. The precursor solution was then treated with horseradish peroxidase to form Gtn-Tyr hydrogel. *In vitro* studies using the hydrogel loaded with siSPARC (siRNA for secreted protein, acidic and rich in cysteine) showed good cell internalization and SPARC silencing. *In vivo* studies in the rabbit model showed that the hydrogel is non-cytotoxic compared to commonly used mitomycin-C and it also showed a reduction in subconjunctival scarring.

2.15. Oxidized alginate (OA)/Alginate dialdehyde (ADA)-Gelatin based hydrogel for tissue engineering

ADA/gelatin system is the most popular ADA-based hydrogel, which has been reported for various tissue engineering applications. The covalent crosslinking between ADA and gelatin occurs between the Ɛ-amino groups of lysine or hydroxylysine of gelatin and the

aldehyde groups of ADA by Schiff's base reaction resulting in aldimine bonds (R-CH = NH) (Nguyen and Lee, 2012). But due to the hemiacetal formation in ADA, the reaction between ADA and gelatin happens at a slow rate. Injectable hydrogels require fast gelation. This is achieved by adding sodium tetraborate (borax) into the ADA solution which in turn results in the formation of a tetraborate complex between the hydroxyl groups of two different ADA polymer chains (Figure 22). The net result is the availability of aldehyde groups for reaction and subsequent gel formation (Balakrishnan et al., 2014a).

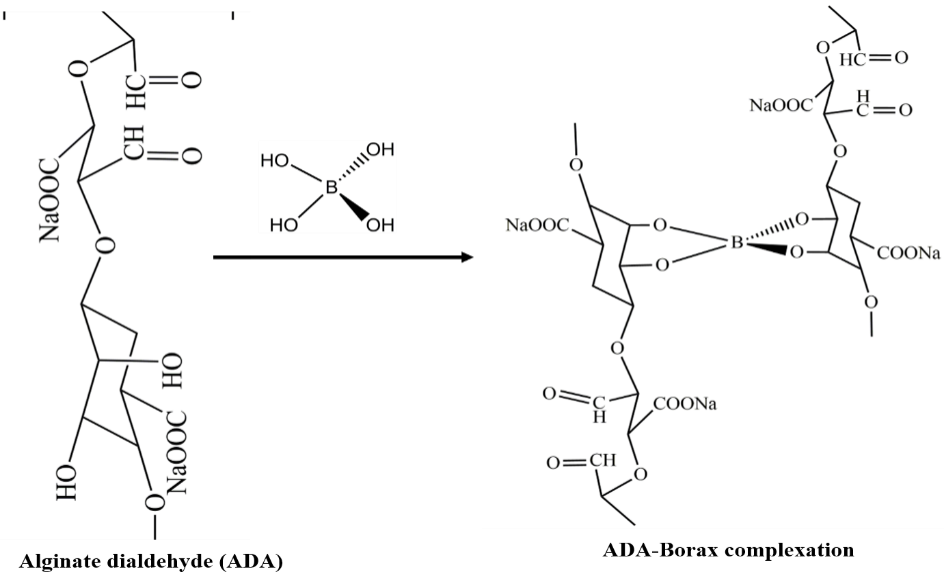

Figure 22. Schematic on the formation of ADA-borax complex.

The forthcoming sections are meant to give a review of the literature on ADA/OA-gelatin hydrogels. Giving the keyword "Alginate dialdehyde" and "Gelatin" in the PUBMED search gave 14 articles published in the past 5 years (2016-2021). Among these, the maximum number of articles (5 nos) was published in the year 2020 (Figure 23 A). Table 1 lists the articles obtained when the above keywords were used. But when the keyword was changed to "Oxidized alginate" and "Gelatin", the number of articles published in the

past 5 years was 33. The maximum number of articles (12 nos) was published in the year 2020 (Figure 23 B). Table 2 lists the articles with these two keywords.

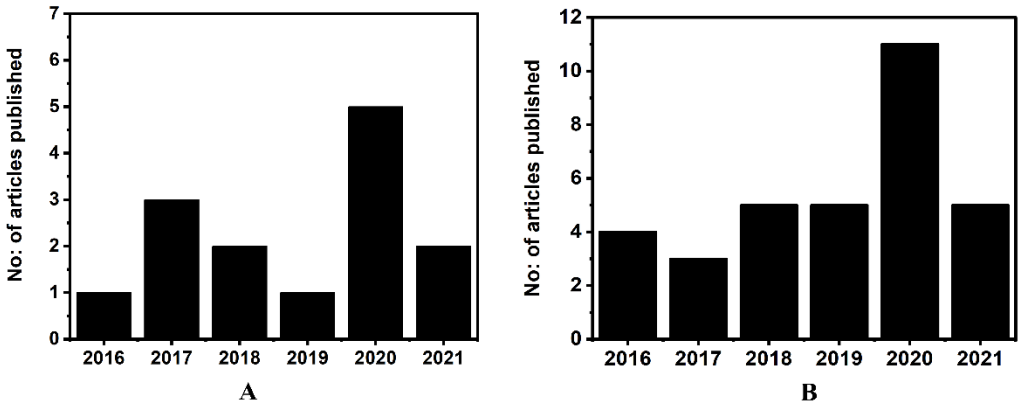

Figure 23. Number of articles published in the past 5 years with two key word pairs: A) Key word pair, 'Alginate dialdehyde' & 'Gelatin'; B) Key word pair, 'Oxidized alginate' & 'Gelatin'.

Table 1. Articles published in the past 5 years with the keyword pair, 'Alginate dialdehyde' and 'Gelatin'.

Sl. No	**Title of the article**	**Journal**	**DOI, Author & year**
1	Scaffold for liver tissue engineering: Exploring the potential of fibrin incorporated alginate dialdehyde-gelatin hydrogel	International Journal of Biological Macromolecules	10.1016/j.ijbiomac.2020.10.256 (Rajalekshmi et al., 2021)
2	Aquatic polymer-based edible films of fish gelatin crosslinked with alginate dialdehyde having enhanced physicochemical properties	Carbohydrate Polymers	10.1016/j.carbpol.2020.117317 (Park et al., 2021)
3	Formulation and Characterization of Alginate Dialdehyde, Gelatin, and Platelet-Rich Plasma-Based Bioink for Bioprinting Applications	Bioengineering (Basel)	10.3390/bioengineering7030108 (T. Somasekharan et al., 2020)
4	Biofabrication and Characterization of Alginate Dialdehyde-Gelatin Microcapsules Incorporating Bioactive Glass for Cell Delivery Application	Macromolecular Bioscience	10.1002/mabi.202000138 (Reakasame et al., 2020)

5	Comparison of Hydrogels for the Development of Well-Defined 3D Cancer Models of Breast Cancer and Melanoma	Cancers (Basel)	10.3390/cancers12082320 (Schmid et al., 2020)
6	Ionically and Enzymatically Dual Cross-Linked Oxidized Alginate Gelatin Hydrogels with Tunable Stiffness and Degradation Behavior for Tissue Engineering	ACS Biomaterials Science & Engineering	10.1021/acsbiomaterials.0c00677 (Distler et al., 2020a)
7	Cell-laden alginate dialdehyde-gelatin hydrogels formed in 3D printed sacrificial gel	Journal of Materials Science: Materials in Medicine	10.1007/s10856-020-06369-7 (Dranseikiene et al., 2020)
8	Printability and Cell Viability in Bioprinting Alginate Dialdehyde-Gelatin Scaffolds	ACS Biomaterials Science & Engineering	10.1021/acsbiomaterials.9b00167 (Soltan et al., 2019)
9	Encapsulation of Rat Bone Marrow Derived Mesenchymal Stem Cells in Alginate Dialdehyde/Gelatin Microbeads with and without Nanoscaled Bioactive Glass for In Vivo Bone Tissue Engineering	Materials (Basel)	10.3390/ma11101880 (Rottensteiner-Brandl et al., 2018)
10	Encapsulation of Mesenchymal Stem Cells Improves Vascularization of Alginate-Based Scaffolds	Tissue Engineering Part A	10.1089/ten.TEA.2017.0496 (Steiner et al., 2018)
11	Preclinical evaluation of hydrogel sealed fluropassivated indigenous vascular prosthesis	Indian Journal of Medical Research	10.4103/ijmr.IJMR_1933_15 (Unnikrishnan et al., 2017)
12	Trilayer Three-Dimensional Hydrogel Composite Scaffold Containing Encapsulated Adipose-Derived Stem Cells Promotes Bladder Reconstruction via SDF-1α/CXCR4 Pathway	ACS Applied Materials & Interfaces	10.1021/acsami.7b10630 (D. Xiao et al., 2017)
13	Cell specificity of magnetic cell seeding approach to hydrogel colonization	Journal of Biomedical Materials Research Part A	10.1002/jbm.a.36147 (Singh et al., 2017)

14	Bioplotting of a bioactive alginate dialdehyde-gelatin composite hydrogel containing bioactive glass nanoparticles	Biofabrication	10.1088/1758-5090/8/3/035005 (Leite et al., 2016)

Table 2 Articles published in the past 5 years with the given keyword "Oxidized Alginate" and "Gelatin".

Sl. No	**Title of the article**	**Journal**	**DOI, Author & Year**
1	Electrically Conductive and 3D-Printable Oxidized Alginate-Gelatin Polypyrrole: PSS Hydrogels for Tissue Engineering	Advanced Healthcare Materials	10.1002/adhm.202001876 (Thomas Distler et al., 2021)
2	Mechanical properties of cell- and microgel bead-laden oxidized alginate-gelatin hydrogels	Biomaterials Science	10.1039/d0bm02117b (T. Distler et al., 2021)
3	Differential Responses to Bioink-Induced Oxidative Stress in Endothelial Cells and Fibroblasts	International Journal of Molecular Sciences	10.3390/ijms22052358 (Genç et al., 2021)
4	Electroactive and antioxidant injectable in-situ forming hydrogels with tunable properties by polyethyleneimine and polyaniline for nerve tissue engineering	Colloids & Surface B Biointerfaces	10.1016/j.colsurfb.2021.111565 (Karimi-Soflou et al., 2021)
5	Viscosity and degradation controlled injectable hydrogel for esophageal endoscopic submucosal dissection	Bioactive Materials	10.1016/j.bioactmat.2020.09.028 (Fan et al., 2021)
6	Potential of laponite incorporated oxidized alginate-gelatin (ADA-GEL) composite hydrogels for extrusion-based 3D printing	Journal of Biomedical Materials Research Part B: Applied Biomaterials	10.1002/jbm.b.34771 (Cai et al., 2020)
7	Biomimetic Alginate/Gelatin Cross-Linked Hydrogels Supplemented with Polyphosphate for Wound Healing Applications	Molecules	10.3390/molecules25215210 (Wang et al., 2020)

8	Complex mechanical behavior of human articular cartilage and hydrogels for cartilage repair	Acta Biomaterilia	10.1016/j.actbio.2020.10.025 (Weizel et al., 2020)
9	Characterization of an oxidized alginate-gelatin hydrogel incorporating a COS-salicylic acid conjugate for wound healing	Carbohydrate Polymers	10.1016/j.carbpol.2020.117145 (Gw et al., 2020)
10	Biofabrication and Characterization of Alginate Dialdehyde-Gelatin Microcapsules Incorporating Bioactive Glass for Cell Delivery Application	Macromolecular Bioscience	10.1002/mabi.202000138 (Reakasame et al., 2020)
11	3D printed oxidized alginate-gelatin bioink provides guidance for C2C12 muscle precursor cell orientation and differentiation via shear stress during bioprinting	Biofabrication	10.1088/1758-5090/ab98e4 (Distler et al., 2020b)
12	Ionically and Enzymatically Dual Cross-Linked Oxidized Alginate Gelatin Hydrogels with Tunable Stiffness and Degradation Behavior for Tissue Engineering	ACS Biomaterials Science & Engineering	10.1021/acsbiomaterials.0c00677 (Distler et al., 2020a)
13	3D printing and characterization of human nasoseptal chondrocytes laden dual crosslinked oxidized alginate-gelatin hydrogels for cartilage repair approaches	Materials Science and Engineering C: Materials for Biological Applications	10.1016/j.msec.2020.111189 (Schwarz et al., 2020)
14	A porous hydrogel-electrospun composite scaffold made of oxidized alginate/gelatin/silk fibroin for tissue engineering application	Carbohydrate Polymers	10.1016/j.carbpol.2020.116465 (Hajiabbas et al., 2020)
15	3D Bioprinting of Carbohydrazide-Modified Gelatin into Microparticle-Suspended Oxidized Alginate for the Fabrication of Complex-Shaped Tissue Constructs	ACS Applied Materials Interfaces	10.1021/acsami.0c05096 (Heo et al., 2020)
16	Injectable self-crosslinking hydrogels for meniscal repair: A study with oxidized alginate and gelatin	Carbohydrate Polymers	10.1016/j.carbpol.2020.115902 (Resmi et al., 2020)
17	An Acoustic Droplet-Induced Enzyme Responsive Platform for the Capture and On-Demand Release of Single Circulating Tumor Cells	ACS Applied Materials Interfaces	10.1021/acsami.9b16566 (Wei et al., 2019)

18	Oxidized alginate/gelatin decorated silver nanoparticles as new nanocomposite for dye adsorption	International Journal of Biological Macromolecules	10.1016/j.ijbiomac.2019.09.076 (Abou-Zeid et al., 2019)
19	Conductive Hydrogen Sulfide-Releasing Hydrogel Encapsulating ADSCs for Myocardial Infarction Treatment	ACS Applied Materials Interfaces	10.1021/acsami.9b01886 (Liang et al., 2019)
20	Magnetic and self-healing chitosan-alginate hydrogel encapsulated gelatin microspheres via covalent cross-linking for drug delivery	Materials Science and Engineering C: Materials for Biological Applications	10.1016/j.msec.2019.04.012 (Chen et al., 2019)
21	Oxidized alginate hydrogels with the GHK peptide enhance cord blood mesenchymal stem cell osteogenesis: A paradigm for metabolomics-based evaluation of biomaterial design	Acta Biomaterialia	10.1016/j.actbio.2019.02.017 (Klontzas et al., 2019)
22	Particle-coated electrospun scaffold: A semi-conductive drug eluted scaffold with layered fiber/particle arrangement	Journal of Biomedical Materials Research Part A	10.1002/jbm.a.36522 (Khorshidi and Karkhaneh, 2018)
23	Construction of Injectable Self-Healing Macroporous Hydrogels via a Template-Free Method for Tissue Engineering and Drug Delivery	ACS Applied Materials Interfaces	10.1021/acsami.8b13077 (L. Wang et al., 2018)
24	Controlling alginate oxidation conditions for making alginate-gelatin hydrogels	Carbohydrate Polymers	10.1016/j.carbpol.2018.06.080 (Emami et al., 2018)
25	Self-crosslinking effect of chitosan and gelatin on alginate based hydrogels: Injectable in situ forming scaffolds	Materials Science and Engineering C: Materials for Biological Applications	10.1016/j.msec.2018.04.018 (Naghizadeh et al., 2018)
26	Synthesis and evaluation of antifungal activities of sodium alginate-amphotericin B conjugates	International Journal of Biological Macromolecules	10.1016/j.ijbiomac.2017.11.030 (Ravichandran and Jayakrishnan, 2018)
27	Oxidized Alginate-Gelatin Hydrogel: A Favorable Matrix for Growth and Osteogenic Differentiation of Adipose-Derived Stem Cells in 3D	ACS Biomaterials Science & Engineering	10.1021/acsbiomaterials.7b00188 (Sarker et al., 2017)

28	Biofabrication of a co-culture system in an osteoid-like hydrogel matrix	Biofabrication	10.1088/1758-5090/aa64ec (Zehnder et al., 2017)
29	Covalently antibacterial alginate-chitosan hydrogel dressing integrated gelatin microspheres containing tetracycline hydrochloride for wound healing	Materials Science and Engineering C: Materials for Biological Applications	10.1016/j.msec.2016.08.086 (Chen et al., 2017)
30	Designing Porous Bone Tissue Engineering Scaffolds with Enhanced Mechanical Properties from Composite Hydrogels Composed of Modified Alginate, Gelatin, and Bioactive Glass	ACS Biomaterials Science & Engineering	10.1021/acsbiomaterials.6b00470 (Sarker et al., 2016)
31	Augmenting in vitro osteogenesis of a glycine-arginine-glycine-aspartic-conjugated oxidized alginate-gelatin-biphasic calcium phosphate hydrogel composite and in vivo bone biogenesis through stem cell delivery	Journal of Biomaterials Applications	10.1177/0885328216667633 (Linh et al., 2016)
32	Electrospun Gelatin Fibers with a Multiple Release of Antibiotics Accelerate Dermal Regeneration in Infected Deep Burns	Macromolecular Bioscience	10.1002/mabi.201600108 (Chen et al., 2016)
33	Design, fabrication and characterization of oxidized alginate-gelatin hydrogels for muscle tissue engineering applications	Journal of Biomaterials Applications	10.1177/0885328216634057 (Baniasadi et al., 2016)

2.16. Effect of Platelet-rich plasma in meniscal repair

Platelet-rich plasma (PRP), an increased concentration of autologous platelets suspended in a small amount of plasma is obtained after centrifugation of blood. PRP plays a major role in haemostasis and is a natural source of various growth factors. The growth factors present in PRP include platelet-derived growth factor (PDGF), transforming growth factor β (TGF-β), vascular endothelial growth factor (VEGF), epidermal growth factor (EGF), insulin-like growth factor (IGF) and fibroblast growth factor (FGF) (Pavlovic et al., 2016). Literature reveals that the growth factors in PRP can stimulate angiogenesis and increase fibroblast cell differentiation when used for soft tissue healing (Petrungaro, 2001). It has

also been reported that PRP reduces scar tissue formation due to its ability to accelerate wound maturity and epithelialization (Wang and Avila, 2007).

The use of PRP in the anterior cruciate ligament (ACL) reconstruction and meniscal repair is a growing area of interest. (Kwak et al., 2017) reported the use of poly-lactic-co-glycolic acid (PLGA) mesh scaffold pre-treated with PRP seeded with human chondrocyte to enhance the healing capacity of the meniscus *in vivo*. The cell-seeded mesh scaffold was placed between two meniscal discs and implanted subcutaneously in nude mice for 6 weeks. Results showed that articular chondrocytes on PRP pre-treated PLGA mesh scaffolds migrated to the interface of the meniscal discs. There was also an increase in cell attachment and healing capacity of the meniscus in a meniscal repair mouse model. (Liu et al., 2019) used a heterocyclic compound Kartogenin (KGN) along with PRP and bone marrow-derived stem cells (BMSCs) to treat meniscal defects in a rabbit model. Results showed that meniscal defects treated with PRP gel seeded BMSCs healed much faster than the wounds treated without BMSCs. Histology evaluation after 3 months showed that the meniscus healed well and there was fibrocartilage-like tissue.

2.17. Lacune in the current scenario and rationale of the present study

Meniscal injury is one of the major injuries in the knee joint. Many sports activities that require sudden stops and turn like football, tennis, basketball, etc. pose a high risk of meniscal injury. In addition to sports activities, people who are involved in laborious occupations are also prone to meniscal injury. Currently, meniscectomy, either partial or total, is the only remedy available to address this. The major drawbacks of this procedure are the high cost of surgery and the development of arthritis as a long-term consequence.

Currently, there are several limitations to the development of an appropriate scaffold for meniscal repair. The main problem is the requirement of an invasive surgery, which involves the risk of infection. Another problem is to shape the material to fit the defect site. Poor-fitting of the scaffold in the defect site will result in dead space leading to fluid accumulation and inflammation. It will also affect the stability of the implant. To address these issues new injectable scaffolds have been developed. This approach is based on the injection of a monomer or polymer that can form into a gel at the site of implantation in response to stimuli. This has the advantage of delivering molecules into small surgical incisions and it helps in the proper integration of scaffolds with the surrounding tissues.

The two products that are currently available in the market are Collagen Meniscal Implant (Menaflex®) and Polyurethane/PCL mixture (Actifit) which are used as a partial meniscal substitute. Menaflex® is a bioresorbable collagen matrix designed to serve as a template for the in-growth of new meniscal tissue. In 2008, Menaflex® got approval from the Food and Drug Administration (FDA). But in the year 2010 FDA cancelled its clearance given for Menaflex.

The current treatment procedures available in India are meniscectomy, either partial or total and suturing of the meniscal tear depending on the tear location, age of the patient and type of tear. Literature shows that meniscal tears in the inner-third avascular area with limited healing potential should be resected (Gwathmey et al., 2012). The limited healing in the central area is due to the lack of blood vessels. Application of load on the meniscus after surgery during sporting activity will lead to re-tear of the meniscus. So, an injectable PRP incorporated hydrogel will be a good choice for the tear at the avascular zone because

of the ability of the hydrogel to deliver growth factors at the site of injury thereby recruiting cells to the injured site and promoting healing without scar tissue formation.

The present work aims to develop biopolymer based in situ forming hydrogel, which gels rapidly on injecting into the meniscal tear. The objectives of the work are listed below:

Objectives

- To develop a suitable alginate dialdehyde-gelatin hydrogel (ADA-Gel) for meniscal repair.
- To characterize the ADA-Gel (Physicochemical, mechanical, gelation behavior, etc).
- To evaluate cell-ADA-Gel interactions *in vitro.*
- To evaluate ADA-Gel as a meniscal substitute in a rabbit model *in vivo.*

A matrix derived from both alginate and gelatin (G) is expected to have useful properties of both polymers. Alginate was oxidized to Alginate dialdehyde (ADA) to improve its biodegradation and solubility. Literature reports the use of injectable ADA/Gelatin hydrogel for cartilage tissue engineering (Balakrishnan et al., 2014a). To date, no studies or reports are available on the use of injectable ADAG for meniscal tear.

For an in situ forming hydrogel, the gelation time should be optimal, ideally within 5 min so that once applied, the hydrogel will stay at the site and does not migrate or dissolve. We used small concentrations of sodium tetraborate (borax) for facilitating rapid gelation between ADA and gelatin. Borax can form a tetraborate complex with hydroxyl groups of polysaccharides so that it can accelerate the gelation process significantly leading to the formation of hydrogels within the required gelation time. Borax also has a long history of medicinal use because of its antiseptic and antiviral activity (Sahin et al., 2016).

The incorporation of Platelet-rich plasma (PRP) to the ADAG hydrogel will be an added advantage to meniscal repair. A study conducted by (Ishida et al., 2007) showed that the incorporation of PRP in gelatin hydrogels enhances the proliferation of meniscal cells and its Glycosaminoglycan (GAG) synthesis *in vitro*. Considering this observation, we incorporated PRP into ADAG hydrogel (ADAGPRP). The in situ forming ADAG and ADAGPRP hydrogels were characterized extensively. The gelation time was determined with respect to the change in concentration of ADA, G and borax. The crosslinking of ADA, G and PRP were confirmed by FTIR spectroscopy, degree of cross-linking of hydrogels was determined by the trinitrobenzene sulphonic acid method (TNBS), mechanical properties by Universal Testing Machine (UTM), morphology by Scanning Electron Microscopy (SEM) and degradation by % weight loss.

The *in vitro* evaluation of the hydrogels was done using fibrochondrocytes cells isolated from rabbit meniscus. The fibrochondrocytes were characterized and seeded on hydrogels to prove the cytocompatibility of hydrogels. Further, the viability and proliferation of cells were evaluated qualitatively by live dead staining, Rhodamine phalloidin staining and quantitatively by alamar blue assay, collagen estimation, Glycosaminoglycan (GAG) and DNA estimation.

In vivo evaluation of ADAG and ADAGPRP was done in the Rabbit model for a study period of 1 and 3 months.

CHAPTER 3

3. MATERIALS AND METHODS

3.1. Materials

Materials used in the work, their purity and sources are listed in table 3 below:

Table 3. List of chemicals, grade, purity and their sources used in the work

Sl. No.	Name of the material/chemical/reagent	Grade / Purity	Source
1	1,9-Dimethyl-Methylene Blue zinc chloride double salt (DMMB)	Dye content 80 %	Sigma Aldrich, USA
2	2-Propanol	ACS reagent, ≥ 99.5 %	Merck, India
3	Acetic acid	glacial, ACS reagent, ≥ 99.7 %	Merck, India
4	Alamar Blue™	Cell Viability Reagent	Invitrogen, USA
5	Alginic acid sodium salt from brown algae	Medium viscosity	Sigma Aldrich, USA
6	Antibiotic-Antimycotic Solution (100X)	Contains 10,000 units of Penicillin, 10,000 µg of Streptomycin and 25 µg of Amphotericin B in a 0.85 % saline solution. Effective against bacteria, fungi, and yeasts.	Genetix, Cell clone, India
7	Collagen, Type I solution from rat tail	Cell culture tested	Sigma Aldrich, USA
8	Collagenase Type 1 and 11 powder	Cell culture	Gibco, USA
9	Direct red 80	Dye content 25 %	Sigma Aldrich, USA
10	Disodium hydrogen phosphate	Anhydrous for analysis EMSURE® ACS, Reag. Ph Eur	Merck, India
11	DMEM-HG	With high-glucose, L-glutamine and sodium pyruvate, 1000 mL	Genetix, Cell clone, India
12	Ethanol, Absolute	99.9 %	Merck, India

13	Ethylenediaminetetraacetic acid disodium salt dihydrate	Reagent grade, 98.5 - 101.5 % (titration)	Sigma Aldrich, USA
14	Fetal Bovine Serum	South American Origin	Genetix, Cell clone, India
15	Gelatin	Type A, gel strength 300	Gelita, Germany
16	Glycine	ACS reagent, ≥ 98.5 %	Sigma Aldrich, USA
17	Hoechst 33258	10µg/ml solution	Origin Lab, India
18	Hydrochloric acid	ACS reagent, 37 %	Merck
19	Hydroxylamine hydrochloride	Reagent plus 99 %	Sigma Aldrich, USA
20	L-Arginine	Reagent grade, ≥ 98 %	Sigma Aldrich, USA
21	L-Proline	99 %	Alpha Aesar, USA
22	Methyl orange	For microscopy (Hist.), indicator (pH 3.0 - 4.4)	Sigma Aldrich, USA
23	MTT Reagent A	Study of cell and mitochondrial health	Sigma Aldrich, USA
24	Paraformaldehyde	Reagent grade, crystalline	Sigma Aldrich, USA
25	Picrylsulfonic acid solution	5 % (w/v) in H_2O, BioReagent, suitable for the determination of primary amines	Merck, India
26	Potassium carbonate	ACS reagent, ≥ 99.0 %	Merck, India
27	Potassium chloride	For analysis EMSURE®	Merck, India
28	Potassium dihydrogen phosphate	For analysis EMSURE® ISO	Merck, India
29	Potassium iodate	Reagent grade – 98 %	Sigma Aldrich, USA
30	Potassium iodide	Emparta	Merck, India
31	Potassium permanganate	For analysis EMSURE® ACS, Reag. Ph Eur	Merck, India
32	Silver nitrate	ACS reagent, ≥ 99.0 %	Sigma Aldrich, USA
33	Sodium azide	AR, 99 %	Spectrochem
34	Sodium bicarbonate	Emparta; 99.7 - 100.3 %	Merck
35	Sodium carbonate	ACS reagent, anhydrous, ≥ 99.5 %	Sigma Aldrich, USA
36	Sodium chloride	Emsure	Merck, India
37	Sodium hydroxide pellets	Emsure	Merck, India

38	Sodium meta periodate	Emsure	Merck, India
39	Sodium metaborate tetrahydrate (Boric acid)	≥ 99 %	Merck, India
40	Sodium tetraborate decahydrate	ACS reagent, ≥ 99.5 %	Sigma Aldrich, USA
41	Sodium thiosulfate pentahydrate	Emplura	Merck, India
42	Spectra/Por3 Dialysis Membrane	3.5KDA	Spectrochem
43	Starch soluble	Emparta	Merck, India
44	Trypsin - EDTA 0.25 %	Contains 0.05 % Trypsin and 1mM EDTA in Hank's Balanced Salt Solution without calcium and magnesium Sterile filtered Porcine parvovirus and mycoplasma tested.	Genetix, Cell clone, India
45	Water	Single Distilled water	

3.2. Methods

3.2.1. Synthetic methods

3.2.1.1. Synthesis of alginate dialdehyde

For synthesizing alginate dialdehyde (ADA), the procedure reported by Balakrishnan et al. (2005) was adopted. ADA is an oxidation product of sodium alginate (SA) and the oxidation was done with sodium metaperiodate. ADA of different degrees of oxidation was prepared for the study. For this sodium alginate (20 % w/v) was suspended in ethanol and treated with different quantities of sodium meta periodate. Number of millimoles of periodate used for the reaction is given in table 4. The reaction mixture was kept stirring at 100 rpm for 6 h and maintained at 25 ^{o}C under dark so that nonspecific oxidation will be prevented (Balakrishnan and Jayakrishnan, 2005).

Table 4. Weight of alginate and periodate used for ADA synthesis

Weight of alginate (g)	Weight of meta periodate (g)	No. of millimoles of alginate	No. of millimoles of periodate
20	6.4	101	32.9
20	10.7	101	50
20	12.9	101	61
20	15.9	101	75.1

At the end of the reaction, the reaction mixture was transferred (about 50 mL each) into dialysis bags (about 40 cm long) and suspended in distilled water, taken in a tray, for dialysis. The water in the tray was replaced with fresh distilled water thrice a day for 3 days. Complete removal of periodate from the dialysate was ensured by checking the medium with an aqueous solution of 1 % silver nitrate. Dialysis was continued till no turbidity or precipitate was obtained with silver nitrate solution. The dialysate was then frozen (-40 ^{0}C), lyophilized (-82 ^{0}C) and stored at -20 °C until use. The yield of ADA obtained was calculated using the following equation:

$$\text{Yield of ADA (\%)} = \left(\frac{\text{Weight of ADA obtained after periodate oxidation}}{\text{Weight of SA taken for the reaction}}\right) \text{x } 100$$

ADA was characterized by ^{1}H Nuclear Magnetic Resonance (NMR) spectroscopy and Raman spectroscopy. It was also analyzed for its degree of oxidation, dialdehyde content and molecular weight.

3.2.1.2. Preparation of hydrogels

Injectable compositions of hydrogels were prepared by reacting ADA (degree of oxidation = 45.4 %) and gelatin (G) in the presence of borax as the catalyst. Different formulations of ADAG hydrogels were prepared by varying the concentrations and ratios of ADA,

gelatin and borax. The formulations prepared, their identification code and their compositions are listed in table 5.

Table 5. Compositions of ADAG hydrogels prepared.

Sl.No.	Formulation Code	Conc. of ADA (w/v) %	Conc. of Gelatin (w/v) %
1	15ADA15G	15	15
2	15ADA20G	15	20
3	20ADA15G	20	15

For preparing hydrogel, at first, ADA was dissolved in the borax solution. Borax of different concentrations (0.025, 0.05, 0.075 and 0.1M) was prepared in distilled water initially. Gelatin solutions were prepared in distilled water (15 and 20 %) at 40ºC. Equal volumes of both solutions of ADA and gelatin were taken in one syringe, mixed thoroughly and injected using an 18 G needle into the saline solution to study the gelation time. Saline was used for mimicking the environment of the knee during arthroscopic joint surgery.

In order to study the properties of hydrogel such as water uptake, degree of crosslinking and compressive strength the gelable composition was injected into a mold of desired dimensions and allowed to gel. The hydrogel thus formed was either dried or lyophilized depending on the studies to be performed. The molded hydrogel was also used for scanning electron microscopy (SEM) and micro-computed tomography (Micro-CT) studies.

Platelet rich plasma (PRP) incorporated hydrogels (ADAGPRP) were also used for the study. The PRP required for the study was isolated from rabbit blood. Whole blood from the rabbit ear vein was drawn directly using a syringe containing a 3.8% citrate solution (0.750 mL for 5 mL of blood). It was centrifuged at 750 g for 5 min at room temperature. After the first centrifugation, the PRP was carefully removed with a pipette inserted above

the buffy coat and transferred to a new, sterile vial. ADAGPRP hydrogels were prepared by mixing equal volumes of ADA solution (15 (w/v) %; dissolved in 0.05 M borax) and Gelatin (20 (w/v) % dissolved in distilled water) solution. Different volumes of PRP (100, 300, 500, 700 and 900 µl) were added to prepare the ADAGPRP hydrogels. PRP was first mixed with ADA thoroughly and to this gelatin was added to obtain the hydrogel. The formulation code and composition of hydrogels prepared are given in table 6.

Table 6. Composition of ADAGPRP hydrogels

Sl. No.	Formulation Code	Conc. of ADA (w/v%)	Conc. of Gelatin (w/v%)	Conc. of Borax (M)	Volume of PRP (µl)
1	15ADA20G100PRP	15	20	0.05	100
2	15ADA20G300PRP	15	20	0.05	300
3	15ADA20G500PRP	15	20	0.05	500
4	15ADA20G700PRP	15	20	0.05	700
5	15ADA20G900PRP	15	20	0.05	900

Since the hydrogel is expected to be bioresorbable, in vitro degradation studies of hydrogels were also carried out. In the clinical conditions hydrogel will be injected into the saline irrigated wound, so degradation studies of the hydrogels were planned to do in saline. Two compositions, namely, 15ADA20G and 15ADA20G300PRP, were selected for degradation studies. The time periods chosen for the degradation studies were 1, 5, 7, 14, 21 and 28 days. The hydrogel was injected into saline solution (5mL) and was allowed to form a gel (4 min). Afterward, the saline was removed and added 5 mL phosphate buffered saline (PBS) with sodium azide and kept at 37 ^{o}C in an incubator under shaking. After each time period, PBS was removed and the hydrogel was lyophilized. Both the extract and hydrogel were used for further analysis.

3.2.2. Material characterization techniques

3.2.2.1. Spectroscopic analysis

3.2.2.2. UV-Visible spectroscopy

UV-Visible spectroscopic analysis of materials was done using a NanoDrop™ 2000 spectrophotometer (M/s. Thermo Scientific, USA). ADA, Gelatin, ADAG hydrogel and the extract obtained after degradation of hydrogels was used for UV spectroscopic analysis. Spectra were recorded in the range of 200 to 400 nm.

3.2.2.3. Fourier Transform Infrared (FTIR) Spectroscopy

Sodium alginate (SA), Gelatin (G), hydrogels and extract collected after in vitro degradation were characterized by FTIR spectroscopy using the attenuated total internal reflection (ATR) method. The spectra were measured in the wavenumber regions 4000 to 400 cm^{-1} using a Nicolet 5700 spectrometer (Thermo Fisher Scientific, USA) coupled with Diamond ATR, which consists of a diamond disc as an internal reflection element. The spectrum of the dry diamond ATR crystal in the ambient atmosphere (air, 22 °C) was used as the background. Spectra were recorded at a spectral resolution of 0.4 cm^{-1} and 32 scans were performed for each measurement. All samples were analyzed in their dry form.

3.2.2.3.1. ^{1}H Nuclear Magnetic Resonance (NMR) spectroscopy

^{1}H NMR spectroscopy was used to assess the chemical structure of SA and ADA. About 10 mg mL^{-1} of ADA was dissolved in D_2O at a temperature of 50 °C. ^{1}H NMR spectra were recorded with a Bruker AMX 500 spectrometer.

3.2.2.3.2. Raman spectroscopy

The Raman spectra of SA, ADA, and hydrogels were recorded using a Confocal Raman Microscope (alpha 300RA, Witec, Germany) with a 532 nm laser.

3.2.2.4. Chemical analysis

3.2.2.4.1. Determination of degree of oxidation

The extent of oxidation of sodium alginate was estimated by iodometric titration of the residual periodate present in the reaction mixture using the modified Muller Friedberger method (Balakrishnan et al., 2005). Briefly, 5mL aliquot of the reaction mixture (taken before dialysis) was neutralized with 10 mL of 10 % sodium bicarbonate solution and iodine was liberated by the addition of 20 % potassium iodide solution (2 mL). This was kept under dark for 15 min. The amount of excess periodate in the reaction mixture was estimated by titrating liberated iodine against standard sodium thiosulphate solution using starch as an indicator. All experiments were done in triplicate. The detailed procedure was given in the annexure.

3.2.2.4.2. Determination of aldehyde content

Aldehyde content of ADA, hydrogels and extracts collected after degradation studies was estimated by means of hydroxylamine hydrochloride method. The hydrogels and extract collected after degradation were lyophilized before analysis. For this, 0.05 g of sample was mixed with 0.25 N hydroxylamine hydrochloride-methyl orange solution. The solution was allowed to stand at room temperature for 2 h and was then titrated against standard sodium hydroxide solution until the pH of the solution reached 4. Values reported are the average of a minimum of three estimations. The detailed procedure was given in the annexure.

3.2.2.4.3. Determination of molecular weight

Dilute solution viscometry was used for determining the molecular weights (Mw) of SA and ADA. For this purpose, a micro viscometer (Lovis 2000 M, Anton Par, USA) was employed. About 5 mL of 0.1 M NaCl solution was used as blank. 1% solution of SA was prepared in 0.1M NaCl. Density of the sample was measured by weighing 1 mL solution in a weighing balance and by using the following equation:

$$\textbf{Density} = \textbf{Mass/Volume}$$

Mw of the polymers was determined using the Mark-Houwink (M-H) equation (Masuelli, 2014):

$$\ln[\eta] = \ln k + a \ln Mw,$$

Where 'k' and 'a' are the (M-H) constants. The 'k' and 'a' values reported for SA were 0.0073 cm^3/g and 0.920, respectively, and for ADA they were 0.0051 cm^3/g and 1, respectively (Masuelli and Illanes, 2014). The intrinsic viscosity [η] data was obtained from the micro viscometer.

3.2.2.5. Gelation time

Gelation time or the time taken for gelation was assessed using a tube inversion method reported elsewhere (Huynh et al., 2018). For this, 2 mL each of ADA and gelatin solutions were mixed together and injected into a test tube. The tubes were then incubated at room temperature. The sol-gel transition time was determined by inverting the tube horizontally every minute. The time from mixing till the content stopped flowing was recorded as the gelation time.

3.2.2.6. Trinitrobenzene sulfonic acid (TNBS) assay

2,4,6-Trinitrobenzene sulfonic acid (TNBS) / Picryl sulfonic acid solution assay was used for estimating the degree of crosslinking of hydrogels (Fields, 1972). It was also used for estimating the amino group contents in the hydrogels as well as in the extract obtained after degradation studies. Briefly, 0.1% TNBS was prepared in 100 mM sodium borate buffer (0.476 g of boric acid and 0.254 g of borax in 100 mL distilled water). pH was adjusted to 9 with 1N NaOH. A standard curve was plotted with Glycine (Stock concentration: 20 µg/mL). Concentrations of glycine used: 10, 5, 2.5, 1.25, 0.62, 0.32, 0.15, 0.07, 0.03, 0.0125 µg/mL. 500 µl of TNBS was added to each sample. Incubated for 30 min at room temperature. Optical absorbance was recorded with a UV spectrophotometer at 420 nm (Shimadzu, Japan). The degree of crosslinking was determined using the equation below:

$$\text{Degree of crosslinking } (\%) = [(NH_2)_{NC} - (NH_2)_C] / (NH_2)_{NC})] * 100$$

Where $(NH_2)_{NC}$ is the mole fraction of the free amino group in gelatin and $(NH_2)_C$ is the mole fraction in the hydrogel after crosslinking.

The amino content in hydrogel and extract after degradation was calculated from the equation obtained from the glycine standard curve as given below.

$$Y = 0.1094X - 0.0013$$

Where Y is the absorbance obtained from the experiment and X is the amount of amino content.

3.2.2.7. Water uptake

For determining the water uptake of hydrogels, ADAG hydrogel samples (70 mm x 15 mm x 2 mm) were immersed in PBS at 37 ^{0}C for 24 h. After 24 h, samples were removed from

PBS and the weight of the swollen samples was recorded (Ws). Samples were then lyophilized and weighed again to determine the dry weight of the polymer (Wo).

$$\text{Water uptake } (\%) = [(\text{Ws} - \text{Wo})/\text{Wo}] * 100$$

3.2.2.8. Compressive strength

The compressive strength of hydrogels was determined at 22 ^{o}C using a Universal Testing Machine (Instron 3365, UK) fitted with a 100 N load cell. Hydrogel samples (10 mm dia x 10 mm height) were prepared as described in section 3.2.1.2 and preconditioned by keeping for 1 h in the test temperature (24 ºC) before testing. A crosshead speed of 1mm/min was maintained during testing. Six specimens were tested and the mean and standard deviation were determined.

3.2.2.9. Surface morphology and 3D microarchitecture

Hydrogel samples having dimensions described in section 3.2.2.8 were used for surface topography and porosity analysis. Lyophilized samples of hydrogels were used for analysis. The surface morphology of the ADAG hydrogel samples was studied using an environmental scanning electron microscope (ESEM) (Hitachi S2400, Japan). The features of the surface and cross-section of the dried samples were recorded after placing the samples on an aluminum stub under vacuum.

The porosity measurements of lyophilized hydrogels were evaluated using micro-computed tomography (micro-CT) (mCT-40, Scanco Medical, Switzerland). The samples were placed in the sample holder (PMMA tube) for detecting the X-ray attenuation and scanning was performed with 45kV X-ray energy, 177 µA intensity and 10 µm resolution (2D slice thickness). Two-dimensional reconstructions were done using the Cone-beam

algorithm. Region of interest in the 2D slices was contoured and 3D evaluation was performed by setting the appropriate threshold value of X-ray attenuation to an actual 3D image of the sample.

3.2.3. *In vitro* biological evaluation

3.2.3.1. Isolation of fibrochondrocytes

Fibrochondrocytes for the study were isolated from New Zealand White (NZW) rabbits. Rabbits were obtained from the Division of laboratory animal science, BMT Wing, SCTIMST, Trivandrum and the experiments were performed there itself in compliance with the relevant laws and guidelines of the institutional animal ethical committee (Approval No. SCT/IAEC 128/2014/85). Meniscal tissues were collected from the rabbit knee joint and were stored in 25 mL of PBS containing 2X antibiotics. After that, the tissues were washed 2 times in PBS containing 2X and 1X antibiotics, respectively. The tissues were minced well and added double volume of collagenase type 1. The tissue was kept for digestion in a shaking water bath for 12-14 h at 37 ^{0}C. The solution was filtered using a 0.2-micron membrane filter into a fresh tube and collagenase reaction was stopped by adding an equal volume of complete medium (DMEM with 10% Fetal Bovine Serum (FBS) and 1% Antibiotics). The mixture was then centrifuged at 2500 rpm for 10 min. The supernatant was discarded and the pellet was resuspended in the medium. Thereafter the pellet was seeded in a 25 cm^2 flask and kept in a humidified incubator (5 % CO_2, 95 % air) at 37 °C. On day 3, after initial plating, the cells were washed twice with PBS to remove the non-adherent cells. When the culture got 80 % confluence, it was trypsinized and sub-

cultured on to new flask (P1 passage). The cells in this passage were used for further *in vitro* cytocompatibility evaluation.

3.2.3.2. Cytocompatibility evaluation

In vitro cytocompatibility evaluation was performed for hydrogel formulations 15ADA20G and 15ADA20G300PRP.

3.2.3.2.1. Direct contact assay

Rabbit meniscal fibrochondrocytes (10,000 cells/well) were seeded onto tissue culture-treated polystyrene surfaces and allowed to form a complete monolayer. Circular shaped hydrogel discs (8 mm dia & 1 mm thickness) was placed on top of the cell monolayer and fed with a complete medium. Efforts were taken to avoid the floating of the hydrogel. The medium was replenished on every alternative day. After 48 h of culture, cell monolayer integrity was observed through phase-contrast microscopy (Olympus, USA).

3.2.3.2.2. LIVE/DEAD cell viability imaging

Hydrogel for the LIVE/DEAD assay was prepared by adding 1 mL of ADAG solution onto a glass coverslip and kept at 37 ^{0}C until gelation. Fibrochondrocytes (1 x 10^{6} cells/coverslip) were seeded on the coverslip containing gel. Cells were allowed to proliferate for 48 h in both cell-alone control and cell-seeded hydrogel. After 48 h of culture, media was removed and hydrogel was washed with sterile PBS, stained with LIVE/DEAD viability kit (Origin, India) and observed under a fluorescent microscope (Olympus DM6000). Experiments were done in triplicate.

3.2.3.2.3. Cell attachment and proliferation

3.2.3.2.3.1. Qualitative evaluation

It is important to observe the morphology of cells that are formed through proliferation and migration (Debnath et al., 2015). Cellular actin (red) was stained by rhodamine or fluorescein-labeled phalloidin and nuclei (blue) with Hoechst. The cell seeding was done as described in section 3.2.3.2.2. After 48 h the cell control and cell seeded on hydrogel were fixed with 4 % paraformaldehyde in PBS, washed with PBS and permeabilized with 0.1 % Triton X-100 (Sigma Aldrich) for 5 min. The cells were again washed with PBS for 3 times and Rhodamine phalloidin stain was added at a concentration of 1:1000 in PBS. This was kept in dark for 30 min. After one more washing in PBS, Hoesct (1:500) was added and incubated for 5 min. The cells were then washed thoroughly with PBS and observed under a fluorescent microscope (Leica, DM6000). The morphology of the formaldehyde-fixed cell seeded hydrogels was also observed using an ESEM.

3.2.3.2.3.2. Quantitative evaluation: Alamar Blue assay

The Alamar Blue® assay was performed to evaluate the metabolic activity of fibrochondrocytes. Alamar blue measures the reducing environment of the living cell. The active component is water soluble resazurin. Actively proliferating cells will chemically reduce alamar blue dye from non-fluorescent blue to fluorescent red (Rampersad, 2012). Fibrochondrocytes were seeded (10^6 cells/well) onto the surface of the hydrogel (8mm dia. x 1mm thick). After each time period cells were washed with PBS at 37 °C. 10 % Alamar Blue® in DMEM media was added to the wells containing hydrogel constructs to assess the cell metabolic activity after 2, 4 and 6 days.

3.2.3.2.4. Immunofluorescence staining – Collagen type I

Cells were seeded for 2, 4 and 6 days as described in section 3.2.3.2.2. After each time period, the coverslip was taken, washed with PBS and fixed in 4 % paraformaldehyde for 20 min. After that, the coverslips were washed with PBS 3 times and blocked with 1% Bovine Serum Albumin (BSA) for 1 hr. It was washed thoroughly with PBS 2-3 times. Coverslips were incubated with primary collagen I antibody (1:100 dilution) for 1 hr. Coverslips were then washed with PBS and incubated with secondary antibody for 30 min. The nucleus was then stained with Hoechst (1:500 dilution) and fluorescent images were taken using a Leica DM6000 microscope.

3.2.3.3. Biochemical analysis of fibrochondrocytes seeded on hydrogel

Hydrogels were seeded with fibrochondrocytes (1×10^6 cells/8 mm hydrogel). After each time period (3, 7 and 14 days), the cell-seeded hydrogel was digested with papain for 24h. After removing the culture media 0.5 ml of papain solution (composition of papain solution was given in the annexure) was added and the cells and hydrogel were properly crushed with a micropipette tip. This was transferred to 1.5 ml vials. Again 0.5 ml of papain was added and again scraped to remove the remaining cells and hydrogels from the well plate. This digest was kept at a 65 ^{0}C water bath for 2 h to ensure complete digestion of cells and hydrogel**.** DNA, Collagen and Glycosaminoglycan (GAG) content of fibrochondrocytes seeded on the hydrogel were evaluated after papain digestion of cell hydrogel construct. For DNA estimation the papain digest was used directly. For GAG and collagen estimation, the papain digest was centrifuged at 12000 rpm for 10 min. The supernatant was removed without disturbing the pellet.

3.2.3.3.1. DNA quantification

From the papain digest, 250 µL was taken and mixed with 150 µL of 100% Isopropyl alcohol (IPA) (ice cold by placing in an ice-water bath or freezer). The solution was then kept at -20 ^{0}C for 30 min and centrifuged at 12,000 rpm for 20 min. The supernatant solution was discarded and the pellet obtained was kept for drying at 60 ^{0}C. The dried pellet was dissolved in 50 - 100 µL of distilled water and the absorbance was taken at 260/280 nm using Nanodrop 2000C.

3.2.3.3.2. Estimation of Glycosaminoglycan

Proteoglycan content in the cell-seeded hydrogel after 3, 7 & 14 days was estimated by dimethyl methylene blue dye binding (DMMB) assay using chondroitin 4-sulfate as standard (Xiao et al., 2017). About 50µl supernatant from papain digest was mixed with 200 µl of 1 X DMMB dye and the absorbance was measured at 525 nm.

3.2.3.3.3. Total collagen content

Sirius Red Assay was done to estimate the collagen synthesis in fibrochondrocytes after being seeded on 15ADA20G and 15ADA20G300PRP hydrogel (Keira et al., 2004). Papain digest was mixed with picric acid saturated Sirius red to measure the total collagen content. 100 µl of the supernatant of papain digest, was mixed with 900µl of picric acid saturated Sirius red and incubated for 30 min at room temperature. This was then centrifuged at 14,000 rpm for 10 min and the supernatant was collected without disturbing the pellet. The tubes were blotted on tissue paper to remove unbound dye. The pellet was resuspended in 500 µl of 0.5N NaOH, and vortexed gently for 2 min to ensure complete dissolution of pellet. From this 100 µl sample was added to 96 well plates and absorbance was taken at

550nm. A standard curve prepared from Type I rat tail collagen was used to calculate the collagen content in each set of experiments.

3.2.3.4. Gene expression studies

Total RNA was isolated using an RNA isolation kit by following the manufacturer's instructions. The RNA was quantified using Nanodrop 2000C Spectrophotometer. cDNA was synthesized by reverse transcriptase PCR in a thermal cycler. The cDNA was amplified by using the Roche light cycler Real-Time PCR system using the KAPA SYBR Fast qPCR master mix. All reactions were performed in triplicates and data was analyzed according to the $\Delta\Delta C_t$ method. Amplification was performed using specific primer sequences as shown in table 7.

Table 7. Primer sequence for qPCR analysis

Oligo name	**Forward/reverse sequence (5' ->3')**
GAPDH	ATCCATTCATTGACCTCCACTAC
	GTACTGGGCACCAGCATCAC
COLLAGEN-1	GATGCGTTCCAGTTCGAGTA
	GGTCTTCCGGTGGTCTTGTA
COLLAGEN-2	CCTGTGCGACGACATAATCTGT
	GGTCCTTTAGGTCCTACGATATCCT
AGGRECAN	GCTACGGAGACAAGGATGAGTTC
	CGTAAAAGACCTCACCCTCCAT

The fold change was expressed graphically and data were represented as mean±SD. The various steps involved in RNA isolation, cDNA synthesis, the time taken and the temperature of each step is given in the annexure.

3.2.3.5. *Ex-vivo* evaluation

In order to check how the hydrogel integrates with host meniscal tissue, an ex-vivo study was performed. For these medial menisci of a pig (autopsied as part of another experiment)

was collected and a longitudinal tear (about 2 cm long) was made in it using a #11 scalpel blade. 15ADA20G300PRP hydrogel was prepared, injected into the meniscal tear and allowed to gel there (Figure 24). The middle portion of the meniscus along with the gel was taken and cultured for 3 days in culture medium at 37 °C and 5 % CO_2. The meniscal tissue with hydrogel was then fixed in formalin and viewed under SEM after critical point drying and gold coating. Formalin-fixed meniscal tissue was also embedded in paraffin to prepare blocks for microtomy and after taking sections they were stained with Hematoxylin and Eosin (H&E).

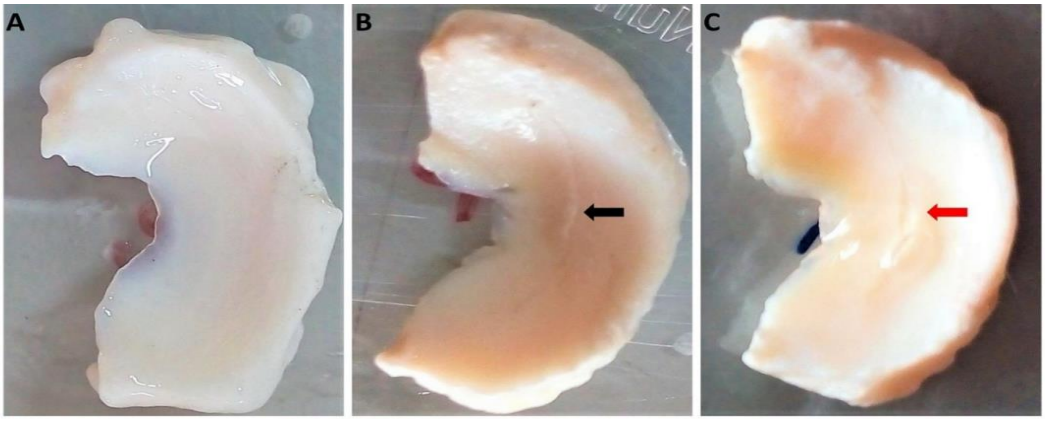

Figure 24. Macroscopic observation of meniscus: A) Control; B) Meniscal tear model (Black arrow shows the tear); C) Tear filled with hydrogel (Red arrow).

3.2.4. *In vivo* biological evaluation

In order to demonstrate the working of the injectable hydrogel system and to establish its functional safety *in vivo*, rabbit model was chosen. Rabbits' meniscus was exposed surgically and a tear was introduced by incision. A gelable hydrogel composition was injected and studied the healing behavior. Implantation studies were performed following the guidelines and recommendations of the Committee for the Purpose of Control and Supervision of Experiments on Animals, India (CPCSEA) and with the approval of the

Institutional Animal Ethics Committee (IAEC), Approval No. SCT/IAEC-128/2014/85. Further details are given in the subsequent sections.

3.2.4.1. Preparation of 15ADA20G and 15ADA20G300PRP hydrogel for implantation

Fresh solutions of ADA (15 w/v. %) and gelatin (20 w/v. %) were prepared and sterilized by UV before implantation. PRP was prepared from the blood of the same animal selected for hydrogel implantation. Gelatin solution was kept at 40 ^{o}C to prevent physical gel formation. At the time of implantation, ADA, PRP and gelatin solutions were taken in a syringe, mixed thoroughly and injected into the meniscus.

3.2.4.2. Surgical procedure

With the rabbit in the supine position, each animal was anesthetized with an intramuscular injection of ketamine (50 mg/kg) and xylazine (5 mg/kg). The hind limbs were shaved and disinfected with a povidone-iodine solution. Following aseptic precautions, a medial parapatellar incision and arthrotomy were performed. The patella was dislocated laterally and the knee was placed in full flexion (Figure 25 A). The fat was removed to make the medial meniscus visible (Figure 25 B black arrow). A radial incision was made on the right medial and lateral menisci (Figure 25 C red arrow). Hydrogel forming composition was injected into the radial tear of both the medial and lateral menisci and the wound was closed after 3-4 min time (Figure 25 D & E). Details of animals and material used for the study were given in table 8.

Table 8. Experimental groups and details of animals used in the study.

Groups	No. of animals for 1 month	No. of animals for 3 months	Gender	Age (Yrs)	Weight (Kg)
Control	3	3	M/F	1-2	2-3
15ADA20G	3	3			
15ADA20G300PRP	3	3			
Total no. of animals	**9**	**9**		**18**	

The skin was closed with 3-0 braided silk sutures (Figure 25 F). Betadine ointment was applied twice daily over the surgical wound site until the wound was healed. The effect of healing with the implanted material was evaluated by sacrificing the animal at 1 and 3 months. Post-operatively animals were put under antibiotic and analgesic coverage for 5 days. Management of postoperative animal care and husbandry was under the supervision of a veterinarian.

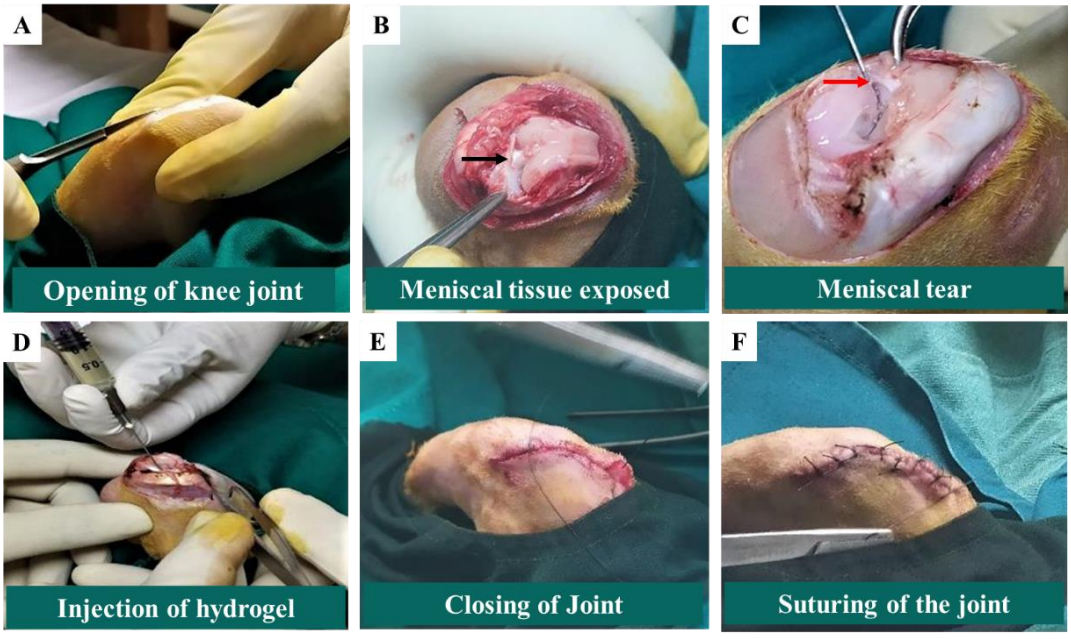

Figure 25. *In vivo* surgical procedure for meniscal tear in rabbit and hydrogel injection.

3.2.4.3. Post-implantation assessment

3.2.4.3.1. Rabbit gait and behavior

Post-surgical behavior and movements of the rabbits inside the cage were monitored for all groups. The gross appearance and integration of the repaired meniscal tissue were assessed by the correct anatomical location of the tissues.

3.2.4.3.2. Histopathological Analysis

Control and test menisci were collected in 10 % Neutral Buffered Formalin and were grossed. Tissues were dehydrated in isopropyl alcohol in ascending grades of dilution, cleared in chloroform and impregnated in paraffin wax. This processing was done using the Automatic Tissue Processor (LEICA TP 1020).

The reagents and time required for processing the tissue sections were given below.

Reagents	**Time**
10% neutral buffered formalin----------	10 min
80% alcohol----------	2 h
95% alcohol I----------	2 h
95% alcohol II----------	2 h
100% alcohol I----------	2 h
100% alcohol II----------	1 h
100% alcohol III----------	1 h
100% chloroform I----------	1 h
100% chloroform II----------	1 h
100% chloroform III----------	2 h
Paraffin wax I----------	2 h
Paraffin wax II----------	2 h

3.2.4.3.3. Embedding

Processed tissues were embedded into paraffin blocks using the Paraffin Embedder (LEICA EG 1160). Tissue samples were removed from the cassettes with warmed pointed forceps. The meniscus was oriented and placed in a mold filled with warm paraffin, in such a way that the cutting surface would cover the implant area with the surrounding tissue. The embedding ring was filled with warm paraffin and the entire mold was placed along with the ring on a cold plate. Once the wax had cooled, the blocks with the embedding ring were removed from the mold and stored till sectioning.

3.2.4.3.4. Sectioning

The sides of the blocks were trimmed and shaped using a wax cutter. Blocks were sectioned using the Automatic Microtome (LEICA RM 2155). The paraffin blocks were initially trimmed till the tissue surface was completely exposed. The exposed surface of the block was cooled with ice cubes and 10µm thick sections were cut. To help expand the tissue sections, they were floated onto the water in a flotation bath (LABINDIA HISTOBATH HI-1210). Sections were picked up onto coated glass slides (Star Frost®).

3.2.4.3.5. Deparaffinization and re-hydration of tissue slide

Tissue slides were deparaffinized and rehydrated as given below

Reagents	**Time (min)**
Xylene I----------	6
Xylene II----------	6
Xylene III----------	6
100 % Isopropyl alcohol (IPA)----------	3
100 % Isopropyl alcohol (IPA)----------	3
80 % Isopropyl alcohol (IPA)----------	3
70 % Isopropyl alcohol (IPA)----------	3

Running tap water---------- 5

3.2.4.3.6. Staining

After deparaffinizing in xylene, rehydrating in descending grades of IPA, the slides were stained with Harri's Haematoxylin and Eosin using an Automatic Stainer (LEICA AUTOSTAINER XL), Safranin O, Alcian blue and Masson's Trichrome (Please see annexure for detailed procedure). After staining, slides were air-dried and mounted with Cytoseal TM 60 (Electron Microscopic Sciences, USA) and coverslipped. Histological analysis of the sections was performed via light microscopy using a trinocular microscope (Nikon Eclipse Model E600, Japan) and images were captured using a digital camera (Nikon model DXM1200F, Japan) with ACT-1 software.

3.2.4.4. Biochemical evaluation

Meniscal tissue collected after explantation from control and test animals was evaluated for its GAG and collagen content. Collected tissues were minced properly and digested in papain solution at 65 ºC overnight. Estimation of GAG and collagen were done as per the procedures given in sections 3.2.3.3.1 and 3.2.3.3.2.

3.2.4.5. Histological scoring of meniscus

To compare the macroscopical, histological, and immunohistochemical results after repair of the meniscal tear, a validated meniscus scoring system was used, which was developed and published for the evaluation of meniscal tear (Angele et al., 2014; Zellner et al., 2013). Scoring parameters for the macroscopical evaluation were stability and defect filling with repair tissue. For histological assessment, the quality of the surface area, the integration of the repair tissue in the native meniscus, cellularity, cell morphology and the content of

proteoglycan were analyzed. The repair was graded by summing up the scores from 0 to 3 of 7 individual subgroups. Consequently, the final scores were between 0 points (no repair) and maximal 21 points (complete reconstitution of the meniscus) (Table 9). The data was collected from 2 blinded scorers, both experienced in the knee anatomy of rabbits and histological assessment.

Table 9. Scoring system for the evaluation of the quality of meniscal repair tissue

	0	**1**	**2**	**3**
Defect filling	No fill	< 25%	25-75%	> 75%
Surface	No surface	Ruptured	Fissured/fibrillated	Meniscus like
Integration	No integration	Partial, unilateral integration	Bilateral partial or unilateral complete integration	Bilateral complete integration
Cellularity	No cells	>10 cell clusters/slide	No cell cluster/slide, cell-ECM-ratio >0.5	Meniscus-like cell-ECM-ratio
Cell morphology	No cells	< 25% meniscus like cells	25–75% meniscus like cells	> cells 75% meniscus-like cells
Content of proteoglycan	No staining for proteoglycan	< 25%	25-75%	> 75%
Stability	No stability	Weak	Stable in shape	Stable to pressure and pulling stress

Another scoring system used for the histologic analysis of regenerated meniscal tissue is the Ishida score (Longo et al., 2013), which includes three components: tissue bonding, the existence of fibrochondrocytes, and Safranin-O staining (range 0–6) in which a higher score indicates better regeneration (Table 10).

Table 10. Ishida score

	0	1	2
Reparative tissue with bonding	No bond with surrounding meniscus	Partial bond with surrounding meniscus	Bilateral bond with surrounding meniscus
Existence of fibrochondrocytes	No fibrochondrocytes in the reparative tissues	Fibrochondrocytes are localized in the reparative tissues	Fibrochondrocytes exist diffusely in the reparative tissues
Staining with Safranin-O	Not stained with Safranin-O	Faintly stained with Safranin-O	Densely stained with Safranin-O

CHAPTER 4

4. RESULTS AND DISCUSSION

4.1. Characterization of raw materials

4.1.1. Fourier Transform Infrared (FTIR) Spectroscopy

4.1.1.1. Sodium alginate

The ATR-FTIR spectra of sodium alginate (Figure 26) showed absorption bands at 3235 cm^{-1} and 2908 cm^{-1} due to the stretching vibration band of the OH group and the -CH vibration bands, respectively. Observed bands at 1601 cm^{-1} and 1407 cm^{-1} were attributed to asymmetric and symmetric stretching vibrations of the COO^- groups, respectively. The peak at 1024 cm^{-1} corresponds to the C–O–C stretching (glycosidic bonds in polysaccharides). Moreover, the bands observed at 945 cm^{-1} and 880 cm^{-1} are specific to the C-H stretching of guluronic and mannuronic acids, respectively. The results were in good agreement with the study conducted by Helmiyati and Aprilliza (2017), using sodium alginate from brown algae as an eco-friendly superabsorbent.

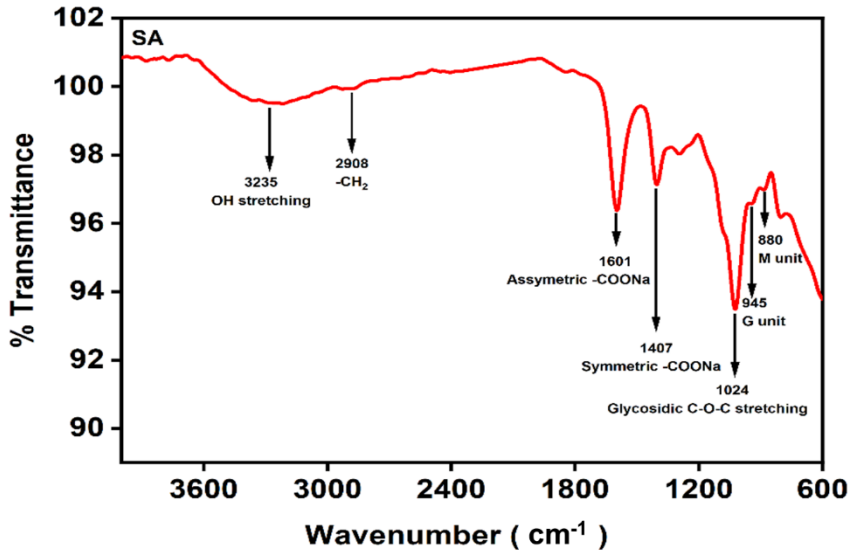

Figure 26. FTIR spectra of Sodium alginate

4.1.1.2. Gelatin

The FTIR spectra of gelatin was shown in figure 27. The amide A band arising from N-H stretching observed at 3232 cm^{-1}, C-H stretching of amide B at 2934 cm^{-1}, C = O stretching of amide I at 1622 cm^{-1} and N-H deformation of amide II at 1500-1550 cm^{-1}. The amide III bands of gelatin were observed at 1222 cm^{-1} (Muyonga et al., 2004; Qadir et al., 2014).

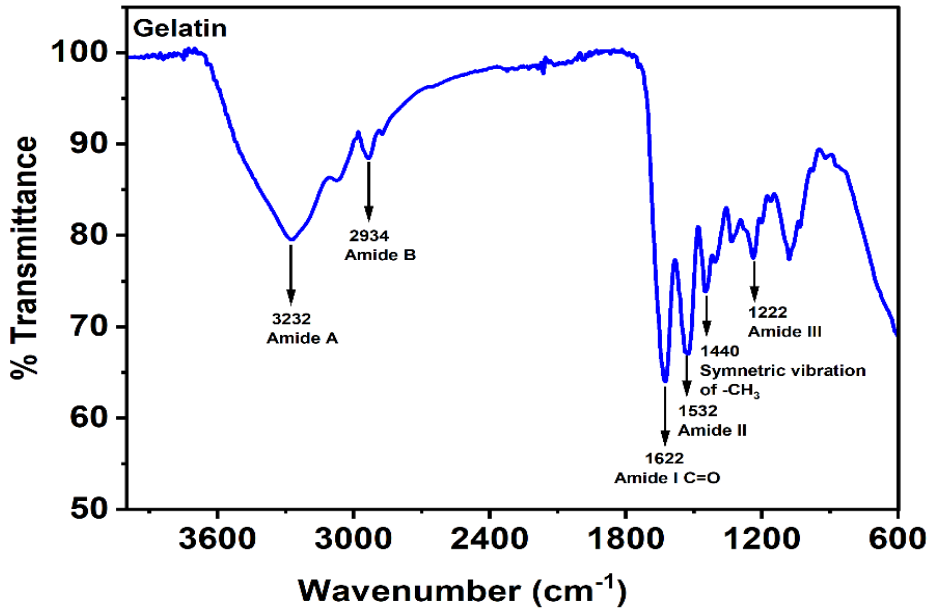

Figure 27. FTIR spectra of gelatin.

4.2. Characterization of ADA

4.2.1. Periodate oxidation of sodium alginate

Alginates are composed of 1,2-cis-linked L-guluronic (G) and D-mannuronic acid (M) units that are arranged in homopolymer or heteropolymer sections (Dinkelaar et al., 2008). During the oxidation of sodium alginate, periodate oxidizes the hydroxyl groups at the second and third carbon positions (C-2 and C-3) of the alginate chain, most preferably the G units (figure 28) into aldehyde groups (Gomez et al., 2007). The aldehyde groups will

react simultaneously with hydroxyl groups of the adjacent unoxidized uronic units in the polymer chain and form cyclic hemiacetals as shown in the red dotted box in figure 27. The aldehyde groups in ADA exist in equilibrium with hemiacetals (Genç et al., 2021).

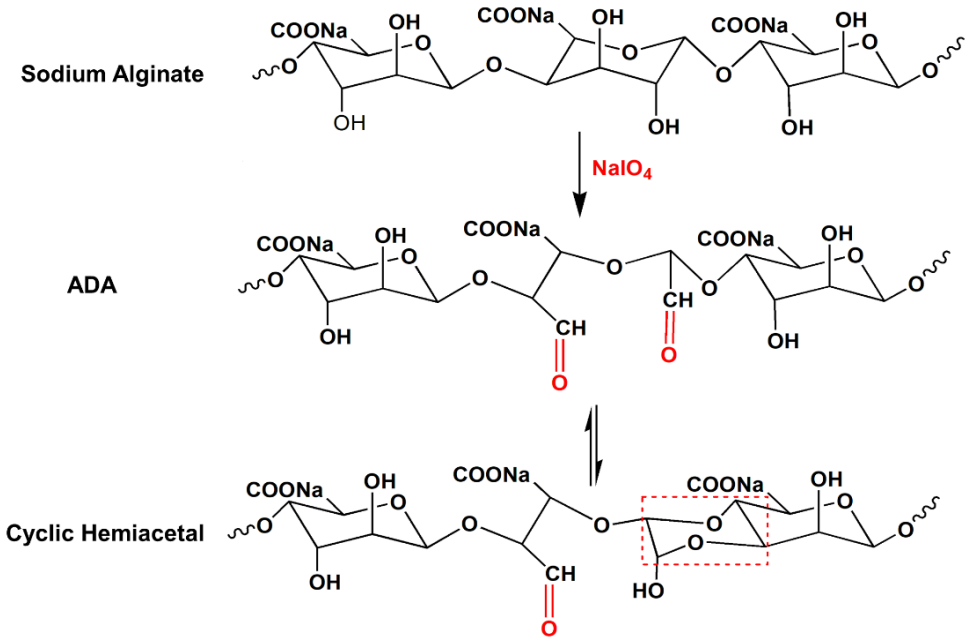

Figure 28. Reaction mechanism for ADA synthesis and its hemiacetal formation.

4.2.2. Degree of oxidation and dialdehyde content

The degree of oxidation (%) of sodium alginate was estimated by measuring the periodate consumption after 6 h of reaction with sodium alginate. The residual periodate in the reaction mixture before dialysis was determined by iodometric titration (Veelaert et al., 1994). In iodometry, potassium iodide was added to the ADA reaction mixture and titrated against sodium bicarbonate. The reaction between periodate left in the mixture and KI leads to the liberation of iodine. The amount of unconsumed periodate was measured by titrating the liberated iodine with standardized sodium thiosulphate using starch as an indicator. The degree of oxidation was found to increase with an increase in the weight

ratio of sodium alginate to periodate as shown in table 11. As the weight ratio increased from 1: 0.6 to 1:1.6, the degree of oxidation increased from 25.8 ± 4.6 % to 66.1 ± 4.4 %. The aldehyde content in ADA was measured by the hydroxylamine hydrochloride method (Maltby and Primavesi, 1949). Hydroxylamine hydrochloride will react with the carbonyl groups of aldehydes in ADA at pH 4 to form polyoxime using a methyl orange indicator. The HCl thus liberated was titrated against standardized sodium hydroxide. The dialdehyde content (Ziegler-Borowska et al., 2018) was also found to increase with the increase in the amount of periodate added (table 11). The dialdehyde content in ADA increased from 19.5 ± 4.7 % to 55.8 ± 3.5 % as the weight ratio increased from 1.0: 0.6 to 1.0: 1.6. The yield of ADA obtained from all the reactions was in the range of 80 - 87 %.

4.2.3. The molecular weight of ADA using viscometry

Molecular weight (MW) is a fundamental property of a polymer and can be determined by viscometry since the intrinsic viscosity of a polymer in its dilute solution state is a function of its molecular weight (Harding et al., 1991). Literature also supports the use of viscometry as a method for the determination of the molecular weight of polysaccharides and their derivatives (Wang et al., 2011; Yaacob et al., 2013).

The viscosity average molecular weight of sodium alginate was found to be 3,39,804 ± 2489 g/mol. The periodate oxidation significantly reduced the molecular weight of alginate from 3,39,804 ± 2489 g/mol to 26,672 ± 3,567 g/mol when 32.9 millimoles of periodate was used for the reaction. From table 11 it was clear that there was a gradual reduction in the viscosity average molecular weight with an increase in the ratio of SA to periodate. As the ratio increased from 1.0 : 0.6 to 1.0 : 1.6 millimoles, the molecular weight of ADA

decreased from 26,672 ± 3,567 to 10,688 ± 1,655 Dalton (Da). The molecular weight of ADA obtained by the viscometry was in good agreement with those reported in the literature (Cai et al., 2007). This reduction may be attributed to the opening of the pyranose ring structure and depolymerization of sodium alginate (Mikkonen et al., 2014).

Table 11. Effect of weight ratio of SA to periodate on the properties of ADA

Weight ratio of SA to Periodate	Degree of oxidation (%)	Dialdehyde content (%)	Yield of ADA (%)	Mw (Da)
1.00 : 0.60	25.8 ± 4.6	19.5 ± 4.7	85.7 ± 2.8	26672 ± 3567
1.00 : 1.06	45.4 ± 2.4	40.3 ± 3.1	86.7 ± 3.3	19447 ± 3365
1.00 : 1.30	54.7 ± 3.3	48.6 ± 4.5	83.2 ± 5.7	12601 ± 2456
1.00 : 1.60	66.1 ± 4.4	55.8 ± 3.5	80.5 ± 3.4	10688 ± 1655

4.2.4. Spectroscopic characterization of ADA

4.2.4.1. Raman spectroscopy

Vibrational spectroscopy has been used for the characterization of polysaccharides. Literature shows that Pereira et al. (2003) and Salomonsen et al. (2008) used Raman spectra for the characterization of identification of alginate and its monomeric units. The Raman spectra of SA and ADA are shown in figure 29. SA shows its characteristics -COO asymmetric and symmetric stretching vibrations at 1613 cm^{-1} and 1417 cm^{-1}, respectively. The C-O single bond stretching vibration at 1314 cm^{-1} and C-O-C stretching at 1096 cm^{-1} of SA can also see in the spectrum.

In the Raman spectrum of ADA, a shift in the C-O single bond peak position from 1314 cm^{-1} to 1343 cm^{-1} indicates the cleavage of vicinal glycols in the alginate chains. The intensities of the SA peak at 1413, 1096 and 956 cm^{-1} were found to decrease in the ADA spectrum suggesting the involvement of β-(1->4)-linked D-mannuronic acid (M) unit in

the oxidation reaction. The involvement of α-(1-4)-linked L-guluronic acid (G) unit in periodate oxidation was suggested by the shifting of the peak at 1314 cm^{-1} and 808 cm^{-1} in ADA spectra (Hernández et al., 2010). The weakening of C-C and C-O bonds was indicated by the shifting of the peak from 1096 cm^{-1} in SA to 1083 cm^{-1} in the spectrum of ADA (Schmid et al., 2008). These results showed that periodate oxidation occurs differently within the M and G blocks.

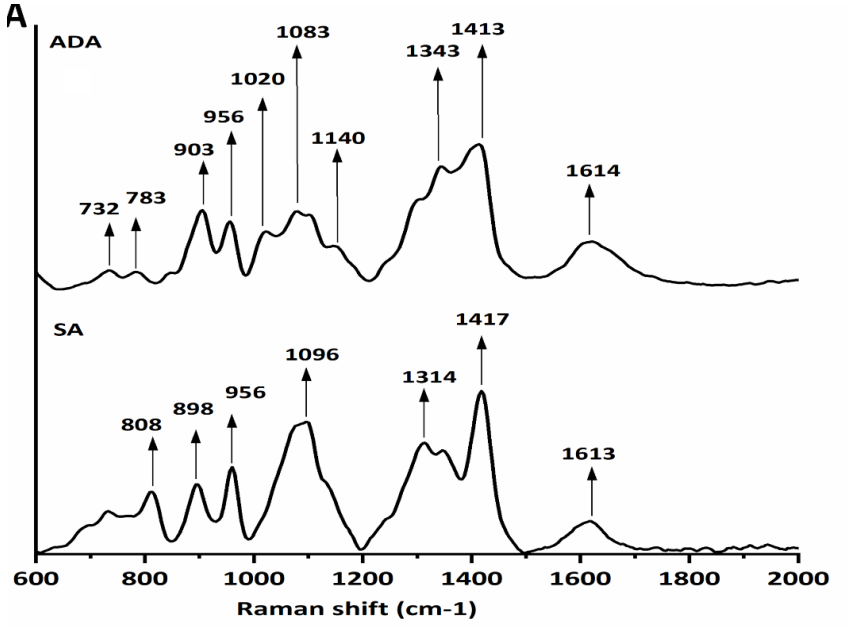

Figure 29. Raman spectra of sodium alginate (SA) and alginate dialdehyde (ADA).

4.2.4.2. ^{1}H NMR spectroscopy

^{1}H NMR spectra of SA and ADA are shown in figure 30. SA showed peaks in the range from 3.6 ppm to 4.0 ppm corresponding to the protons of G and M units. After the oxidation of SA to ADA, the ^{1}H NMR spectrum of ADA showed a signal at 4.2 ppm corresponding to the protons of the oxidized G units. The appearance of two new signals at 5.35 ppm and 5.60 ppm are attributed to hemiacetalic proton (red arrows) formed from aldehyde and

neighboring hydroxyl groups as shown in the reaction mechanism in figure 28 which also confirmed the oxidation of SA to ADA (Tian et al., 2016; Wang et al., 2019).

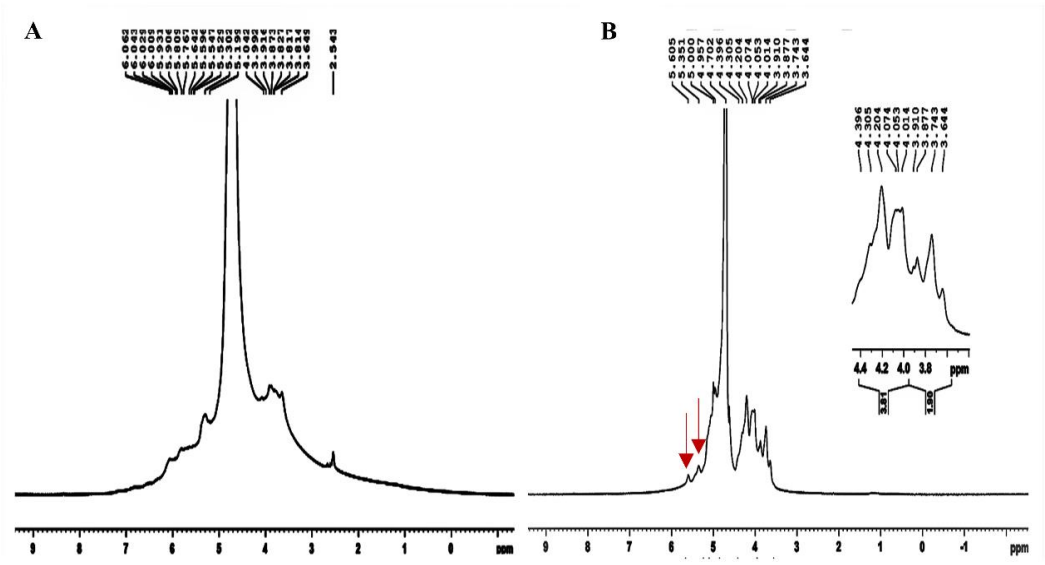

Figure 30. NMR Spectra of: (A) Sodium alginate; (B) Alginate dialdehyde.

4.3. Formation of hydrogel through Schiff's base crosslinking

As shown in figure 28, ADA forms inter cyclic hemiacetal linkage, which limits the availability of aldehyde groups for reaction with amino groups of gelatin. This will lead to an increase in the gelation time. For an injectable system, gel formation should be fast. Literature shows that, when borax was added to ADA solution, the hydroxyl groups of ADA has served as a ligand for the formation of a tetraborate complex with borax as shown in the red dotted box in figure 31 (Balakrishnan et al., 2014b). Reports state that borax forms complex with diols of polysaccharides (Bishop et al., 2004) and increases their solubility. This makes the aldehyde groups available for reaction with the pendent ε-amino groups of lysine, an amino acid monomer, present in gelatin enabling faster gelation via Schiff's base (C=N) formation (represented by blue color in figure 31). So, there is a dual

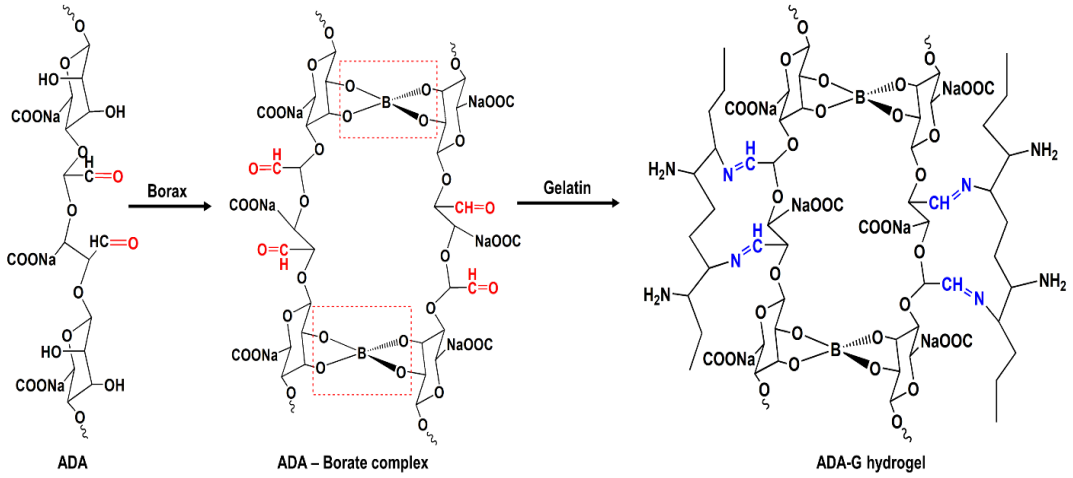

Figure 31. Scheme for borate complexation with ADA and formation of ADA-Gelatin hydrogel in the presence of borax.

crosslinking happening at the time of hydrogel formation namely physical crosslinking of ADA chains with borax followed by chemical crosslinking with gelatin resulting in an in situ gelling self-crosslinked systems without any extraneous crosslinking agents.

Platelet-rich plasma (PRP) contains more than 1100 different proteins, growth factors, angiogenic factors and chemokines (Boswell et al., 2012; Pavlovic et al., 2016). So like

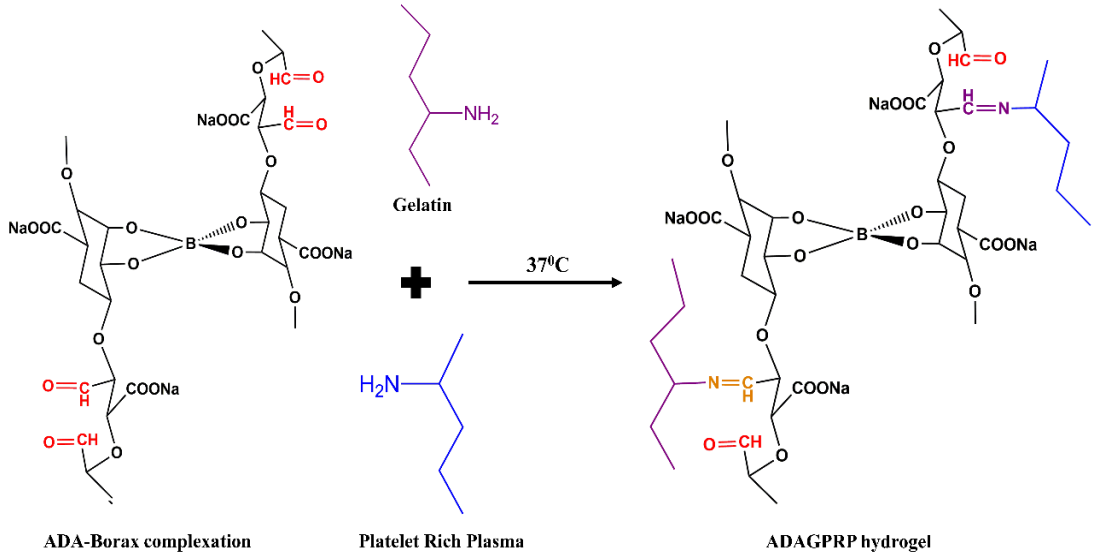

Figure 32. Scheme showing the formation of ADAGPRP hydrogel in the presence of borax.

gelatin, PRP also has amino groups which can crosslink with the aldehyde groups in ADA to form Schiff's base crosslinking (Somasekharan et al., 2020). Figure 32 shows the schematic representation for ADAGPRP hydrogel preparation. The aldehyde groups in ADA were shown in red color. The -C=N- linkage formed by gelatin is shown in orange color and that by PRP is shown by purple color in figure 32.

4.4. Characterization of hydrogel

4.4.1. Physicochemical characterization

4.4.1.1. Gelation time

Time taken by the injectable liquid composition from the onset of mixing the individual components to forming into a solid hydrogel has great clinical significance (Moeinzadeh and Jabbari, 2015). Methods for monitoring gelation time rely on simple techniques. Gelation time can be determined by the tube inversion method or from rheological measurements (Chung et al., 2002).

4.4.1.1.1. Tube inversion/tube tilting method

The time taken by material to change its state from flow (sol) to no flow (gel) when inverting/tilting is the simplest method for determining the gelation time (Chung et al., 2002). Due to its simplicity and efficiency, this method has been widely used for determining gelation time. During knee surgery, saline is used for irrigating the surgical area to keep it hydrated and distend the joint (Li et al., 2016; Shinjo et al., 2002). From figure 33 A, it may observe that the hydrogel (red arrow) could be properly injected into the saline (black arrow). When the bottle was inverted, hydrogel and saline formed a

separate phase which indicates that Schiff's base crosslinking can take place in the presence of saline.

4.4.1.1.2. Effect of concentration of ADA and gelatin on the gelation time

Figure 33 B shows the influence of concentration of ADA and gelatin on the gelation time of hydrogel. As the concentration of ADA increased from 15 % (15ADA15G) to 20 % (20ADA15G) the gelation time of hydrogel decreased from 15.4 ± 1.6 min to 2.2 ± 0.19 min. The borax concentration was kept at 0.025 mol/L. On the otherhand when the concentration of gelatin increased from 15 % (15ADA15G) to 20 % (15ADA20G) the gelation time of hydrogel decreased from 15.4 ± 1.6 min to 6.9 ± 0.15 min. The concentration of borax was maintained at 0.025 mol/L. The gelation time was found to be decreasing when the concentration of ADA and gelatin increased irrespective of the concentration of borax. Literature also supports these results. It has been reported that when ADA-GEL hydrogel was used for fabricating microcapsules, increasing the concentration of gelatin decreased the gelation time of ADA-GEL hydrogel (Reakasame et al., 2020).

The clinically relevant gelation time of 4-5 min was obtained when the composition of hydrogel was 15 % ADA and 20 % G (15ADA20G) with a borax concentration of 0.05mol/L.

4.4.1.1.3. Effect of PRP addition on the gelation time of 15ADA20G hydrogel

15ADA20G hydrogel was chosen for PRP incorporation. Different volumes of PRP (100, 300, 500, 700 and 900 µl) were added during hydrogel preparation. The effect of PRP addition on gelation time is shown in figure 33 C. As the volume of PRP increased from 100 to 900 µl the gelation time was also increased from 4.07 ± 0.1 min to 9.75 ± 0.5 min.

To maintain the clinically required gelation time of 4-5 min, the maximum permissible volume of PRP was 300 µl. The increased gelation time above this volume of PRP may be attributed to the dilution effect of PRP in the 15ADA20G hydrogel system.

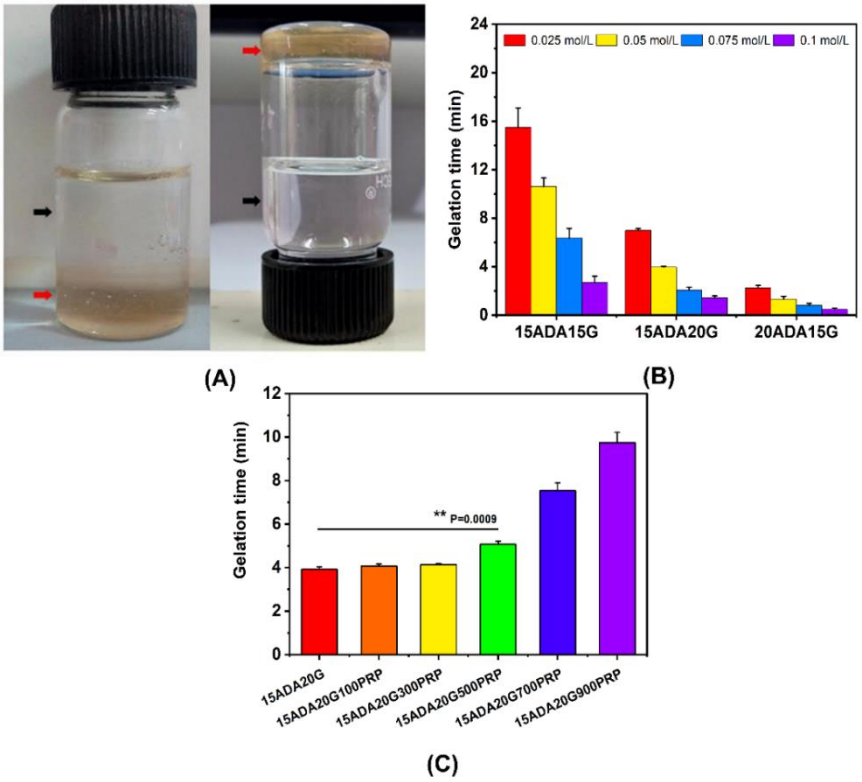

Figure 33. Gelation time and associated parameters: (A) Gelation time determined by tube inversion method at 37^{o}C (black arrows show saline and red arrows show hydrogel); (B) Effect of ADA and gelatin concentration on the gelation time of hydrogel; (C) Effect of addition of various volume of PRP on the gelation time of 15ADA20G hydrogel.

4.4.1.1.4. Rheology

Rheology is an ideal method for the determination of viscoelastic properties, as it is sensitive, quick and requires a small volume of hydrogel per measurement (Alonso et al., 2021). It can provide information about the crosslinking as well as gelation time of hydrogels (Jiang et al., 2016; Otero-Espinar et al., 2018).

Time sweep rheology analysis of 15ADA20G hydrogel was done to confirm the gelation time. The G' represents the elastic storage modulus and G" represents the viscous loss moduli. At the beginning of the gelation process G' and G" was very low, with G" greater than G' which indicates the sol state of 15ADA20G. As time progresses, The G' and G" started increasing and the elastic hydrogel was formed through crosslinking of ADA and gelatin through Schiff's base reaction with G' > G". At a particular time, G' crossed over G" (gel point) indicating the transition from liquid to gel state of 15ADA20G. Figure 34 A shows the crossover point (red arrow) of G' and G" at 2.9 min. ADA and gelatin were mixed thoroughly for 1 min before injecting onto the rheometer plate. So, the total gelation time from the beginning of mixing was 3.9 min which confirmed the result obtained from the tube inversion method. A sharp increase in G' after the crossover point indicates the formation of a distinct 3D network in the hydrogel system (Weng et al., 2007).

The time sweep rheology analysis 15ADA20G300PRP was also done since up to this volume the clinically required gelation time of 4-5 min was obtained by tube inversion method (Figure 33 C). The gelation time of 4.14 min obtained from the tube inversion method was confirmed by the result from time sweep rheology analysis. The gelation time obtained from rheology was 3.3 min (red arrow in figure 34 B). As described for 15ADA20G, a 1 min mixing time should be added along with this. So, the gelation time of 15ADA20G300PRP was 4.3 min.

4.4.1.2. Raman spectra of hydrogel

Raman spectroscopy studies the vibrational energy of molecules. It is a suitable method to investigate the molecular interactions that generate the hydrogel network. Raman spectra

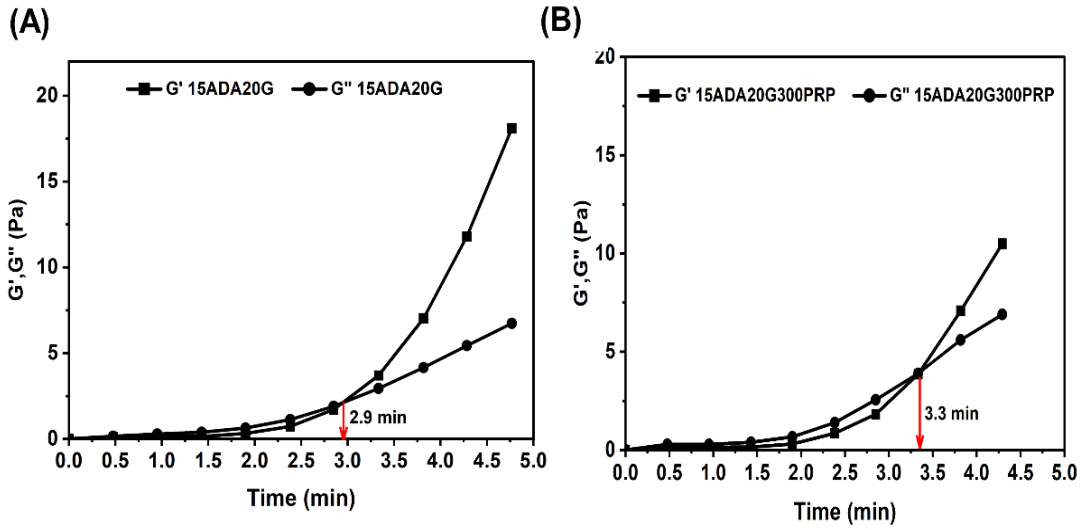

Figure 34. Time sweep rheology analysis of: (A)15ADA20G and (B)15ADA20G300PRP hydrogel.

provide fingerprints of a system, although the information is complementary and selection rules are different compared to FTIR spectra. An advantage of using Raman spectroscopy compared with IR spectroscopy in studying hydrogels is the fact that Raman spectroscopy is insensitive to the presence of water in the compounds, while IR spectra would be dominated by the broad -OH band due to the presence of water (Ionita, 2016).

Raman spectrum of gelatin (Figure 35 A) showed an intense band at 1666 cm^{-1}, corresponding to the amide I vibration, which primarily indicates C=O stretching vibration. The bands at 1453 cm^{-1} and 1250 cm^{-1} correspond to C–H bending and amide III vibrations, respectively. These two peaks are the characteristic absorption bands of the gelatin protein structure.

Raman spectra of Platelet Rich Plasma (PRP) (Figure 35 A) showed a small band at 1651 cm^{-1} corresponding to the Amide 1, C=O stretching. A very strong peak at 1511 cm^{-1} is due to the NH_3 symmetric bending of proteins. A small band at 1443 cm^{-1} corresponds to

the CH_2 bending. A small peak at 1274 cm^{-1}, a strong peak at 1152 cm^{-1} and a medium peak at 1002 cm^{-1} corresponds to the =C-H in-plane deformation vibration of unsaturated fatty acids, C-C bond stretching vibration of proteins and aromatic δ ring mode of Phenylalanine respectively (García-Rubio et al., 2019; Zhu et al., 2011).

The Raman spectrum of ADAG hydrogel exhibits absorption bands at 1658 cm^{-1} due to v(C=N) suggesting the formation of Schiff's base between aldehyde groups in ADA and amino groups in gelatin. The band at 1658 cm^{-1} is broad probably because of overlapping with the band at 1666 cm^{-1} of amide I of gelatin. Moreover, the intensity of the characteristic peak of gelatin at 1250 cm^{-1} due to amide III was decreased in the spectrum of the hydrogel, confirming the involvement of this group in the crosslinking reaction.

Raman spectra of ADAGPRP (Figure 35 B) also have a strong peak at 1657 cm^{-1} confirming the formation of Schiff's base between the amino groups in PRP and aldehyde groups in gelatin. In the ADAGPRP spectra disappearance of the characteristic peak in PRP at 1511 cm^{-1}, 1152 cm^{-1} and 1002 cm^{-1} indicates the incorporation of PRP in the hydrogel. Compared to ADAG hydrogel spectra, there is a shifting of the peak 1405 and 1254 cm^{-1} to 1451 and 1257 cm^{-1}, respectively, also confirms the incorporation of PRP in the hydrogel.

4.4.1.3. Degree of crosslinking

The degree of crosslinking of ADAG and ADAGPRP was quantitatively determined by trinitrobenzene sulfonic acid (TNBS) assay (Bubnis and Ofner, 1992). The reaction of TNBS with the primary amino groups in the proteins is used to determine the number of free amino groups in the samples. The degree of crosslinking is determined from the

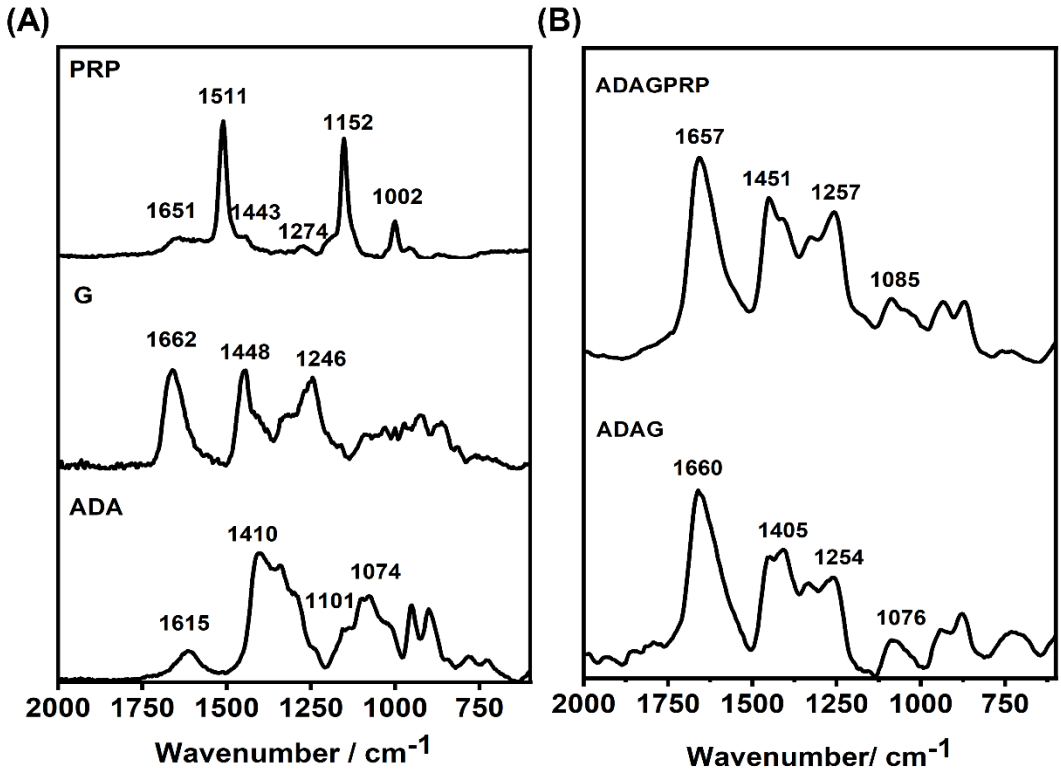

Figure 35. Raman spectra; (A)ADA, Gelatin (G) and PRP; (B) ADAG and ADAGPRP hydrogel.

difference between the chemically determined number of uncrosslinked amino groups (free amines) before and after crosslinking. While determining the degree of crosslinking, it has been assumed that each lost amino group participates in one crosslinking reaction (Grover et al., 2012).

4.4.1.3.1. Effect of ADA and gelatin concentration on the degree of crosslinking of hydrogel

When the composition of hydrogel changed from 15ADA15G to 15ADA20G the degree of crosslinking of hydrogel increased from 43.9 ± 1.7 % to 54.4 ± 1.4 % with a significant difference of $P<0.004$ (Figure 36 A). This may be due to the availability of more amino groups of gelatin for reaction with aldehyde groups in ADA. In the same way when the

ADA content in the hydrogel increased as seen in 15ADA15G to 20ADA15G, the degree of crosslinking increased significantly (P=0.000004) from 43.9 ± 1.7 % to 66.9 ± 2.7 % (Figure 36 A). This proves that when more aldehyde groups are available for reaction, they will react with the amino groups of gelatin thereby increasing the degree of crosslinking.

4.4.1.3.2. Effect of volume of PRP on the degree of crosslinking of 15ADA20G hydrogel

Based on the gelation time 15ADA20G hydrogel was chosen for PRP addition. From figure 36 B it was clear that as the volume of PRP increased from 100 to 900 µl the degree of crosslinking of 15ADA20G hydrogel decreased from 53.9 ± 1.8 % to 28 ± 1.5 %. The significant decrease in the degree of crosslinking would be due to the unavailability of aldehyde groups to react with the amino groups in PRP. The higher volume of PRP in the hydrogel was creating a dilution effect. There was no significant difference between the degree of crosslinking of 15ADA20G (54.4 ± 1.4 %), 15ADA20G100PRP (53.9 ± 1.8 %) and 15ADA20G300PRP (51.7 ± 0.5 %) (P>0.05) (Figure 36 B). So up to 300 µl PRP, there

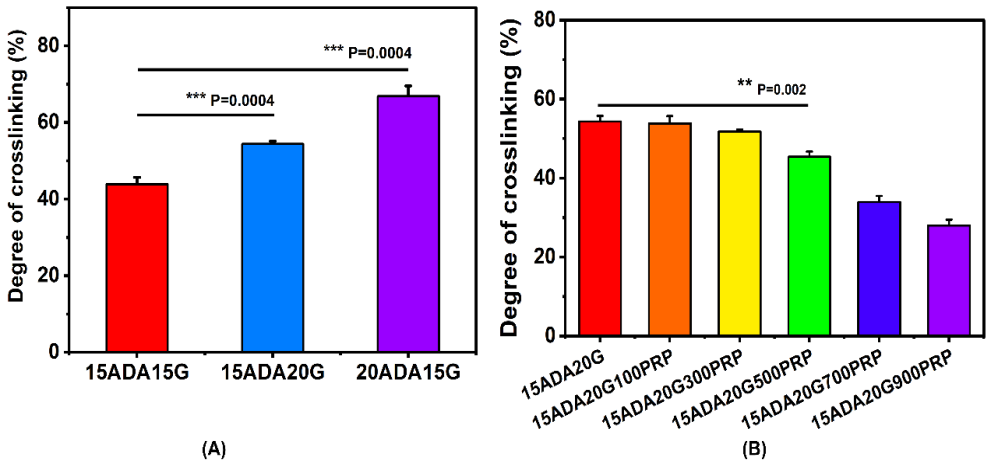

Figure 36. Degree of crosslinking of hydrogel compositions: (A) Effect of the concentration of ADA and Gelatin; (B) Effect of PRP addition on the degree of crosslinking of 15ADA20G hydrogel.

may be a sufficient quantity of aldehyde groups available for reaction with amino groups in PRP along with gelatin.

4.4.1.4. Water uptake

Hydrogels are 3D crosslinked networks of hydrophilic polymers, that undergo swelling instead of dissolution in water. The ability to display a measurable change in the hydrogel network volume by uptaking a thermodynamically stable solvent in response to external stimuli is a fundamental property of hydrogels (Lee and Park, 1996). The ability of hydrogels to absorb water is attributed to the presence of hydrophilic groups in the polymer used for hydrogel preparation. Due to the contribution of these groups and various domains in the network, the polymer gets hydrated to different degrees, even more than 90% of its weight, depending on the nature of the aqueous environment and polymer composition (Gulrez et al., 2011).

4.4.1.4.1. Effect of concentration of ADA and gelatin on the water uptake of hydrogel

The water uptake of 15ADA20G (470 ± 22 %) was significantly lower than 15ADA15G (530 ± 24 %) with a P-value of 0.03, indicating a higher degree of crosslinking of the former. In the same way as the ADA content in the composition increased from 15 to 20 % as seen in 15ADA15G to 20ADA15G, the water uptake of hydrogel decreased significantly from 530 ± 24 % to 336 ± 80 % with a P-value of 0.0005 (Figure 37 A).

4.4.1.4.2. Effect of addition of PRP on the water uptake properties of 15ADA20G hydrogel

Figure 36 B shows the effect of the addition of different volumes of PRP on the water uptake of 15ADA20G hydrogel. As the volume of PRP increases from 100 to 900 µl, the

water uptake of 15ADA20G hydrogel also increased significantly from 526 ± 19 % to 1468 ± 94 %. So as the degree of crosslinking of 15ADA20G hydrogel decreased after the addition of PRP, the water uptake also increased.

Literature also showed that the increased crosslinking density diminishes the voids in the hydrogel network that holds water (Wang and Wang, 2010). Here the decreasing trend in the water uptake shown in figure 36 A can be explained by the difficulty in the diffusion of water into the hydrogel network with high cross-linking density (Kowalski et al., 2019). This is related to the more compact and smaller mesh size formed in the hydrogel network as the concentration of polymer varies. In the case of ADAGPRP hydrogel, the increased volume of PRP in the 15ADA20G hydrogel resulted in a dilution effect thereby decreasing the crosslinking density and increasing the water uptake due to the larger mesh size of the hydrogel network.

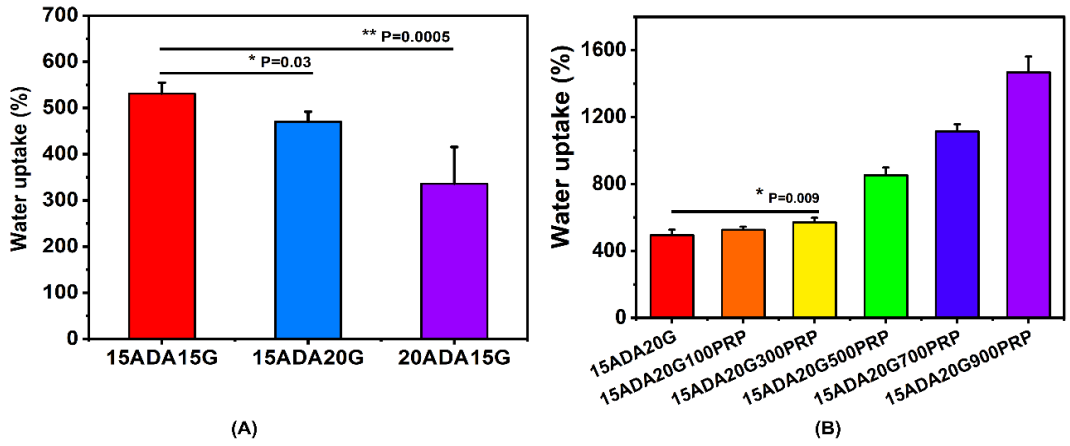

Figure 37. Water uptake; (A) Effect of concentration of ADA and Gelatin on the water uptake; (B) Effect of volume of PRP on the water uptake of 15ADA20G hydrogel.

4.4.1.5. Compressive strength of the hydrogel

The compressive strength is one of the mechanical tests (Svensson et al., 2005) used to examine the load-bearing capability of different types of hydrogels. This technique

involves placing the hydrogel of defined height and diameter between two platens as shown in figure 38 A-C and compressing it. The pressure applied to the surface of the hydrogel (Figure 38 B) and the distance the hydrogel is compressed (Figure 38 C) was used to calculate the compressive strength of hydrogels (Ahearne and Liu, 2008). Comparable mechanical properties are desirable for modulating the cellular adhesion in cytoskeletal organizations (Wolf et al., 2012).

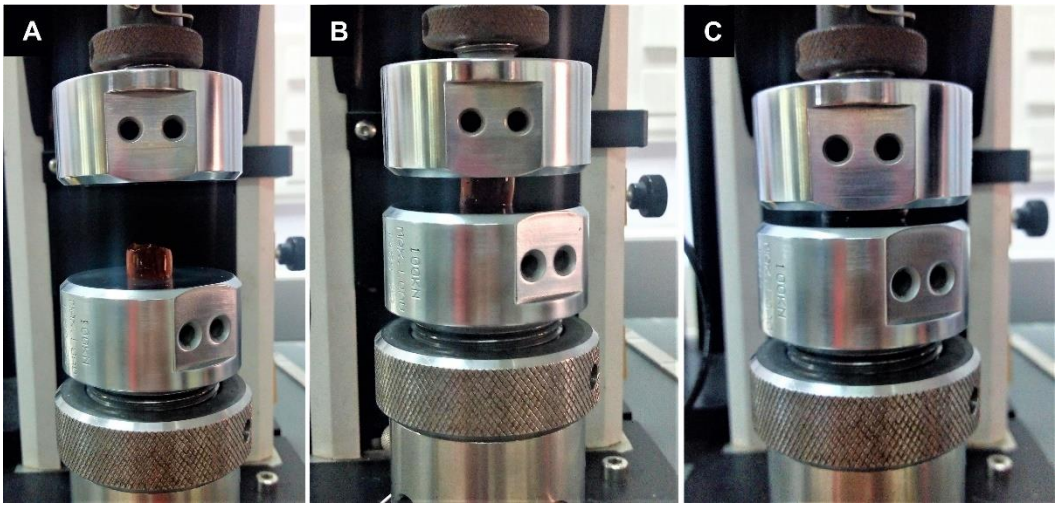

Figure 38. Compressive testing of hydrogels: A) Hydrogel placed between the jigs; B) Hydrogel at the time of compression testing; C) Deformation of hydrogel at maximum compressive load.

4.4.1.5.1. Effect of solution concentration of ADA and gelatin

The compressive strength (CS) of 15ADA20G (295 ± 32 kPa) was found to be significantly higher (P=0.04) than that of 15ADA15G (220 ± 22 kPa) showing the influence of increased concentration of gelatin. But when the concentration of ADA was increased from 15 % (15ADA15G, CS = 220 ± 22 kPa) to 20 % (20ADA15G, CS = 164 ± 24 kPa) (Figure 39 A), there was a significant decrease (P= 0.004) in the compressive strength. This decrease in compressive strength was attributed to a higher degree of crosslinking between ADA and gelatin. A higher degree of crosslinking made the hydrogel

brittle and cause it to fail at a lower compressive load. It may be noted that the compressive properties of the native meniscus fall in the range of 100 – 400 kPa (Hasan et al., 2014). So, as far as mechanical properties are considered, the injectable 15ADA20G could be considered as a prospective material for the repair of a partially defective meniscus.

4.4.1.5.2. Effect of addition of PRP on the compressive strength of the 15ADA20G hydrogel

Figure 39 B shows the effect of the addition of PRP on the compressive strength of 15ADA20G hydrogel. As the concentration of PRP increased from 100 to 900 µl, the compressive strength of 15ADA20G hydrogel increased from 331 ± 18 to 793 ± 32 KPa. From the water uptake and degree of crosslinking it was observed that up to 300 µl PRP can be added to 15ADA20G hydrogel without affecting its properties. Here, an increase in compressive strength of 15ADA20G hydrogel after the addition of PRP may be due to the lesser degree of crosslinking resulting in a highly porous and elastic polymer network (Bajpai et al., 2006). As described in section 4.4.1.5.1 the native rabbit meniscus has a

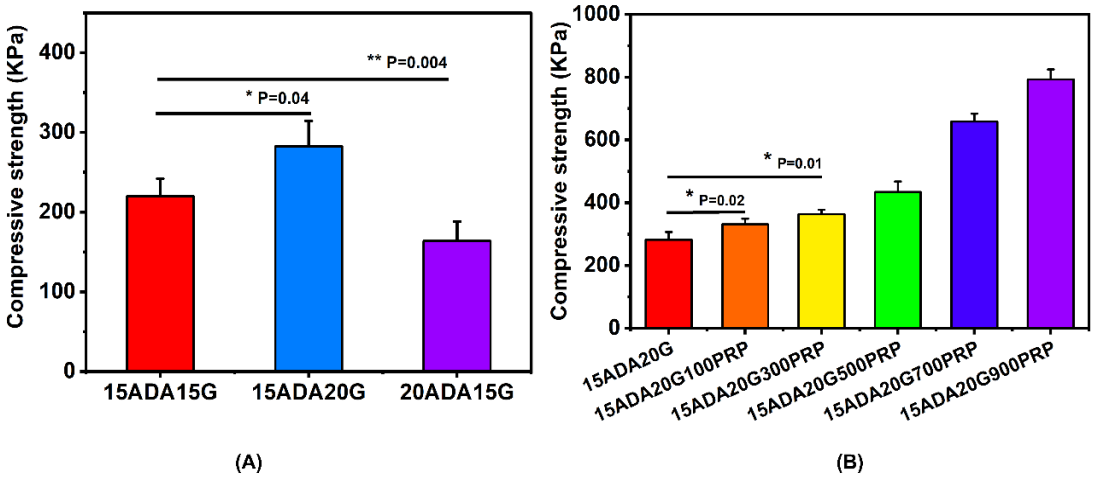

Figure 39. Compressive strength; (A) Effect of concentration of ADA and Gelatin on the compressive strength; (B) Effect of volume of PRP on the compressive strength of 15ADA20G hydrogel.

compressive strength ranging from 100 - 400 kPa. So based on the degree of crosslinking, water uptake and compressive strength up to 300 µl of PRP can be added to 15ADA20G hydrogel without affecting its properties.

4.4.1.6. Porosity, Morphology and 3D microarchitecture

In tissue engineering, the architecture and microstructure of hydrogel greatly influence *in vitro* and *in vivo* functional responses (Palmroth et al., 2020). The degree of porosity of hydrogel has a significant effect on the water uptake and mechanical properties. When the porosity increases the stiffness of the hydrogel decreases and the water uptake increases. (Gerecht et al., 2007; Gupta and Shivakumar, 2012). The porosity and pore architecture and pore interconnectivity play a significant role in cell survival, proliferation, migration and ECM secretion (Lien et al., 2009; Mandal and Kundu, 2009). The porosity of hydrogels also plays a significant role in nutrient diffusion and waste removal (Bružauskaitė et al., 2016).

Several techniques like Scanning Electron Microscopy (SEM), mercury and liquid extrusion porosimetry and Micro Computed Tomography (Micro-CT) have been used for porosity measurements. Each of these techniques has advantages and disadvantages, and a combination of different techniques is often required to achieve an in-depth study of the morphological features of the hydrogel. Here we have used SEM and Micro-CT for evaluating the surface morphology and total porosity of hydrogel, respectively. Apart from SEM, Micro-CT will provide a full assessment of the porous structures both in terms of pore size and interconnected porosity (Bertoldi et al., 2011).

4.4.1.6.1. Morphology and porosity of 15ADA20G hydrogel

Since 15ADA20G composition was chosen as the optimum in terms of gelation time and compressive strength, SEM analysis was done for this material. Results show an interconnected porous nature for this hydrogel composition (Figure 40 A). Typical Micro-CT images/data of 15ADA20G hydrogel after lyophilization is shown in figure 40 B-D. Figure 40 B is the 3D reconstructed image of the hydrogel. Figure 40 C shows the porosity distribution within the hydrogel network. From the Micro-CT image, it is clear that there is a wide size distribution of pores in the hydrogel indicated by the color distribution from grey (small pores), green, yellow and red (large pores) (Rajalekshmi et al., 2021).

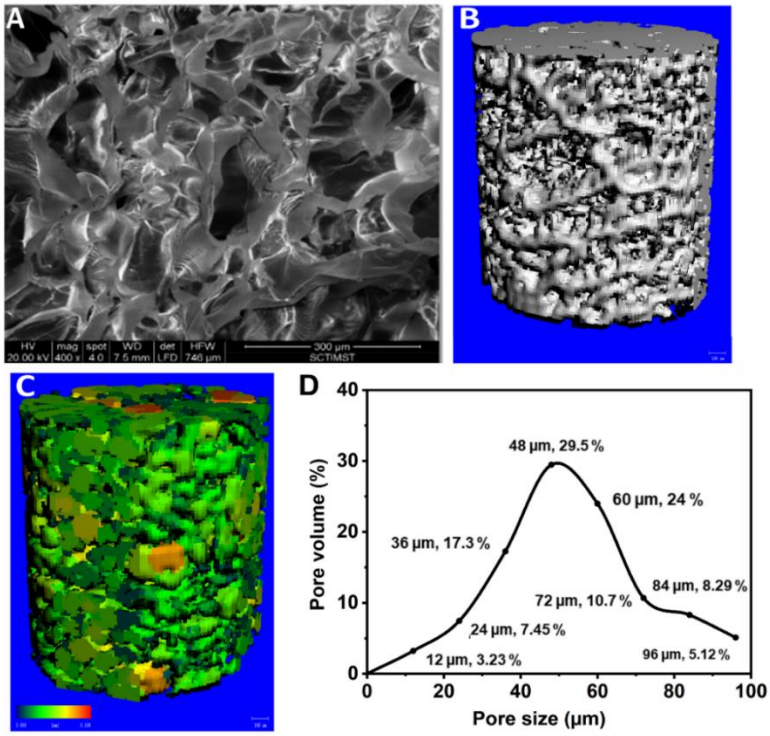

Figure 40. Morphology and 3D microarchitecture of 15ADA20G hydrogel: A) Scanning Electron Micrograph of lyophilized hydrogel; B) 3D reconstruction image of hydrogel obtained from Micro-CT; C) Pore size distribution and D) pore volume (%) distribution.

The quantitative evaluation of pore size distribution (Figure 40 D) showed that the hydrogel contains pore sizes ranging from 12 µm to 100 µm with the majority of the pores lies in the range of 36 µm (17.3 %) - 60 µm (24 %) which is represented by green color in the porosity distribution image (Figure 40 C). The 15ADA20G system showed an average porosity of 51 %, wall thickness of 48 µm, pore diameter of 60 µm and anisotropy of 1.239. This result was similar to that obtained for PVA hydrogels used for meniscal functional repair. PVA hydrogels had a pore distribution ranging from 15 to 400 µm, with most of the pore diameters falling in the 20-100 µm (Coluccino et al., 2018).

4.4.1.6.2. Effect of addition of PRP on the morphology and porosity of 15ADA20G hydrogel

Among the hydrogel compositions containing PRP, 15ADA20G300PRP was chosen as the optimum composition in terms of gelation time, degree of crosslinking, water uptake and compressive strength. The surface morphology of lyophilized hydrogel observed under SEM is shown in figure 41 A. The interconnected porous nature of the 15ADA20G300PRP hydrogel observed here was similar to that observed for 15ADA20G.

Figure 41 B-D represents the Micro-CT images/data of lyophilized 15ADA20G300PRP hydrogel. Figure 41 B is the 3D reconstructed image of the lyophilized hydrogel. As described for 15ADA20G, there is a wide size distribution of pores in 15ADA20G300PRP hydrogel indicated by the color distribution from grey (small pores) to red (large pores).

The quantitative evaluation of pore size distribution in 15ADA20G300PRP hydrogel (Figure 41 D) showed that the material contains pores of size ranging from 12 µm to 100

µm with the majority of the pores lies in the range 36 µm (23.8 %) - 60 µm (12.7 %), which is represented by grey to green color in the porosity distribution image (Figure 41 C).

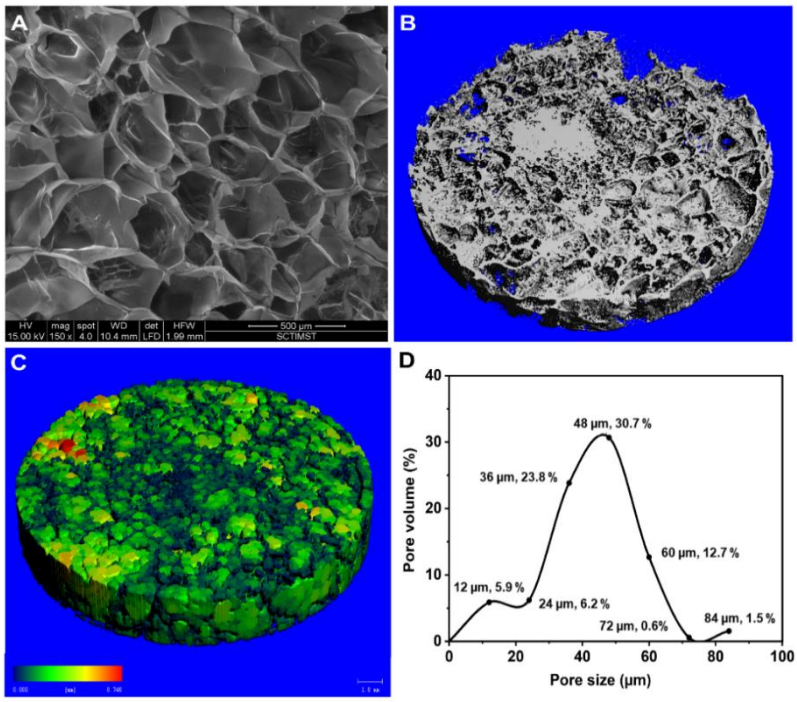

Figure 41. Morphology and 3D microarchitecture of 15ADA20G300PRP hydrogel: A) Scanning Electron Micrograph of lyophilized hydrogel; B) 3D reconstruction image of hydrogel obtained from Micro-CT; C) Pore size distribution and D) pore volume (%).

4.4.1.7. Degradation of hydrogel

The degradation profile of hydrogels must be considered as an important property whenever designing scaffolds for tissue regeneration. Since many injectable hydrogels form highly condensed structures with nanometer-size pores, micron-scale sized cells find it difficult to proliferate and infiltrate into the bulk of the material. Biodegradation cleaves the covalent bonds within the polymer matrix leading to increased porosity. For proper tissue regeneration, there should be a precise balance between hydrogel degradation and tissue integration (Dimatteo et al., 2018). Slow biodegradation may cause an increased

inflammatory response and can promote fibrosis (Alijotas-Reig et al., 2013). But materials that degrade too quickly cannot provide an adequate structural framework and initial support required for the cells to attach, proliferate and form an extracellular matrix (ECM) (Chang and Wang, 2011). To overcome these limitations, several methods have been used to design injectable scaffolds which can accommodate tissue regeneration while retaining bulk stability (Bencherif et al., 2012; Griffin et al., 2015).

The performance of the injected hydrogels was affected by the nature of the degradation mechanism and the products that are released into the host site. The released products may change the local cell environment and can negatively affect tissue regeneration (Madaghiele et al., 2014). Here the degradation profile of injectable 15ADA20G and 15ADA20G300PRP was studied. The product released from the hydrogel into the PBS was evaluated.

4.4.1.7.1. UV-Visible spectra

UV visible spectra of individual components used for 15ADA20G hydrogel preparation were shown in figure 42 A. The maximum absorbance of ADA is at 204 nm (figure 42 A Blackline). The result was in accordance with that obtained for dialdehyde galactomannan, where they obtained absorbance at 202 nm after the periodate oxidation of guar gum (Umamaheswari et al., 2012). The aqueous solution of borax gave negative absorbance in the UV spectra ranging from 190 to 600 nm (Figure 42 A, red line). This result is also supported by the research published by Gujral, 2015, where they studied the UV spectra of borax dissolved in various solvents. When borax was added to the ADA solution, the absorption maxima of ADA was shifted from 204 nm to 235 nm (Figure 42 A, blue line).

This redshift could be due to the tetraborate complex formation between the hydroxyl groups in ADA and the boron in borax. The spectra of gelatin (Figure 42 A, green line) show two bands, one at 227 nm and the other at 280 nm due to the peptide bond and side chains of the aromatic groups present in it $\pi \rightarrow \pi^*$ and $n \rightarrow \pi^*$ transitions, respectively (Antosiewicz and Shugar, 2016). The UV spectra of PRP have two bands (figure 42 B, black line). The band at 230 nm corresponds to the amide backbone of proteins and that at 280 nm due to the presence of chromophoric amino acids in the proteins along with other small chromophoric molecules found in plasma (Dickinson and McClements, 1995; Mattley et al., 2000).

Figure 42 B shows the blends of ADA, G and PRP solutions. The blend of ADA and G with and without PRP (ADAG (figure 41B, black line) and ADAGPRP (figure 42 B, red line)) did not show the peak of Schiff base at 320 nm since the spectra were taken just by mixing dilute solutions of ADA and G and PRP. The aldehyde and amino groups may not be reacting to form Schiffs base since the concentration was very low.

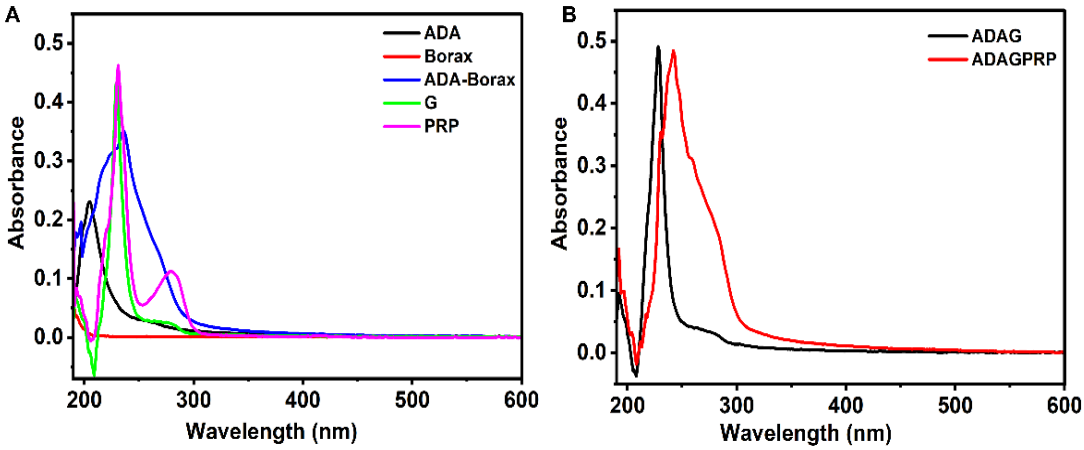

Figure 42. UV Visible spectra A) individual components used for hydrogel preparation B) blend of ADAG and ADAGPRP.

4.4.1.7.1.1. Extract collected from hydrogel

UV spectra of extract collected at respective time periods after the degradation of hydrogel were evaluated for the products released from the hydrogel.

Figure 43 A shows the UV-Vis spectra of the extract collected from day 1 to day 28 of 15ADA20G hydrogel. The spectra of the extract have a peak around 311 nm which was not seen in the ADAG blend (Figure 41B, black line). Literature reports that the peak around 300–350 nm involves $\pi \rightarrow \pi*$ transitions of the C = N group in the Schiff's base (Cinarli et al., 2011). This gives an inference that the degradation product from the hydrogel was forming a Schiff base between the available aldehyde groups from small chains of ADA and amino groups from degraded gelatin. As days progressed from day 1 to day 14 the height of the Schiffs base peak increased. But for day 21 and day 28 the height of the Schiff base was visually reduced. This may be due to the saturation of the extract solution after day 14. Also, the components in the extract again started degrading and give a spectrum almost similar to day 1.

A similar trend was also followed by the extract of 15ADA20G300PRP hydrogel as shown in figure 43 B. The extract also showed a similar peak at 311 nm corresponding to the Schiffs base formed between the aldehyde groups and amino groups in both gelatin and PRP. Here also the maximum Schiff's base formation was found up to day 14. On day 21 and day 28, the spectrum was similar to that obtained for day 3. This may be due to the release of more degradation products due to the presence of PRP in addition to gelatin in the hydrogel.

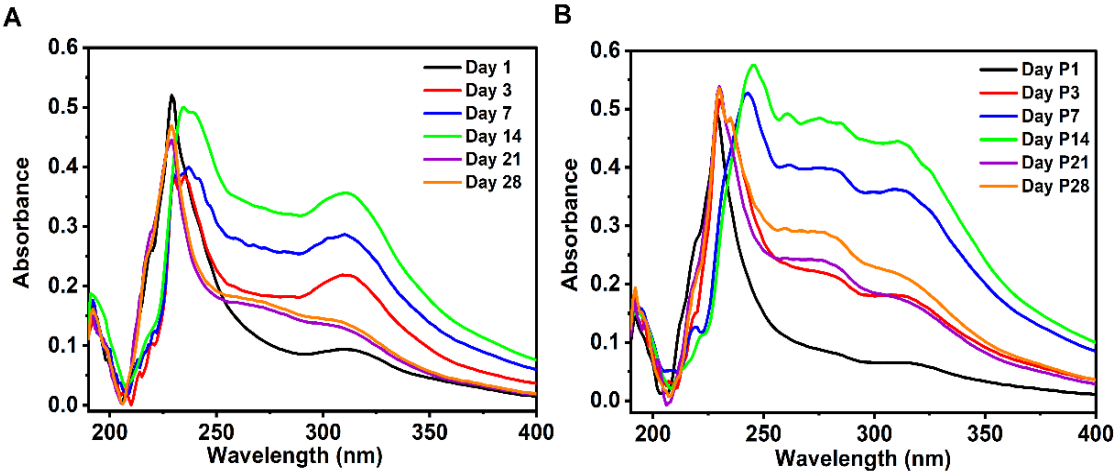

Figure 43. UV visible spectra: (A) extract collected after each time period of 15ADA20G hydrogel degradation; (B) extract collected after each time period of 15ADA20G300PRP hydrogel degradation.

4.4.1.7.2. FTIR spectra

The FTIR spectra of lyophilized extract collected after degradation of hydrogel with and without PRP were evaluated for the degradation products (Figure 44 A-C). The spectra of the extract were compared with that of hydrogel spectra (ADAG). Figure 44 A shows the FTIR spectra of ADAG hydrogel. The Schiffs base peak in the hydrogel was seen at 1611 cm^{-1}. The height of the amide II peak of gelatin at 1539 cm^{-1} was found to decrease in the hydrogel spectrum, which shows the involvement of the amide II peak in crosslinking with aldehyde groups of ADA.

Figures 44 B and C show the FTIR spectra of extracts collected after each time period of 15ADA20G and 15ADA20g300PRP hydrogel degradation, respectively. Both the FTIR spectra showed similarity to that of the ADAG hydrogel spectrum. The peak at 1614 and 1542 cm^{-1} corresponding to Schiff base and amide II peak in gelatin was also seen in the spectrum of both extracts irrespective of hydrogel composition and time period. This also

confirms the result obtained from UV-Vis spectra for the formation of Schiff base in the extract after the degradation of hydrogel.

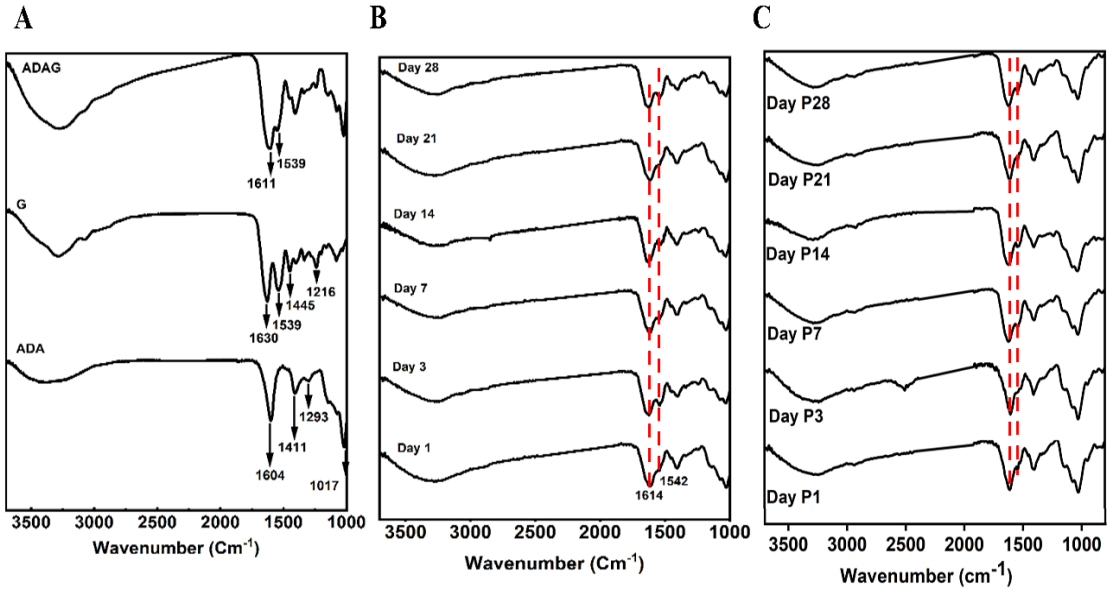

Figure 44. FTIR spectra: A) ADA,G and ADAG hydrogel; B) 15ADA20G extract; B) 15ADA20G300PRP extract ; Dotted line represents the peak similar to ADAG hydrogel.

4.4.1.7.3. Aldehyde content in the extract and hydrogel

Figure 45 A & B shows the aldehyde content in the extract collected after each time period from 15ADA20G and 15ADA20G300PRP hydrogel. It was observed that as the day progressed from 1 to 14 there was a decrease in the aldehyde content in the extracts collected from both the hydrogels. In the 15ADA20G extract, the aldehyde content decreased from 5.8 ± 0.05 % (day 1) to 3.7 ± 0.03 % (day 14) and that of 15ADA20G300PRP extract the decrease was from 5.9 ± 0.06 % (day P1) to 3.08 ± 0.02 % (day P14) as time progressed from day 1 to 14 significantly ($P<0.0005$). But there was an increase in the aldehyde content from day 21 to 38. In the 15ADA20G extract, the increase was from 5.7 ± 0.2 % (day 21) to 6.8 ± 0.06 % (day 14) and that of 15ADA20G300PRP extract the increase was from 3.2 ± 0.04 % (day P21) to 4.9 ± 0.03 % (day P28) as time

progressed from day 21 to 28 significantly (P<0.0005). The decrease in the aldehyde content up to day 14 (15ADA20G) and day 21(15ADA20G300PRP) in the extract may be due to the Schiff base formation between the aldehyde and amino groups present in the extract. The increase in the aldehyde content at days 21 and 28 may be due to the degradation of the Schiff base formed.

In the case of degraded hydrogel (Figure 45 C & D), collected after each time period, the aldehyde content was decreasing as days progressed from 1 to 28 in 15ADA20G and 15ADA20G300PRP. For 15ADA20G hydrogel, the decrease was from 14.4 ± 0.6 % (day 1) to 7.8 ± 0.1 % (day 28) and for 15ADA20G300PRP, the decrease was from 17.6 ± 0.3 % (day P1) to 7.8 ± 0.1 % (day P28) significantly (P<0.0005). The decrease in aldehyde content was due to the degradation of hydrogel.

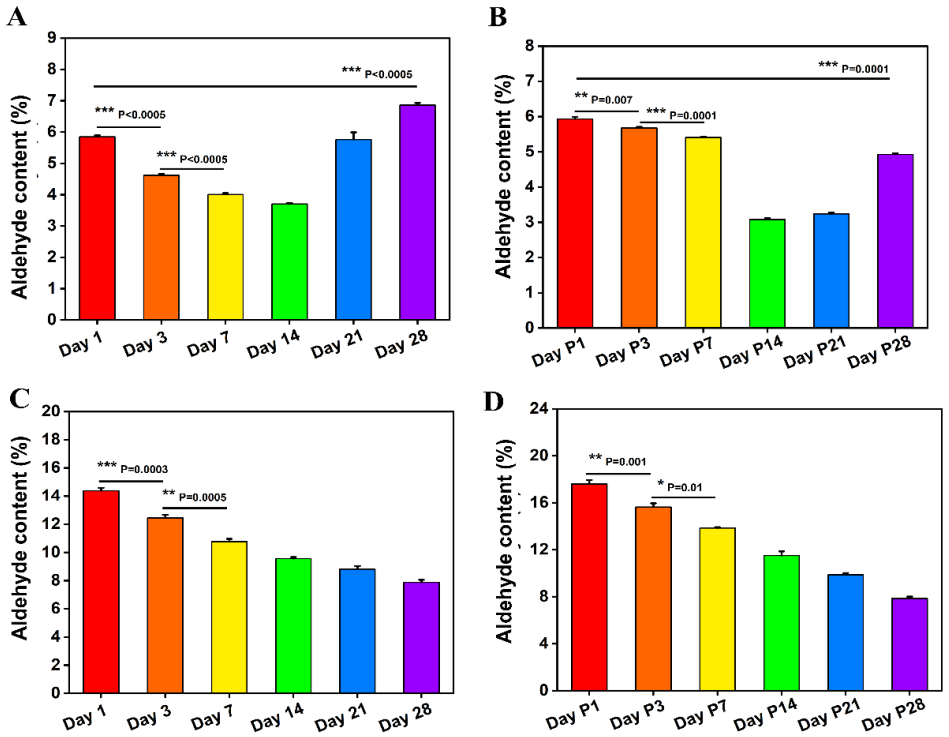

Figure 45. Aldehyde content after each time period A) 15ADA20G extract; B)15ADA20G300PRP extract; C) 15ADA20G hydrogel; D) 15ADA20G300PRP hydrogel.

4.4.1.7.4. Amino group estimation in the extract and in the hydrogel

Figure 46 A & B shows the amino content in the extract collected after each time period from 15ADA20G and 15ADA20G300PRP hydrogel. It was observed that as the day progressed from 1 to 28 there was a significant increase in the amino content in extracts collected from both the hydrogels. In the 15ADA20G extract, the amino content increased from 1.2 ± 0.03 % (day 1) to 2.03 ± 0.06 % (day 28) and that of 15ADA20G300PRP extract increased from 1.4 ± 0.08 % (day P1) to 2.5 ± 0.3 % (day P28) significantly ($P<0.0005$). But in the case of degraded hydrogel (Figure 46 C & D) collected after each time period, the amino content was decreasing as days progressed from 1 to 28 in 15ADA20G and

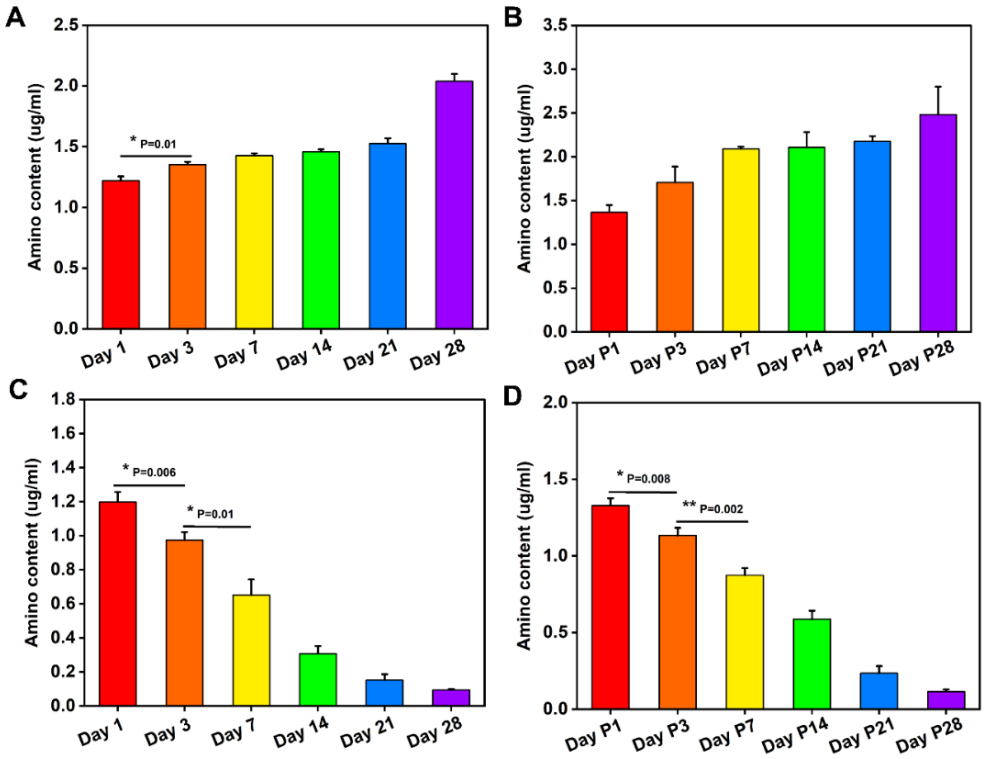

Figure 46. Amino content after each time period: A) 15ADA20G extract; B)15ADA20G300PRP extract; C) 15ADA20G hydrogel; D) 15ADA20G300PRP hydrogel.

15ADA20G300PRP. For 15ADA20G hydrogel, the decrease was from 1.3 ± 0.03 % (day 1) to 0.09 ± 0.003 % (day 28) and for 15ADA20G300PRP, the decrease was from 1.6 ± 0.04 % (day P1) to 0.1 ± 0.01 % (day P28) significantly ($P<0.0005$). The significant increase and decrease in the amino content in the extract and hydrogel, respectively, collected after each time period can be attributed to the hydrolytic degradation of gelatin.

4.4.1.7.5. Release of growth factor from 15ADA20G300PRP hydrogel

Literature shows that the amount of platelet-derived growth factor-BB (PDGF-BB) in PRP was relatively high, so it was selected as a representative to show the release kinetics of growth factors from PRP (Qiu et al., 2016). As determined by enzyme-linked immunosorbent assay (ELISA), PRP contained 273.9 ± 30.1 ng/ml of PDGF-BB. As day progressed from P1 to P28 the release of PDGF-BB increased from 44.3 ± 4.5 ng/ml to 91.1 ± 4.7 ng/ml (Figure 47 A). So at day P1, there was an initial burst release of 17 ± 0.9 % and as the day progressed to P28 the release % was 33.5 ± 2.5 % (Figure 47 B).

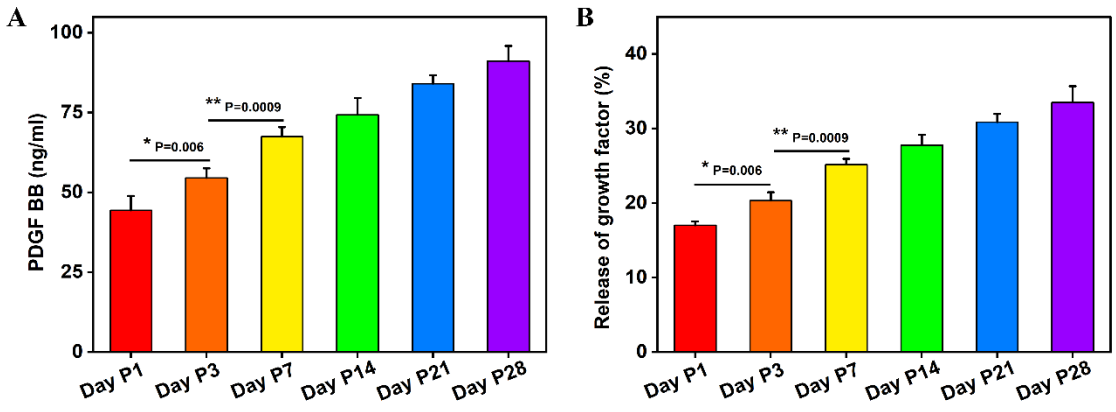

Figure 47. Release of PDGF BB growth factor from hydrogel A) release in ng/ml; B) release in %.

4.4.2. *In vitro* evaluation

4.4.2.1. Cell morphology and proliferation of isolated fibrochondrocytes

Fibrochondrocytes were isolated from rabbit meniscus. The meniscal tissue obtained after collagenase digestion was used for seeding in the flask. Cells started coming out from the explant (black arrow) after 3-4 days of culture as shown in figure 48 A. Two different cell types could be observed initially: round chondrocyte-like cells (arrowhead, Figure 48 A & B) and fibroblastic spindle-shaped cells. After 4–5 days the round chondrocyte-like cells started to disappear from the culture and after 1-2 weeks all cells had a fibroblastic spindle-shaped appearance. Similar observations were also seen while characterizing meniscal cells isolated from the human meniscus (Verdonk et al., 2005).

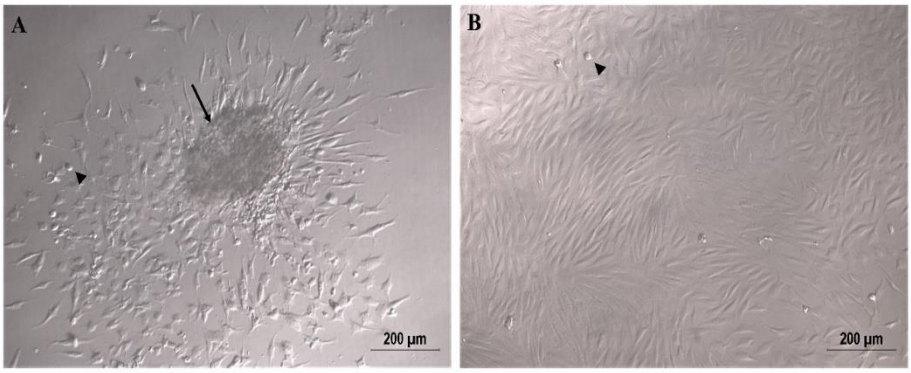

Figure 48. Phase contrast micrographs of fibrochondrocytes isolated from rabbit meniscus A) cells coming out from digested meniscal tissue (black arrow); B) monolayer of fibrochondrocytes; Arrow head: chondrocytes

4.4.2.2. *In vitro* evaluation of cytocompatibility of fibrochondrocytes seeded on hydrogels

4.4.2.2.1. Qualitative evaluation of cytocompatibility

Cell viability and proliferation are two important features to be considered when selecting materials for tissue regeneration and repair (Khan, 2019). Cytocompatibility of

fibrochondrocytes towards 15ADA20G and 15ADA20G300PRP hydrogels were evaluated by the direct contact method. Fibrochondrocytes were seeded on the top of hydrogels and allowed to proliferate for 48h. Phase-contrast micrographs (Figure 49 B and C) showed that fibrochondrocytes (dotted lines) proliferated on the surface of both the hydrogels (black arrow). Cells maintained similar morphology similar to control cells (Figure 49 A).

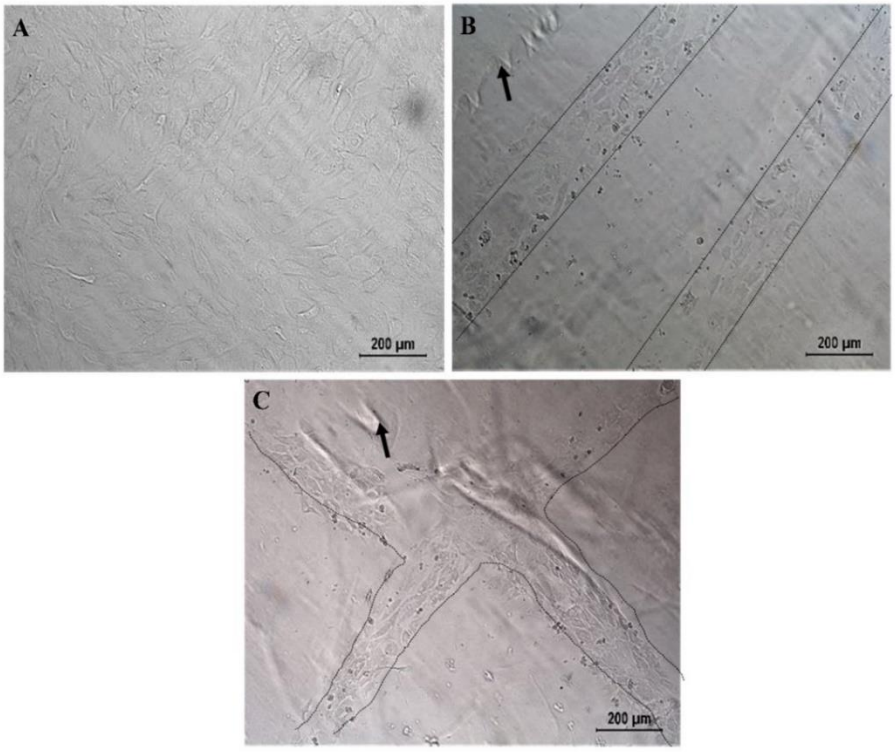

Figure 49. *In vitro* cytocompatibility evaluation; A) Control fibrochondrocytes; B) Cells seeded on 15ADA20G; C) cells seeded on 15ADA20G300PRP. Arrow represents hydrogel; Dotted lines: pattern of cell growth.

Visualization of cells in LIVE/DEAD cell viability assay was done using Acridine orange and EtBr staining (Kasibhatla et al., 2006). The staining help to distinguish normal, apoptotic and dead cells based on the fluorescence (Liu et al., 2015). Here, similar to control fibrochondrocytes (Figure 50 A), green fluorescence was shown by cells in direct

contact with the 15ADA20G (Figure 50 B) and 15ADA20G300PRP (Figure 50 C), which indicates its cytocompatible nature. Even though few dead cells (red) were also detected in all conditions, the number of live cells was higher compared to dead cells.

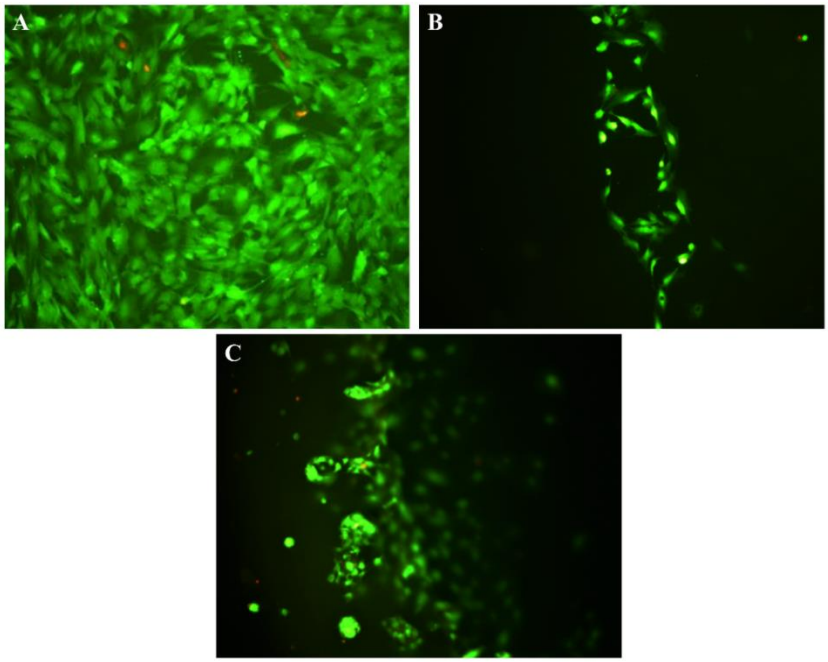

Figure 50. Confocal micrographs of fibrochondrocytes - Live-dead assay: A) Control fibrochondrocytes ; Cells seeded on B) 15ADA20G, C)15ADA20G300PRP

To analyze the proliferation of fibrochondrocytes on hydrogels, actin cytoskeleton staining was done with rhodamine-phalloidin/Hoechst *in vitro*. All the cell nuclei stained with Hoechst are in blue, and the F-actin filaments are in red. Similar to control cells (Figure 51 A), 15ADA20G (Figure 51 B) and 15ADA20G300PRP (Figure 51 C) support actin proliferation accompanied by filopodia extensions.

Type 1 collagen is abundantly present in fibrocartilage (Maynard and Downes, 2019). Here Collagen I antibody staining of fibrochondrocytes was done after seeding on top of hydrogels. Like the control fibrochondrocytes (Figure 52 A), 15ADA20G (Figure 52 B)

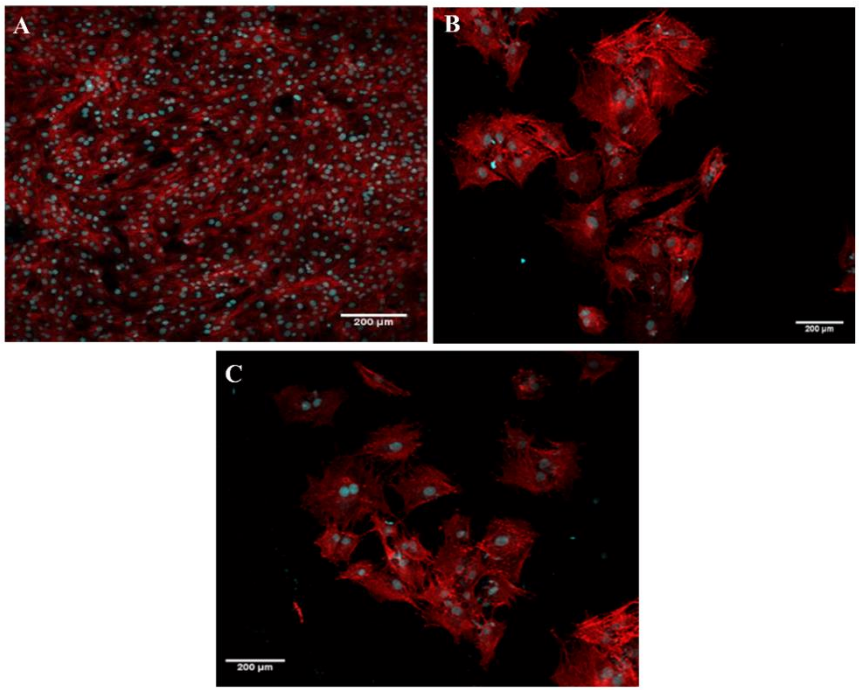

Figure 51. Confocal micrographs: Rhodamine-phalloidin/ Hoechst staining A) control fribrochondrocytes; cell seeded on B)15ADA20G, C)15ADA20G300PRP showing actin cytoskeletal morphology.

and 15ADA20G300PRP (Figure 52 C) hydrogels seeded with cells also showed positive staining of collagen type I. The results were similar to that obtained by Guo et al., 2021, where they seeded Polycaprolactone-decellularized meniscal extracellular matrix (PCL-MECM) scaffolds with fibrochondrocytes isolated from rabbit meniscus showed positive staining for collagen type 1.

Even though SEM was used to observe the pore size and the surface topography of scaffolds (Bhaarathy et al., 2014), it also enables the study of morphology, cell attachment and spreading of cells on the scaffolds (Sarika et al., 2014).

Spindle shaped cells (red arrow) can be seen attached to the surface of both 15ADA20G (figure 53 A) and 15ADA20G300PRP (figure 53 B) hydrogels. Similar observations were

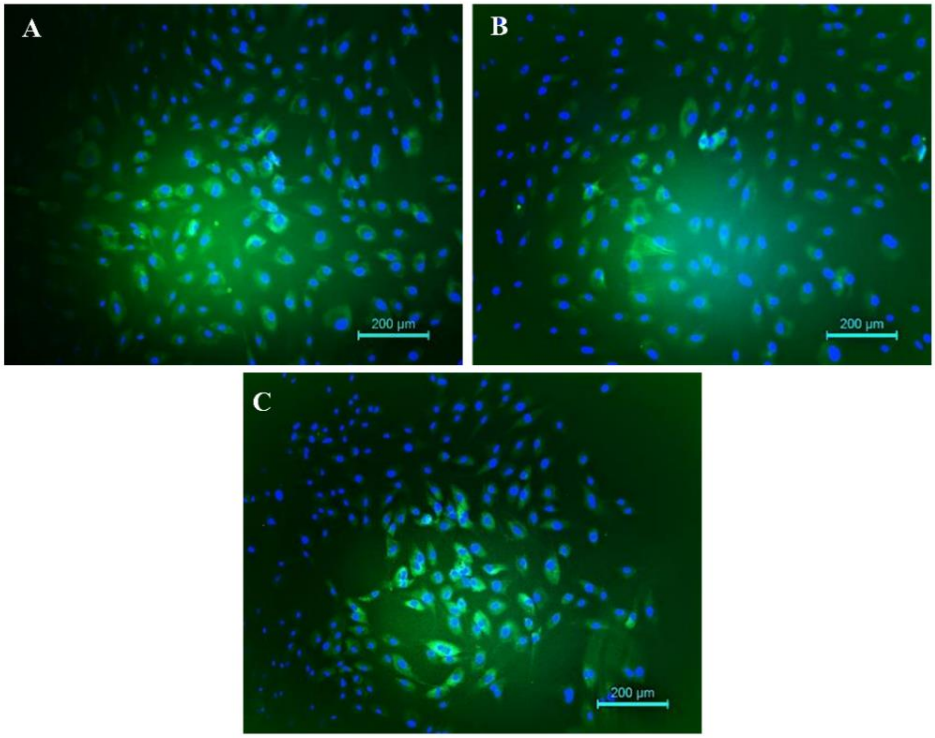

Figure 52. Confocal micrographs: Collagen 1 staining A) control fribrochondrocytes; cell seeded on B)15ADA20G, C)15ADA20G300PRP.

found when human meniscus cells were seeded on coaxial electrospun scaffolds. Here also cells attached to the entire surface of the scaffolds with an elongated morphology (Baek et al., 2019).

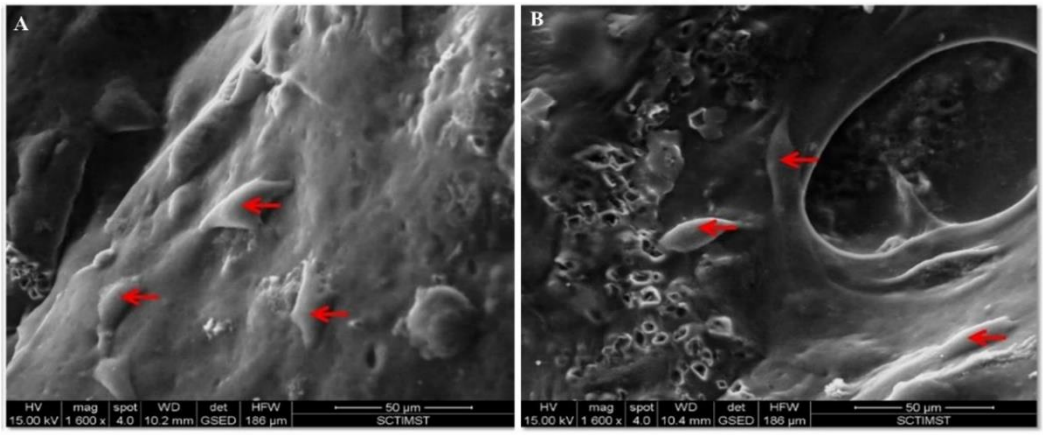

Figure 53. ESEM analysis of fibrochondrocyte seeded hydrogels: A) 15ADA20G; B) 15ADA20G300PRP. Red arrow represents the cells attached to the hydrogel surface.

4.4.2.2.2. Quantitative evaluation for cell proliferation

For the healing of meniscal tear migration of cells from the surrounding tissue is important. The influence of the various components of hydrogels on the metabolic activity of fibrochondrocytes was assessed by the reduction of resazurin to resorufin by the Alamar blue assay. It has been reported that ADAG hydrogels aid in the epithelial cell migration and healing of wounds (Balakrishnan et al., 2005b).

When fibrochondrocytes were cultured in the presence of 15ADA20G hydrogel, there was a significant ($P<0.05$) increase in cell proliferation as the time progressed from day 3 (95 ± 8 %) to day 21 (171 ± 12 %) (Figure 54 A). The addition of PRP on 15ADA20G hydrogel has an advantage on cell proliferation. There was a significant increase in the proliferation of cells on day 3 (109 ± 6 %), 7 (141 ± 10 %), 14 (159 ± 6 %) and 21 (191 ± 12 %) compared to 15ADA20G hydrogel.

The DNA content is assumed to be proportional to the cell number, revealing the proliferation of cells on a scaffold over time. From figure 54 B it was clear that DNA content increased significantly ($p < 0.05$) from 18.7 ± 0.3 to 35.1 ± 0.7 ng/mg for 15ADA20G as the days progressed from 3 to 21. When PRP was added to 15ADA20G, the DNA content increased from 26.1 ± 0.6 (day 3) to 42.7 ± 0.99 ng/mg (day 21). The DNA content had a significant increase when PRP was added to 15ADA20G hydrogel with respect to time.

The adhesion and proliferation of fibrochondrocytes could probably be due to the presence of cell binding Arg–Gly–Asp (RGD) adhesive motifs in gelatin which can be identified by cellular integrin proteins (Yang et al., 2016). Literature shows that growth factors will aid

in meniscal cell proliferation (Chen et al., 2018). The increased cell proliferation on 15ADA20G300PRP hydrogel may be due to the presence of growth factors in PRP.

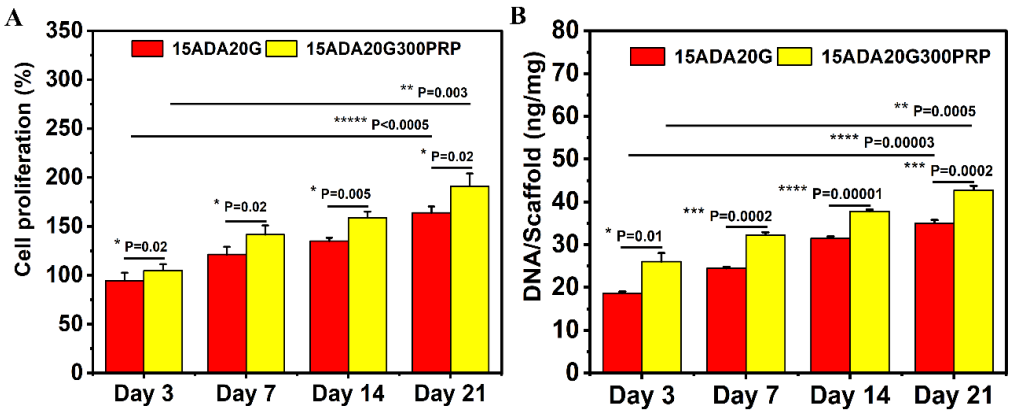

Figure 54. Quantitative evaluation of fibrochondrocyte proliferation: A) Alamar blue assay; B) DNA quantification.

4.4.2.3. Biochemical content analysis

Quantification of DNA, glycosaminoglycan (GAG), and collagen were used to measure the proliferation of fibrochondrocytes and ECM deposition (Yuan et al., 2016). Fibrochondrocytes can maintain a sufficient amount of GAG and collagen to resist external mechanical loading (Kim et al., 2018). So, quantitative analysis of GAG secreted by cells will provide an indication of the suitability of hydrogel for this application. Figure 55 A shows the sGAG normalized per unit scaffold mass of 15ADA20G and 15ADA20G300PRP. The GAG content increased significantly ($p < 0.05$) from 0.46 ± 0.01 μg/mg to 0.81 ± 0.03 μg/mg, 1.17± 0.01 μg/mg and 1.51 ± 0.02 μg/mg for 3, 7, 14 and 21 days, respectively, for 15ADA20G hydrogel and for 15ADA20G300PRP the sGAG increased significantly ($p<0.05$) from 0.78 ± 0.01 μg/mg to 1.2 ± 0.009 μg/mg, 1.61 ± 0.003 μg/mg and 1.93 ± 0.006 μg/mg. The addition of PRP significantly increased the

GAG production of 15ADA20G hydrogel by 58.9 %, 67.5 %, 72.6 % and 78.2 % for 3, 7, 14 and 21 days, respectively.

To evaluate the GAG secreted by fibrochondrocytes, we calculated GAG normalized for DNA content. This increased over time, as measured at days 3, 7, 14 and 21 days ($p \leq 0.05$). A significant increase in the GAG content was seen between 15ADA20G and 15ADA20G300PRP irrespective of the time periods (Figure 55 B).

Literature shows that mannuronic acid content in the alginate can also contribute to increased GAG production (Rey-Rico, Klich, Cucchiarini, & Madry, 2016). Compared to 15ADA20G hydrogel the GAG content per scaffold was higher for 15ADA20G300PRP hydrogel. PRP has various growth factors in it. Literature shows that the addition of growth factors to the monolayer of fibrochondrocytes helps in the production of GAG (Pangborn and Athanasiou, 2005). The incorporation of growth factors into electrospun PCL scaffolds also showed an increase in GAG production compared to control (Ionescu et al., 2012).

Figure 55 C shows the collagen content normalized per unit scaffold mass of 15ADA20G and 15ADA20G300PRP. The collagen content increased significantly ($p < 0.05$) from 8 ± 0.09 μg/mg (day 3) to 29.3 ± 0.1 μg/mg (day 21) for 15ADA20G hydrogel and for 15ADA20G300PRP the collagen content increased significantly ($p<0.05$)from 13.5 ± 1.6 μg/mg (day 3) to 37.4 ± 0.2 μg/mg (day 21). From figure 55 C it was also clear that the addition of PRP significantly increased the collagen content compared to 15ADA20G hydrogel irrespective of time periods. Using total collagen content normalized to corresponding DNA to assess collagen secretion, the collagen/DNA content in both the hydrogels showed the same trend as collagen production/scaffold at day 3 to day 21 (Figure

55 D). Collagen/DNA content was significantly higher ($p<0.05$) in 15ADA20G300PRP hydrogel for all the time period compared to 15ADA20G which indicates the effect of PRP in collagen secretion by the cells.

The increase in the collagen content in PRP incorporated hydrogel was due to the presence of various growth factors in it. Literature also reported that the addition of the growth factor TGF-β1 to the coculture of articular chondrocyte and fibrochondrocyte results in a 20 % increase in collagen deposition (Kalpakci et al., 2011).

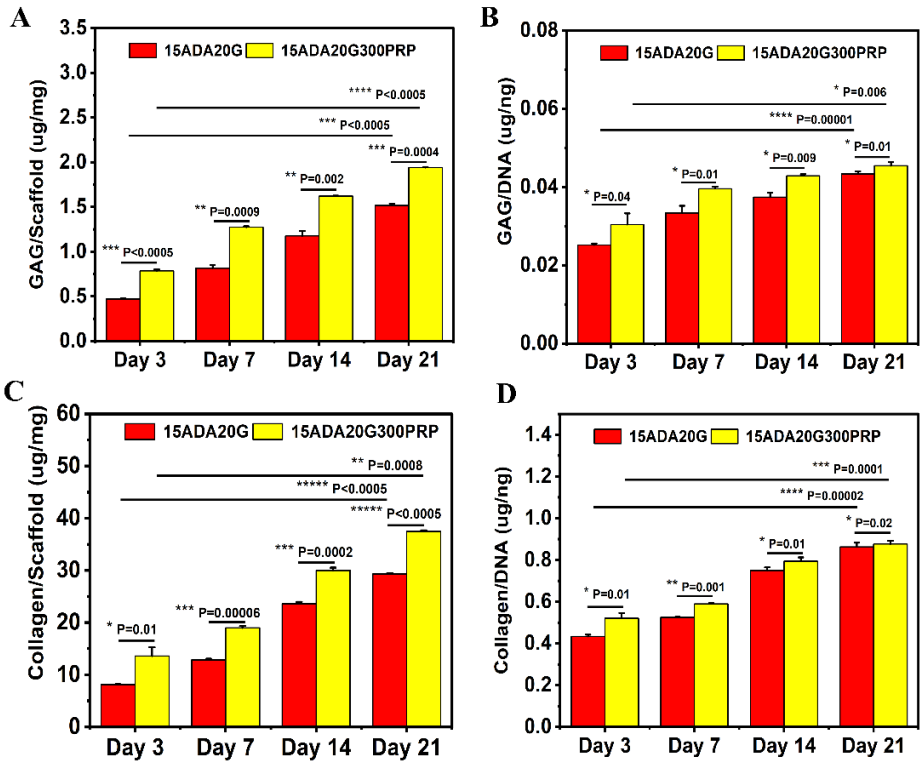

Figure 55. Biochemical content: A) GAG/scaffold; B) GAG/DNA; C) Collagen/scaffold; D) Collagen/DNA.

4.4.2.4. Real-Time PCR

Quantitative real-time RT-PCR was performed to assess the expression of collagen I (COL1A1), collagen II (COL2A1) and aggrecan (ACAN) in 15ADA20G and

15ADA20G300PRP hydrogels at 7 and 14 days. The target expression was normalized by GAPDH as a reference gene. Cells cultured in a monolayer were taken as control. On days 7 and 14, compared to control, 15ADA20G and 15ADA20G300PRP hydrogel showed a significant increase ($P<0.05$) in the expression of COL1A1, COL2A1 and ACAN (Figure 56 A-C). As the day progressed from 7 to 14 the COL1A1 gene expression of 15ADA20G and hydrogel increased from 4.7 ± 0.15 fold to 6.7 ± 0.51 fold and that of 15ADA20G300PRP increased from 6.7 ± 0.43 to 8.4 ± 0.36 fold. For the COL2A1 gene, the fold change was from 2.8 ± 0.26 to 4.4 ± 0.27 fold for 15ADA20G and 4.5 ± 0.4 to 6.1 ± 0.1 fold for 15ADA20G300PRP hydrogel, respectively, as days progressed from 7 to 14. The gene expression of ACAN increased from 4.1 ± 0.3 to 5.7 ± 0.5 for 15ADA20G and 6.1 ± 0.15 to 7.9 ± 0.7 fold for 15ADA20G300PRP as days progressed from 7 to 14. From figure 55 A-C it was also clear that the addition of PRP stimulated the expression of all these genes compared to 15ADA20G hydrogel.

Literature reveals that the addition of PRP to collagen hydrogel increased the gene expression of collagen 1 compared to the control group on 14 days of culture (Cheng et al., 2010). Collagen II and aggrecan gene expression were increased when adipose stem cells encapsulated in a 3D alginate scaffold were cultured in PRP containing DMEM media (Beigi et al., 2018).

4.4.2.5. *Ex vivo* evaluation of meniscal tear filled with hydrogel

Integration of hydrogel with meniscal tissue was one of the major issues related to injectable hydrogels. To assess the integration, a longitudinal tear was made in the pig meniscus and it was filled with hydrogel. The meniscal tear could be filled

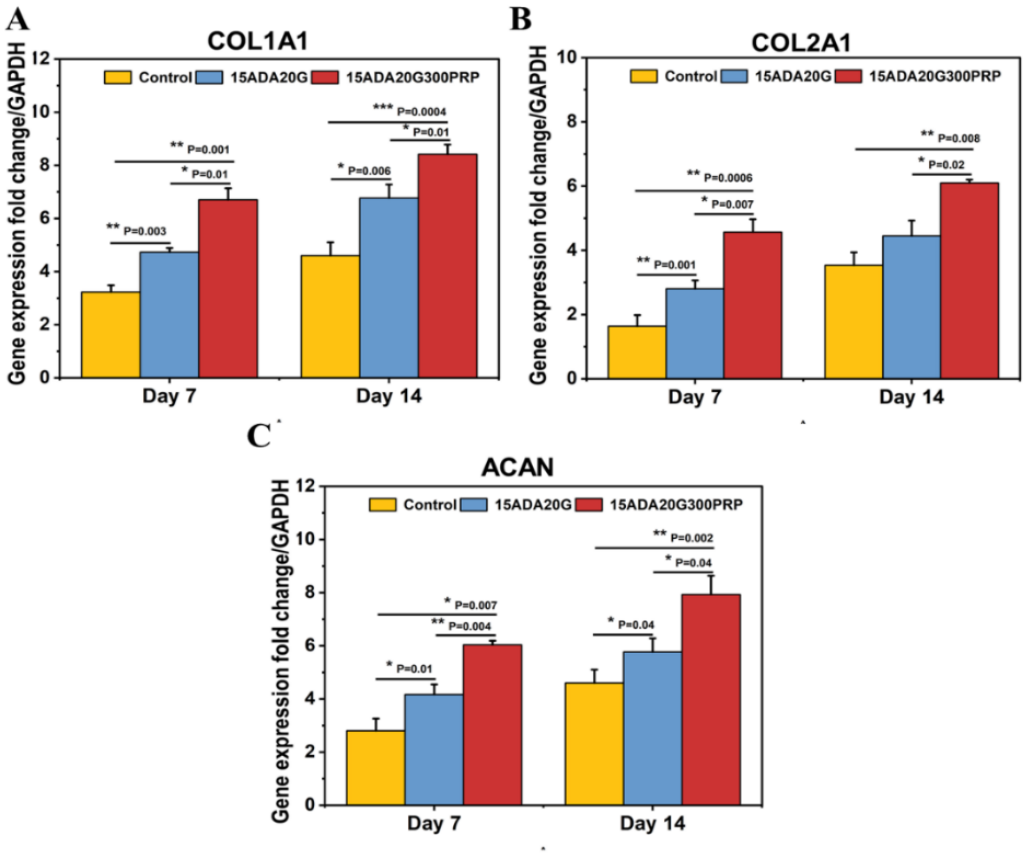

Figure 56. Real-time gene expression results showing fold increases of A) Collagen 1; B) Collagen II and C) Aggrecan.

successfully with 15ADA20G hydrogel and the gel tends to integrate with the surrounding tissue within 3 days in culture medium.

ESEM images (Figure 57 A) of gold-coated meniscal gel explant shows good integration of hydrogel (red arrow) to meniscal tissues. This observation was similar to that reported for oxidized carboxymethyl cellulose-gelatin injectable hydrogels used for cartilage repair (Balakrishnan et al., 2014a). This integration could probably be due to the presence of residual aldehyde groups present in ADA which in turn react with amino groups of collagen present in the tissue (Kanth et al., 2009). H & E staining (Figure 57 B & C) of

injectable hydrogel filled meniscal tear (black arrow) showed good space conformity and seamless tissue hydrogel interface. Figure 57 C shows the magnified image which clearly shows the integration of hydrogel with the surrounding tissues. Both fusiform and round-shaped cells can be seen in close vicinity to the hydrogel. The hydrogel remained intact with no signs of degradation.

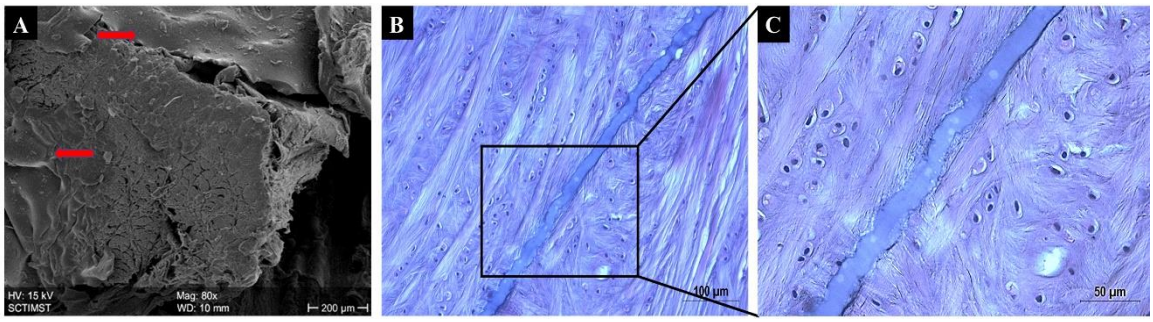

Figure 57. *Ex vivo* transplantation of hydrogel in an experimental meniscal defect model : A) ESEM of hydrogel/meniscal in interface (Red arrows indicate the hydrogel); B &C) Histology of hydrogel filled meniscal tear after 3 days of culture - H & E staining at different magnifications.

4.4.3. *In vivo* evaluation

4.4.3.1. Rabbit gait and behavior

Post-surgery experimental rabbits showed normal gait and behavior where they can walk, feed and drink ad libitum (Figure 58 A). There were no complications or significant weight gain observed. There was no postoperative infection at the wound site and all the wounds healed uneventfully (figure 58 B).

4.4.3.2. Gross evaluation of joint

The macroscopic observation of the operated joints was shown in figure 59. Panel I (A-D) shows the alignment and shape of the meniscus after 3 months post-surgery. The dotted line in figure 59 panel I A indicate the lateral (L) and medial (M) meniscii. In the control

Figure 58. Rabbit behaviour: A) Gait and movement; B) Knee joint after 3 months.

animal (Figure 59 panel I B) there observed a slight degeneration in the medial meniscus where the tear was made (Black arrow). But in both the hydrogel groups (Figure 59 panel I B & C) the medial meniscus was intact with no sign of degeneration and appear similar to the native meniscus.

Panels II and III of figure 59 represent the femur and tibia of the operated knee joint after three months. No sign of degeneration was seen in the control and test groups.

4.4.3.3. Histological evaluation and semi-quantitative scoring

Representative microphotographs of H & E, safranin O, Alcian Blue and Masson's trichrome staining after 1 month and 3 months of surgery are shown in Figure 60 (A-L) and Figure 60 (M-X), respectively. In the control group, the tear was seen (black arrow) at 1 month (Figure 60 A). In the 15ADA20G group, histological analysis done 1 month after surgery showed the presence of hydrogel in the meniscal tear (red arrow in the H & E staining, Figure 60 E). There was cell migration and proliferation from the peripheral tissue. But the hydrogel remnants were not seen in the 15ADA20G300PRP group even at

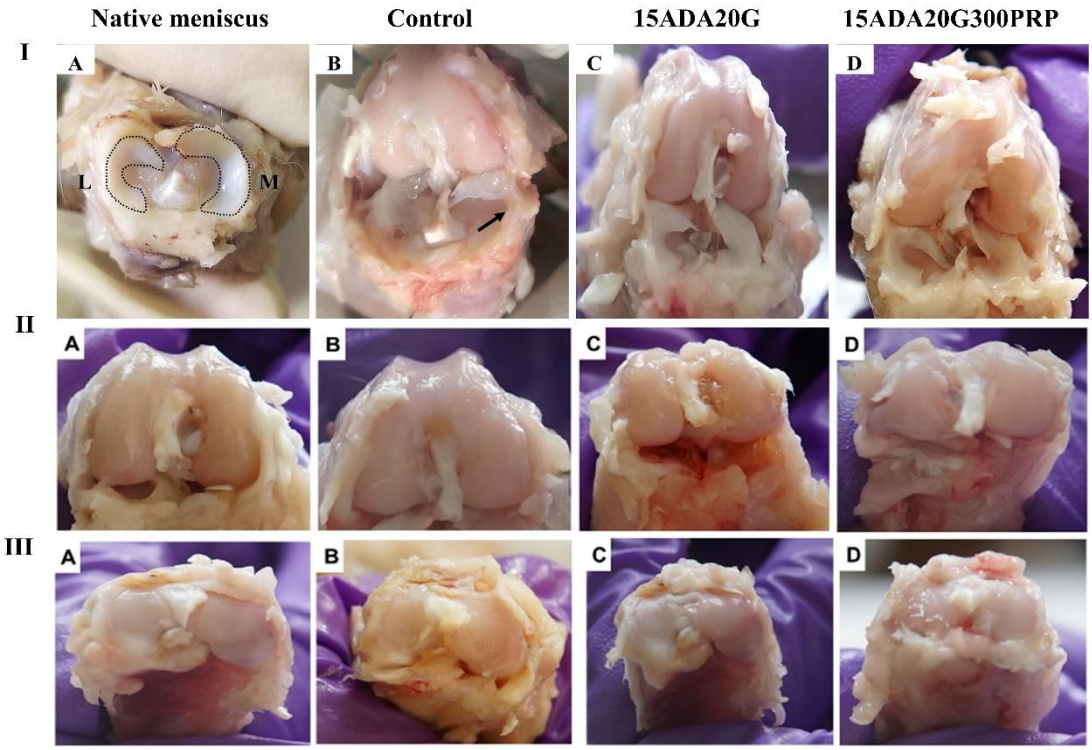

Figure 59. Macroscopic observation of operated knee joint at 3 months I) Menisci; II) Femur and III) Tibia.

one month post surgery. Here the cell migration from the surrounding tissues was higher compared to the 15ADA20G group (yellow arrow) (Figure 60 I). At 3 months post surgery no hydrogel was observed in both the 15ADA20G (Figure 60 Q) and 15ADA20G300PRP groups (Figure609 U)). There was only partial healing of meniscal tear in the control group at 3 months (Figure 60 M black arrow). Compared to control, the meniscal tear filled with both hydrogel compositions healed better. The reparative tissue was attached to the edges of the native meniscal tissue. The boundary between newly formed tissue and native meniscus was not seen. The newly formed tissue at 3 months post surgery had oval-shaped cells and rich GAG components, which stained red with safranin O in 15ADA20G300PRP hydrogel groups (Figure 60 V). The regenerated tissues (Figure 60 V) showed similar

staining to that of the inner portion of the native meniscus (Figure 60 II). Literature also showed that healthy meniscus showed a higher concentration of GAGs in the inner area (Polito et al., 2020). Consistent with safranin-O staining, alcian blue staining was higher in the 15ADA20G300PRP hydrogel (Figure 60 W) group and was similar to that of the native meniscus (Figure 60 III). Masson's trichrome of the meniscal tissue sections revealed the presence of collagen (Kang et al., 2006). The collagen structures regenerated meniscus at 3 months post surgery (Figure 60 L) were similar to those of native meniscus (Figure 60 IV) and more organized than those of neomenisci at one month (Figure 60 X, 15ADA20G300PRP group, Masson's Trichrome staining).

Meniscal tissue regeneration induced by the injection of 15ADA20G and 15ADA20G300PRP hydrogels compared to control were analyzed by a validated and published semi-quantitative meniscus scoring system (Figure 61 A and B) (Oda et al., 2015; Zellner et al., 2017). The Ishida score based on the reparative tissue bonding, presence of fibrochondrocytes and Safranin-O staining was significantly high for both hydrogel groups compared to control. The quality of the regenerated tissue in the 15ADA20G300PRP (5.50 ± 0.15 and 5.90 ± 0.05), evaluated based on Ishida score, was significantly higher than that in control (2.00 ± 0.06, $p = 0.0002$ and 3.0 ± 0.1, $p = 0.0002$) and 15ADA20G (5.00 ± 0.12, $p = 0.03$ and 5.5 ± 0.1, $p = 0.03$), respectively, for first and 3rd month post surgery (Figure 61 A). In another scoring system based on the overall quality of the repaired meniscal tissue, the 15ADA20G300PRP (16.7 ± 0.2 and 17.1 ± 0.1) group has a significantly higher score compared to the control (9.9 ± 0.1, $p = 0.0003$ and

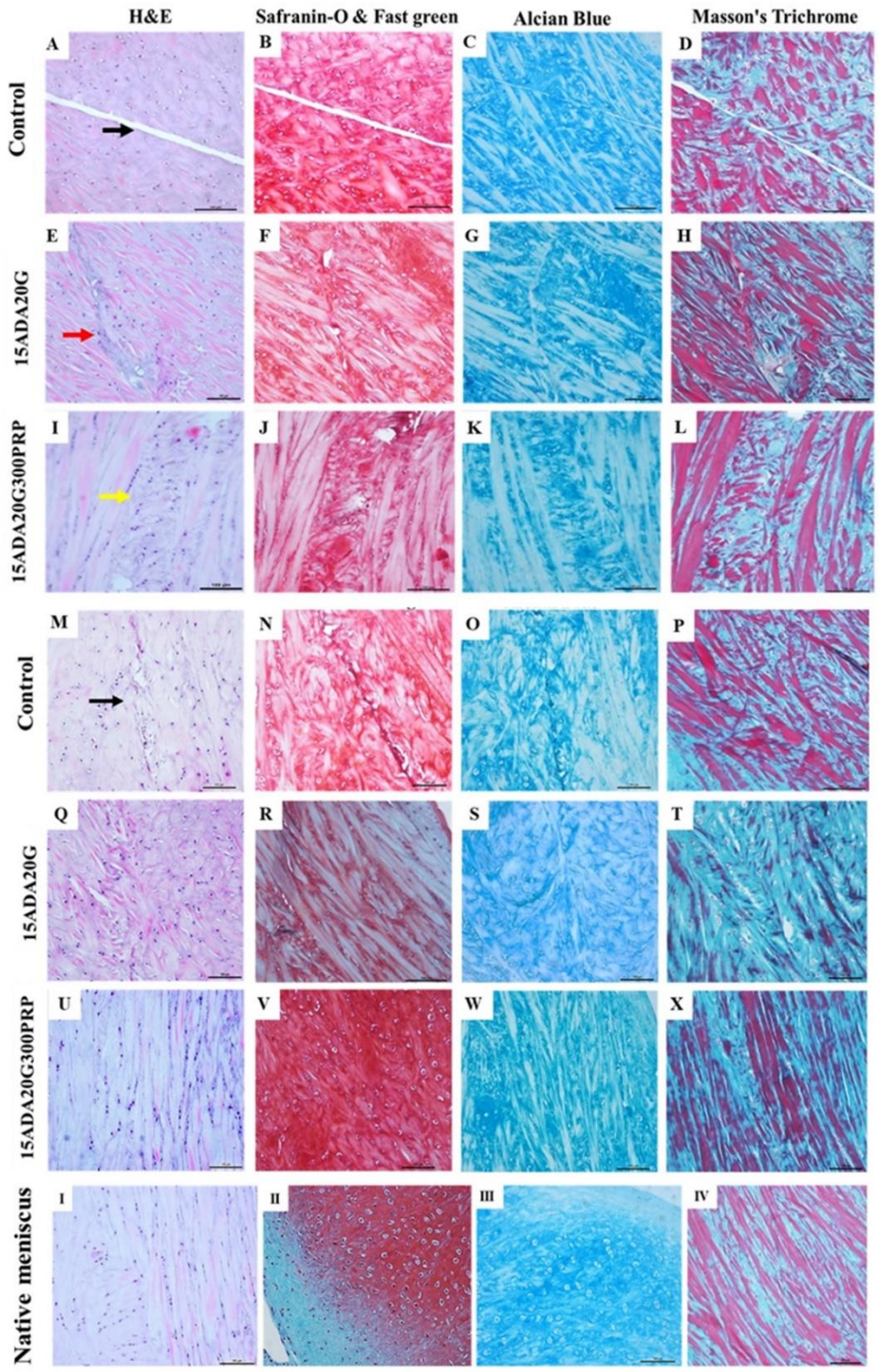

Figure 60. Histopathological evaluation of meniscal tear after injecting with 15ADA20G and 15ADA20G300PRP hydrogel compared to control and native meniscus at 1 month and 3 months.

9.8 ± 0.2, p =0.0003) and 15ADA20G (14.9 ± 0.06, p = 0.01 and 16.8 ± 0.1, p = 0.01) for

1 month and 3 months post-surgery, indicating its better regenerative potential.

The addition of PRP clearly benefits the healing of the meniscal tear. From the literature, it was clear that the use of PRP was better than the use of a single isolated growth factor (Longo et al., 2011). Since PRP is an autologous blood preparation that contains abundant growth factors such as TGF-β, PDGF, VEGF and HGF, it can regulate the activities to stimulate the production of extracellular matrix (Forriol, 2009; Pangborn and Athanasiou, 2005). Literature also supports the results that PRP benefits in better healing of meniscal tear when used along with various natural polymers like gelatin (Ishida et al., 2007) and hyaluronan (Yan et al., 2020).

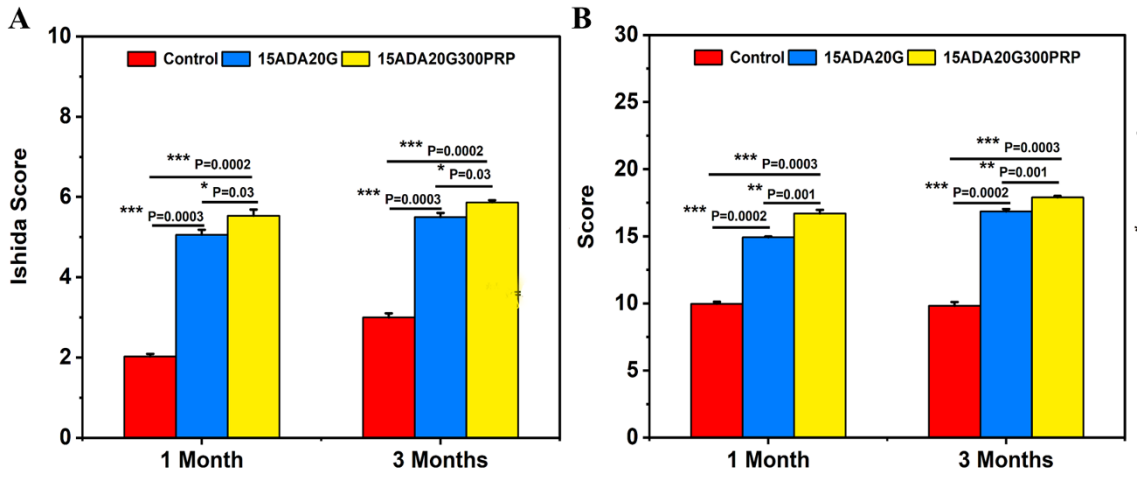

Figure 61. Semi-quantitative meniscal scoring: A) Ishida score; B) Scoring based on quality of regenerated tissue.

4.4.3.4. Biochemical content evaluation in explant meniscus

The GAG and collagen estimation of explanted meniscal tissue collected after 1 and 3 months of hydrogel implantation was shown in figure 62 A & B. The GAG and collagen content was compared with that of the native meniscus. The native meniscus has a GAG and collagen content of 10 ± 0.2 µg/mg and 241.9 ± 3.2 µg/mg, respectively. At one month

post surgery, the GAG and collagen content in the regenerated tissue was less compared to the native meniscus in 15ADA20G (4.50 ± 0.09 µg/mg and 116.9 ± 2.9 µg/mg) and 15ADA20G300PRP (5.00 ± 0.08 µg/mg and 168 ± 1.6 µg/mg) groups, respectively. But at 3 months there was a significant increase in the GAG and collagen content of the regenerated tissue in 15ADA20G (6.00 ± 0.08 µg/mg and 136.9 ± 1.1 µg/mg) and in 15ADA20G300PRP (6.7 ± 0.04 µg/mg and 188.3 ± 1.2 µg/mg) groups, respectively. GAG and collagen content in the 15ADA20G300PRP hydrogel implanted meniscus was higher than the 15ADA20G group. The increase in the GAG and collagen content in the 15ADA20G300PRP was due to the various growth factors present in PRP. During the degradation of hydrogel, the release of PDGF was noted. Literature shows that growth factors may promote meniscal repair and regeneration via different mechanisms like recruitment and enhancement of fibrochondrogenic cell proliferation and stimulation of ECM production (Chen et al., 2018).

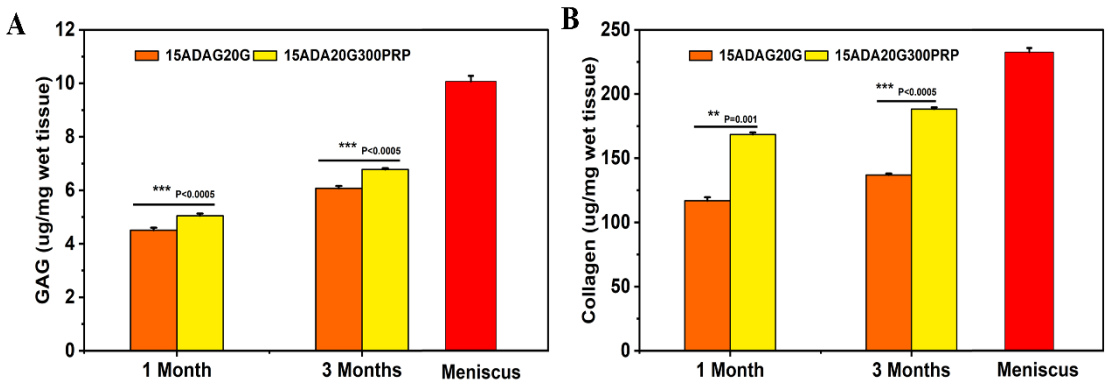

Figure 62. Biochemical content evaluation in explant tissue: A) GAG; B) Collagen.

A similar trend was also shown *in vitro* when fibrochondrocytes seeded 15ADA20G300PRP hydrogels were cultured for 21 days. Even though the GAG and

collagen content in the hydrogel group was less compared to the native meniscus, there was an increase due to tissue regeneration as time progressed from 1 to 3 months. Literature also supports the results. When PGA/PLGA scaffold seeded with allogenic meniscal cells was implanted into the rabbit menisci, the newly-formed tissue at the 10th week has collagen and GAG content similar to that of native tissue (Kang et al., 2006).

CHAPTER 5

5. SUMMARY AND CONCLUSION

This work was undertaken with the specific aim of developing an injectable hydrogel system based on ADA and gelatin with and without PRP for meniscal tear healing. To achieve these aims the plan of work was undertaken under four phases with the objectives: (i) To develop a suitable alginate dialdehyde-gelatin hydrogel (ADA-Gel) for meniscal repair, (ii) To characterize the ADA-Gel (Physicochemical, mechanical, gelation behavior, etc.), (iii) To evaluate cell-ADA Gel interactions *in vitro,* and (iv) To evaluate ADA-Gel as a meniscal substitute in a rabbit model *in vivo.*

An array of self-crosslinking, in situ forming, injectable hydrogel compositions were prepared using ADA, gelatin and PRP. The formation of the hydrogel was aided through the borate complexation of ADA and Schiff's base reaction. The gelation time of hydrogels was tuned by adjusting the concentration of borax so that the clinically required working time of about 4 min was obtained. The degree of crosslinking, water uptake and compressive strength of hydrogel were controlled by varying the concentration of ADA and Gelatin and PRP. The final formulation chosen was 15ADA20G and 15ADA20G300PRP. The porous structure of both the hydrogels and its pore size distribution enabled fibrochondrocytes to proliferate on the hydrogel matrix.

The *in vitro* evaluation using fibrochondrocytes proved the cytocompatible nature of both hydrogels. The addition of PRP has an added advantage in the cell proliferation, ECM synthesis and expression of various genes related to the meniscal tissue. *Ex vivo* evaluation

of hydrogel on pig meniscal tear showed proper integration of hydrogel with the surrounding tissues.

Further, the *in vivo* implantation of hydrogel in the meniscal tear in rabbits showed good healing compared to control. Histology showed good integration of hydrogel with the surrounding meniscal tissue and better cellular infiltration into the torn area when 15ADA20G300PRP hydrogel was injected. The regenerated tissue was similar to the native meniscal tissue when PRP incorporated hydrogel was injected. The regenerated tissue could enhance the GAG and collagen content comparable to that of the native meniscus. The use of simple chemistry and ease of control of the cellular behavior makes this hydrogel a potential biomaterial for mending meniscal tears in clinical orthopedic reconstructive surgeries.

The future perspective of this work includes the implantation and evaluation of the injectable hydrogel system in a large animal model.

REFERENCES

Abou-Zeid, R.E., Awwad, N.S., Nabil, S., Salama, A., Youssef, M.A., 2019. Oxidized alginate/gelatin decorated silver nanoparticles as new nanocomposite for dye adsorption. Int. J. Biol. Macromol. 141, 1280–1286.

Abram, S.G.F., Hopewell, S., Monk, A.P., Bayliss, L.E., Beard, D.J., Price, A.J., 2020. Arthroscopic partial meniscectomy for meniscal tears of the knee: a systematic review and meta-analysis. Br. J. Sports Med. 54, 652–663.

Adams, M.E., Billingham, M.E., Muir, H., 1983. The glycosaminoglycans in menisci in experimental and natural osteoarthritis. Arthritis Rheum. 26, 69–76.

Ahearne, M., Liu, I.K.-K., 2008. Mechanical Characterisation of Hydrogels for Tissue Engineering Applications. Top. Tissue Eng 4.

Alban, S., Schauerte, A., Franz, G., 2002. Anticoagulant sulfated polysaccharides: Part I. Synthesis and structure–activity relationships of new pullulan sulfates. Carbohydr. Polym. 47, 267–276.

Alonso, J.M., Andrade del Olmo, J., Perez Gonzalez, R., Saez-Martinez, V., 2021. Injectable Hydrogels: From Laboratory to Industrialization. Polymers 13, 650.

Andrish, null, 1996. Meniscal Injuries in Children and Adolescents: Diagnosis and Management. J. Am. Acad. Orthop. Surg. 4, 231–237.

Angele, P., Kujat, R., Koch, M., Zellner, J., 2014. Role of mesenchymal stem cells in meniscal repair. J. Exp. Orthop. 1, 12.

Anz, A.W., Hackel, J.G., Nilssen, E.C., Andrews, J.R., 2014. Application of biologics in the treatment of the rotator cuff, meniscus, cartilage, and osteoarthritis. J. Am. Acad. Orthop. Surg. 22, 68–79.

Arnoczky, S.P., Warren, R.F., 1982. Microvasculature of the human meniscus. Am. J. Sports Med. 10, 90–95.

Arnoczky, S.P., Warren, R.F., Spivak, J.M., 1988. Meniscal repair using an exogenous fibrin clot. An experimental study in dogs. J. Bone Joint Surg. Am. 70, 1209–1217.

Baek, J., Lotz, M.K., D'Lima, D.D., 2019. Core-Shell Nanofibrous Scaffolds for Repair of Meniscus Tears. Tissue Eng. Part A 25, 1577–1590.

Bai, X., Fang, R., Zhang, S., Shi, X., Wang, Z., Chen, X., Yang, J., Hou, X., Nie, Y., Li, Y., Tian, W., 2013. Self-cross-linkable hydrogels composed of partially oxidized alginate and gelatin for myocardial infarction repair. J. Bioact. Compat. Polym. 28, 126–140.

Bajpai, S.K., Bajpai, M., Shah, F.F., 2016. Alginate dialdehyde (AD)-crosslinked casein films: synthesis, characterization and water absorption behavior. Des. Monomers Polym. 19, 406–419.

Bajpai, S.K., Bajpai, M., Sharma, L., 2006. Investigation of Water Uptake Behavior and Mechanical Properties of Superporous Hydrogels. J. Macromol. Sci. Part A 43, 507–524.

Balakrishnan, B., Jayakrishnan, A., 2005. Self-cross-linking biopolymers as injectable in situ forming biodegradable scaffolds. Biomaterials 26, 3941–3951.

Balakrishnan, B., Joshi, N., Jayakrishnan, A., Banerjee, R., 2014a. Self-crosslinked oxidized alginate/gelatin hydrogel as injectable, adhesive biomimetic scaffolds for cartilage regeneration. Acta Biomater. 10, 3650–3663.

Balakrishnan, B., Joshi, N., Jayakrishnan, A., Banerjee, R., 2014b. Self-crosslinked oxidized alginate/gelatin hydrogel as injectable, adhesive biomimetic scaffolds for cartilage regeneration. Acta Biomater. 10, 3650–3663.

Balakrishnan, B., Lesieur, S., Labarre, D., Jayakrishnan, A., 2005. Periodate oxidation of sodium alginate in water and in ethanol-water mixture: a comparative study. Carbohydr. Res. 340, 1425–1429.

Baniasadi, H., Mashayekhan, S., Fadaoddini, S., Haghirsharifzamini, Y., 2016. Design, fabrication and characterization of oxidized alginate–gelatin hydrogels for muscle tissue engineering applications , Design, fabrication and characterization of oxidized alginate–gelatin hydrogels for muscle tissue engineering applications. J. Biomater. Appl. 31, 152–161.

Banks, S.R., Enck, K., Wright, M., Opara, E.C., Welker, M.E., 2019. Chemical Modification of Alginate for Controlled Oral Drug Delivery. J. Agric. Food Chem. 67, 10481–10488.

Baynat, C., Andro, C., Vincent, J.P., Schiele, P., Buisson, P., Dubrana, F., Gunepin, F.X., 2014. Actifit® synthetic meniscal substitute: Experience with 18 patients in Brest, France. Orthop. Traumatol. Surg. Res., Proceedings of the French Arthroscopy Society 100, S385–S389.

Beaufils, P., Becker, R., Verdonk, R., Aagaard, H., Karlsson, J., 2015. Focusing on results after meniscus surgery. Knee Surg. Sports Traumatol. Arthrosc. 23, 3–7.

Beigi, M.-H., Atefi, A., Ghanaei, H.-R., Labbaf, S., Ejeian, F., Nasr-Esfahani, M.-H., 2018. Activated platelet-rich plasma improves cartilage regeneration using adipose stem cells encapsulated in a 3D alginate scaffold. J. Tissue Eng. Regen. Med. 12, 1327–1338.

Bertoldi, S., Farè, S., Tanzi, M.C., 2011. Assessment of scaffold porosity: the new route of micro-CT. J. Appl. Biomater. Biomech. JABB 9, 165–175.

Berton, A., Longo, U.G., Candela, V., Greco, F., Martina, F.M., Quattrocchi, C.C., Denaro, V., 2020. Quantitative Evaluation of Meniscal Healing Process of Degenerative Meniscus Lesions Treated with Hyaluronic Acid: A Clinical and MRI Study. J. Clin. Med. 9.

Bhaarathy, V., Venugopal, J., Gandhimathi, C., Ponpandian, N., Mangalaraj, D., Ramakrishna, S., 2014. Biologically improved nanofibrous scaffolds for cardiac tissue engineering. Mater. Sci. Eng. C Mater. Biol. Appl. 44, 268–277.

Bhattacharyya, T., Gale, D., Dewire, P., Totterman, S., Gale, M.E., McLaughlin, S., Einhorn, T.A., Felson, D.T., 2003. The clinical importance of meniscal tears demonstrated by magnetic resonance imaging in osteoarthritis of the knee. J. Bone Joint Surg. Am. 85, 4–9.

Biçer, E.K., Aydoğdu, S., Sur, H., 2016. The Structure, Function, and Healing of the Meniscus. In: Korkusuz, F. (Ed.), Musculoskeletal Research and Basic Science. Springer International Publishing, Cham, pp. 405–427.

Bishop, M., Shahid, N., Yang, J., Barron, A.R., 2004. Determination of the mode and efficacy of the cross-linking of guar by borate using MAS 11B NMR of borate cross-linked guar in combination with solution 11B NMR of model systems. Dalton Trans. 2621–2634.

Bleakley, C.M., O'Connor, S., Tully, M.A., Rocke, L.G., MacAuley, D.C., McDonough, S.M., 2007. The PRICE study (Protection Rest Ice Compression Elevation): design of a randomised controlled trial comparing standard versus cryokinetic ice applications in the management of acute ankle sprain [ISRCTN13903946]. BMC Musculoskelet. Disord. 8, 125.

Boswell, S.G., Cole, B.J., Sundman, E.A., Karas, V., Fortier, L.A., 2012. Platelet-Rich Plasma: A Milieu of Bioactive Factors. Arthroscopy 28, 429–439.

Bouhadir, K.H., Lee, K.Y., Alsberg, E., Damm, K.L., Anderson, K.W., Mooney, D.J., 2001. Degradation of Partially Oxidized Alginate and Its Potential Application for Tissue Engineering. Biotechnol. Prog. 17, 945–950.

Bracht, H., Verdonk, R., Verbruggen, G., Elewaut, D., Verdonk, P., 2007. Cell-based meniscus tissue engineering. Top. Tissue Eng. 3.

Bružauskaitė, I., Bironaitė, D., Bagdonas, E., Bernotienė, E., 2016. Scaffolds and cells for tissue regeneration: different scaffold pore sizes—different cell effects. Cytotechnology 68, 355–369.

Bubnis, W.A., Ofner, C.M., 1992. The determination of epsilon-amino groups in soluble and poorly soluble proteinaceous materials by a spectrophotometric method using trinitrobenzenesulfonic acid. Anal. Biochem. 207, 129–133.

Buma, P., Ramrattan, N.N., van Tienen, T.G., Veth, R.P.H., 2004. Tissue engineering of the meniscus. Biomaterials 25, 1523–1532.

Cai, F.-F., Heid, S., Boccaccini, A.R., 2020. Potential of laponite incorporated oxidized alginate-gelatin (ADA-GEL) composite hydrogels for extrusion-based 3D printing. J. Biomed. Mater. Res. B Appl. Biomater.

Cai, K., Zhang, J., Deng, L., Yang, L., Hu, Y., Chen, C., Xue, L., Wang, L., 2007. Physical and Biological Properties of a Novel Hydrogel Composite Based on Oxidized Alginate, Gelatin and Tricalcium Phosphate for Bone Tissue Engineering. Adv. Eng. Mater. 9, 1082–1088.

Campbell, S.E., Sanders, T.G., Morrison, W.B., 2001. MR imaging of meniscal cysts: incidence, location, and clinical significance. AJR Am. J. Roentgenol. 177, 409–413.

Cengiz, I.F., Pereira, H., Espregueira-Mendes, J., Oliveira, J.M., Reis, R.L., 2017. Treatments of Meniscus Lesions of the Knee: Current Concepts and Future Perspectives. Regen. Eng. Transl. Med. 3, 32–50.

Chamberlain, N.H., Cunningham, G.E., Speakman, J.B., 1946. Alginic Acid Diacetate. Nature 158, 553–553.

Chanasit, W., Gonzaga, Z.J.C., Rehm, B.H.A., 2020. Analysis of the alginate O-acetylation machinery in Pseudomonas aeruginosa. Appl. Microbiol. Biotechnol. 104, 2179–2191.

Chatain, F., Adeleine, P., Chambat, P., Neyret, P., Société Française d'Arthroscopie, 2003. A comparative study of medial versus lateral arthroscopic partial meniscectomy on stable knees: 10-year minimum follow-up. Arthrosc. J. Arthrosc. Relat. Surg. Off. Publ. Arthrosc. Assoc. N. Am. Int. Arthrosc. Assoc. 19, 842–849.

Chen, H., Xing, X., Tan, H., Jia, Y., Zhou, T., Chen, Y., Ling, Z., Hu, X., 2017. Covalently antibacterial alginate-chitosan hydrogel dressing integrated gelatin microspheres

containing tetracycline hydrochloride for wound healing. Mater. Sci. Eng. C Mater. Biol. Appl. 70, 287–295.

Chen, J., Liu, Z., Chen, M., Zhang, H., Li, X., 2016. Electrospun Gelatin Fibers with a Multiple Release of Antibiotics Accelerate Dermal Regeneration in Infected Deep Burns. Macromol. Biosci. 16, 1368–1380.

Chen, M., Guo, W., Gao, S., Hao, C., Shen, S., Zhang, Z., Wang, Zhenyong, Wang, Zehao, Li, X., Jing, X., Zhang, X., Yuan, Z., Wang, M., Zhang, Y., Peng, J., Wang, A., Wang, Y., Sui, X., Liu, S., Guo, Q., 2018. Biochemical Stimulus-Based Strategies for Meniscus Tissue Engineering and Regeneration. BioMed Res. Int. 2018, e8472309.

Chen, P.-R., KANG, P.-L., SU, W.-Y., Lin, F.-H., Chen, M.-H., 2005. The evaluation of thermal properties and in vitro test of carbodiimide or glutaraldehyde cross-linked gelatin for PC 12 cells culture. Biomed. Eng.-Appl. Basis Commun. - BIOMED ENG-APPL BASIS COMMUN 17.

Chen, X., Fan, M., Tan, H., Ren, B., Yuan, G., Jia, Y., Li, J., Xiong, D., Xing, X., Niu, X., Hu, X., 2019. Magnetic and self-healing chitosan-alginate hydrogel encapsulated gelatin microspheres via covalent cross-linking for drug delivery. Mater. Sci. Eng. C 101, 619–629.

Cheng, M., Wang, H., Yoshida, R., Murray, M.M., 2010. Platelets and plasma proteins are both required to stimulate collagen gene expression by anterior cruciate ligament cells in three-dimensional culture. Tissue Eng. Part A 16, 1479–1489.

Chiari, C., Koller, U., Kapeller, B., Dorotka, R., Bindreiter, U., Nehrer, S., 2008. Different Behavior of Meniscal Cells in Collagen II/I,III and Hyaff-11 Scaffolds In Vitro. Tissue Eng. Part A 14, 1295–1304.

Chun, Y.Y., Yap, Z.L., Seet, L.F., Chan, H.H., Toh, L.Z., Chu, S.W.L., Lee, Y.S., Wong, T.T., Tan, T.T.Y., 2021. Positive-charge tuned gelatin hydrogel-siSPARC injectable for siRNA anti-scarring therapy in post glaucoma filtration surgery. Sci. Rep. 11, 1470.

Chung, Y.-M., Simmons, K.L., Gutowska, A., Jeong, B., 2002. Sol−Gel Transition Temperature of PLGA-g-PEG Aqueous Solutions. Biomacromolecules 3, 511–516.

Cinarli, A., Gürbüz, D., Tavman, A., Birteksöz, A.S., 2011. Synthesis, spectral characterizations and antimicrobial activity of some Schiff bases of 4-chloro-2-aminophenol. Bull. Chem. Soc. Ethiop. 25.

Cole, B.J., Carter, T.R., Rodeo, S.A., 2003. Allograft meniscal transplantation: background, techniques, and results. Instr. Course Lect. 52, 383–396.

Coluccino, L., Gottardi, R., Ayadi, F., Athanassiou, A., Tuan, R.S., Ceseracciu, L., 2018. Porous Poly(vinyl alcohol)-Based Hydrogel for Knee Meniscus Functional Repair. ACS Biomater. Sci. Eng. 4, 1518–1527.

Cooper, D.E., Arnoczky, S.P., Warren, R.F., 1991. Meniscal repair. Clin. Sports Med. 10, 529–548.

Debnath, T., Ghosh, S., Potlapuvu, U.S., Kona, L., Kamaraju, S.R., Sarkar, S., Gaddam, S., Chelluri, L.K., 2015. Proliferation and Differentiation Potential of Human Adipose-Derived Stem Cells Grown on Chitosan Hydrogel. PLOS ONE 10, e0120803.

Dhillon, M.S., John, R., Sharma, S., Prabhakar, S., Behera, P., Saxena, S., Singh, H., Chouhan, D., 2017. Epidemiology of Knee Injuries in Indian Kabaddi Players. Asian J. Sports Med. 8.

Di Matteo, B., Moran, C.J., Tarabella, V., Viganò, A., Tomba, P., Marcacci, M., Verdonk, R., 2016. A history of meniscal surgery: from ancient times to the twenty-first century. Knee Surg. Sports Traumatol. Arthrosc. Off. J. ESSKA 24, 1510–1518.

Dinkelaar, J., van den Bos, L.J., Hogendorf, W.F.J., Lodder, G., Overkleeft, H.S., Codée, J.D.C., van der Marel, G.A., 2008. Stereoselective Synthesis of L-Guluronic Acid Alginates. Chem. – Eur. J. 14, 9400–9411.

Distler, T., Kretzschmar, L., Schneidereit, D., Girardo, S., Goswami, R., Friedrich, O., Detsch, R., Guck, J., Boccaccini, A.R., Budday, S., 2021. Mechanical properties of cell- and microgel bead-laden oxidized alginate-gelatin hydrogels. Biomater. Sci.

Distler, T., McDonald, K., Heid, S., Karakaya, E., Detsch, R., Boccaccini, A.R., 2020a. Ionically and Enzymatically Dual Cross-Linked Oxidized Alginate Gelatin Hydrogels with Tunable Stiffness and Degradation Behavior for Tissue Engineering. ACS Biomater. Sci. Eng. 6, 3899–3914.

Distler, Thomas, Polley, C., Shi, F., Schneidereit, D., Ashton, M.D., Friedrich, O., Kolb, J.F., Hardy, J.G., Detsch, R., Seitz, H., Boccaccini, A.R., 2021. Electrically Conductive and 3D-Printable Oxidized Alginate-Gelatin Polypyrrole:PSS Hydrogels for Tissue Engineering. Adv. Healthc. Mater. n/a, 2001876.

Distler, T., Solisito, A.A., Schneidereit, D., Friedrich, O., Detsch, R., Boccaccini, A.R., 2020b. 3D printed oxidized alginate-gelatin bioink provides guidance for C2C12 muscle

precursor cell orientation and differentiation via shear stress during bioprinting. Biofabrication 12, 045005.

Djabourov, M., Leblond, J., Papon, P., 1988. Gelation of aqueous gelatin solutions. I. Structural investigation. J. Phys. 49, 319–332.

Djagny, V.B., Wang, Z., Xu, S., 2001. Gelatin: a valuable protein for food and pharmaceutical industries: review. Crit. Rev. Food Sci. Nutr. 41, 481–492.

Doral, M.N., Bilge, O., Huri, G., Turhan, E., Verdonk, R., 2018. Modern treatment of meniscal tears. EFORT Open Rev. 3, 260–268.

Dranseikiene, D., Schrüfer, S., Schubert, D.W., Reakasame, S., Boccaccini, A.R., 2020. Cell-laden alginate dialdehyde–gelatin hydrogels formed in 3D printed sacrificial gel. J. Mater. Sci. Mater. Med. 31, 31.

Emami, Z., Ehsani, M., Zandi, M., Foudazi, R., 2018. Controlling alginate oxidation conditions for making alginate-gelatin hydrogels. Carbohydr. Polym. 198, 509–517.

Englund, M., Roemer, F.W., Hayashi, D., Crema, M.D., Guermazi, A., 2012. Meniscus pathology, osteoarthritis and the treatment controversy. Nat. Rev. Rheumatol. 8, 412–419.

Espino, D.M., Shepherd, D.E., Hukins, D.W., 2014. Viscoelastic properties of bovine knee joint articular cartilage: dependency on thickness and loading frequency. BMC Musculoskelet. Disord. 15, 205.

Esposito, A.R., Moda, M., Cattani, S.M. de M., de Santana, G.M., Barbieri, J.A., Munhoz, M.M., Cardoso, T.P., Barbo, M.L.P., Russo, T., D'Amora, U., Gloria, A., Ambrosio, L., Duek, E.A. de R., 2013. PLDLA/PCL-T Scaffold for Meniscus Tissue Engineering. BioResearch Open Access 2, 138–147.

Fairbank, T.J., 1948. Knee Joint Changes After Meniscectomy. J. Bone Joint Surg. Br. 30-B, 664–670.

Fan, C., Xu, K., Huang, Y., Liu, S., Wang, T., Wang, W., Hu, W., Liu, L., Xing, M., Yang, S., 2021. Viscosity and degradation controlled injectable hydrogel for esophageal endoscopic submucosal dissection. Bioact. Mater. 6, 1150–1162.

Faunø, P., Nielsen, A.B., 1992. Arthroscopic partial meniscectomy: a long-term follow-up. Arthrosc. J. Arthrosc. Relat. Surg. Off. Publ. Arthrosc. Assoc. N. Am. Int. Arthrosc. Assoc. 8, 345–349.

Fields, R., 1972. [38] The rapid determination of amino groups with TNBS. In: Methods in Enzymology, Enzyme Structure, Part B. Academic Press, pp. 464–468.

Figueroa, F., Figueroa, D., Calvo, R., Vaisman, A., Espregueira-Mendes, J., 2019. Meniscus allograft transplantation: indications, techniques and outcomes. EFORT Open Rev. 4, 115–120.

Fisher, A.G.T., 1936. The Disk-shaped External Semilunar Cartilage. Br. Med. J. 1, 688–690.

Forriol, F., 2009. Growth factors in cartilage and meniscus repair. Injury 40 Suppl 3, S12-16.

Fox, A.J.S., Bedi, A., Rodeo, S.A., 2012. The Basic Science of Human Knee Menisci. Sports Health 4, 340–351.

Fox, J.M., Rintz, K.G., Ferkel, R.D., 1993. Trephination of incomplete meniscal tears. Arthrosc. J. Arthrosc. Relat. Surg. Off. Publ. Arthrosc. Assoc. N. Am. Int. Arthrosc. Assoc. 9, 451–455.

Franklin, M.J., Douthit, S.A., McClure, M.A., 2004. Evidence that the algI/algJ gene cassette, required for O acetylation of Pseudomonas aeruginosa alginate, evolved by lateral gene transfer. J. Bacteriol. 186, 4759–4773.

Furth, M.E., Atala, A., 2014. Chapter 6 - Tissue Engineering: Future Perspectives. In: Lanza, R., Langer, R., Vacanti, J. (Eds.), Principles of Tissue Engineering (Fourth Edition). Academic Press, Boston, pp. 83–123.

Gao, Y., Li, Z., Huang, J., Zhao, M., Wu, J., 2020. In situ formation of injectable hydrogels for chronic wound healing. J. Mater. Chem. B 8, 8768–8780.

García-Rubio, D.L., Mora, M.B. de la, Badillo-Ramírez, I., Cerecedo, D., Saniger, J.M., Benítez-Benítez, J.L., Villagrán-Muniz, M., 2019. Analysis of platelets in hypertensive and normotensive individuals using Raman and Fourier transform infrared-attenuated total reflectance spectroscopies. J. Raman Spectrosc. 50, 509–521.

Gardner, E., O'Rahilly, R., 1968. The early development of the knee joint in staged human embryos. J. Anat. 102, 289–299.

Genç, H., Hazur, J., Karakaya, E., Dietel, B., Bider, F., Groll, J., Alexiou, C., Boccaccini, A.R., Detsch, R., Cicha, I., 2021. Differential Responses to Bioink-Induced Oxidative Stress in Endothelial Cells and Fibroblasts. Int. J. Mol. Sci. 22.

George, M., Abraham, T.E., 2006. Polyionic hydrocolloids for the intestinal delivery of protein drugs: alginate and chitosan--a review. J. Control. Release Off. J. Control. Release Soc. 114, 1–14.

Gerecht, S., Townsend, S.A., Pressler, H., Zhu, H., Nijst, C.L.E., Bruggeman, J.P., Nichol, J.W., Langer, R., 2007. A porous photocurable elastomer for cell encapsulation and culture. Biomaterials 28, 4826–4835.

Ghadially, F.N., Lalonde, J.M., Wedge, J.H., 1983. Ultrastructure of normal and torn menisci of the human knee joint. J. Anat. 136, 773–791.

Ghosh, P., Taylor, T.K., 1987. The knee joint meniscus. A fibrocartilage of some distinction. Clin. Orthop. 52–63.

Gilsenan, P.M., Ross-Murphy, S.B., 2000. Rheological characterisation of gelatins from mammalian and marine sources. Food Hydrocoll. 14, 191–195.

Goble, E.M., Kohn, D., Verdonk, R., Kane, S.M., 1999. Meniscal substitutes--human experience. Scand. J. Med. Sci. Sports 9, 146–157.

Gomez, C.G., Rinaudo, M., Villar, M.A., 2007. Oxidation of sodium alginate and characterization of the oxidized derivatives. Carbohydr. Polym. 67, 296–304.

Grover, C.N., Gwynne, J.H., Pugh, N., Hamaia, S., Farndale, R.W., Best, S.M., Cameron, R.E., 2012. Crosslinking and composition influence the surface properties, mechanical stiffness and cell reactivity of collagen-based films. Acta Biomater. 8, 3080–3090.

Gulrez, S.K.H., Al-Assaf, S., Phillips, G.O., 2011. Hydrogels: Methods of Preparation, Characterisation and Applications, Progress in Molecular and Environmental Bioengineering - From Analysis and Modeling to Technology Applications. IntechOpen.

Guo, W., Chen, M., Wang, Zhenyong, Tian, Y., Zheng, J., Gao, S., Li, Y., Zheng, Y., Li, X., Huang, J., Niu, W., Jiang, S., Hao, C., Yuan, Z., Zhang, Y., Wang, M., Wang, Zehao, Peng, J., Wang, A., Wang, Y., Sui, X., Xu, W., Hao, L., Zheng, X., Liu, S., Guo, Q., 2021.

3D-printed cell-free PCL–MECM scaffold with biomimetic micro-structure and micro-environment to enhance in situ meniscus regeneration. Bioact. Mater. 6, 3620–3633.

Guo, W., Liu, S., Zhu, Y., Yu, C., Lu, S., Yuan, M., Gao, Y., Huang, J., Yuan, Z., Peng, J., Wang, A., Wang, Y., Chen, J., Zhang, L., Sui, X., Xu, W., Guo, Q., 2015. Advances and Prospects in Tissue-Engineered Meniscal Scaffolds for Meniscus Regeneration. Stem Cells Int. 2015.

Gupta, N.V., Shivakumar, H.G., 2012. Investigation of Swelling Behavior and Mechanical Properties of a pH-Sensitive Superporous Hydrogel Composite. Iran. J. Pharm. Res. IJPR 11, 481–493.

Gw, O., Sc, K., Th, K., Wk, J., 2020. Characterization of an oxidized alginate-gelatin hydrogel incorporating a COS-salicylic acid conjugate for wound healing. Carbohydr. Polym. 252, 117145–117145.

Gwathmey, F.W., Golish, S.R., Diduch, D.R., 2012. Complications in Brief: Meniscus Repair. Clin. Orthop. 470, 2059–2066.

Hajiabbas, M., Alemzadeh, I., Vossoughi, M., 2020. A porous hydrogel-electrospun composite scaffold made of oxidized alginate/gelatin/silk fibroin for tissue engineering application. Carbohydr. Polym. 245, 116465.

Harding, S., Varum, K., Stokke, B., Smidsrød, O., 1991. Molecular weight determination of polysaccharides. Adv. Carbohydr. Anal. 1, 63–144.

Hasan, J., Fisher, J., Ingham, E., 2014. Current strategies in meniscal regeneration. J. Biomed. Mater. Res. B Appl. Biomater. 102, 619–634.

Head, F.S.H., 1950. Effect of Light on the Reaction between Periodates and α-Glycols. Nature 165, 236–237.

Hede, A., Jensen, D.B., Blyme, P., Sonne-Holm, S., 1990. Epidemiology of meniscal lesions in the knee. 1,215 open operations in Copenhagen 1982-84. Acta Orthop. Scand. 61, 435–437.

Hede, A., Larsen, E., Sandberg, H., 1992. The long term outcome of open total and partial meniscectomy related to the quantity and site of the meniscus removed. Int. Orthop. 16, 122–125.

Helmiyati, Aprilliza, M., 2017. Characterization and properties of sodium alginate from brown algae used as an ecofriendly superabsorbent. IOP Conf. Ser. Mater. Sci. Eng. 188, 012019.

Heo, D.N., Alioglu, M.A., Wu, Y., Ozbolat, V., Ayan, B., Dey, M., Kang, Y., Ozbolat, I.T., 2020. 3D Bioprinting of Carbohydrazide-Modified Gelatin into Microparticle-Suspended Oxidized Alginate for the Fabrication of Complex-Shaped Tissue Constructs. ACS Appl. Mater. Interfaces 12, 20295–20306.

Hernández, R., Sacristán, J., Mijangos, C., 2010. Sol/Gel Transition of Aqueous Alginate Solutions Induced by Fe2+ Cations. Macromol. Chem. Phys. 211, 1254–1260.

Herwig, J., Egner, E., Buddecke, E., 1984. Chemical changes of human knee joint menisci in various stages of degeneration. Ann. Rheum. Dis. 43, 635.

Hoque, M.E., Nuge, T., Tshai, K.Y., Nordin, N., Prasad, V., 2015. Gelatin Based Scaffolds For Tissue Engineering – A review. Polym. Res. J. 9, 15–32.

Howell, R., Kumar, N.S., Patel, N., Tom, J., 2014. Degenerative meniscus: Pathogenesis, diagnosis, and treatment options. World J. Orthop. 5, 597–602.

Huynh, C.T., Liu, F., Cheng, Y., Coughlin, K., Alsberg, E., 2018. Thiol-Epoxy "Click" Chemistry to Engineer Cytocompatible PEG-based Hydrogel for siRNA-Mediated Osteogenesis of hMSCs. ACS Appl. Mater. Interfaces 10.

Ionescu, L.C., Lee, G.C., Huang, K.L., Mauck, R.L., 2012. Growth Factor Supplementation Improves Native and Engineered Meniscus Repair in Vitro. Acta Biomater. 8, 3687–3694.

Ionita, G., 2016. Characterization and Tailoring the Properties of Hydrogels Using Spectroscopic Methods, Emerging Concepts in Analysis and Applications of Hydrogels. IntechOpen.

Ishida, K., Kuroda, R., Miwa, M., Tabata, Y., Hokugo, A., Kawamoto, T., Sasaki, K., Doita, M., Kurosaka, M., 2007. The Regenerative Effects of Platelet-Rich Plasma on Meniscal Cells In Vitro and Its In Vivo Application with Biodegradable Gelatin Hydrogel. Tissue Eng. 13, 1103–1112.

Izuta, Y., Ochi, M., Adachi, N., Deie, M., Yamasaki, T., Shinomiya, R., 2005. Meniscal repair using bone marrow-derived mesenchymal stem cells: experimental study using green fluorescent protein transgenic rats. The Knee 12, 217–223.

Jackson, D.W., McDevitt, C.A., Simon, T.M., Arnoczky, S.P., Atwell, E.A., Silvino, N.J., 1992. Meniscal transplantation using fresh and cryopreserved allografts. An experimental study in goats. Am. J. Sports Med. 20, 644–656.

Jamilah, B., Harvinder, K.G., 2002. Properties of gelatins from skins of fish—black tilapia (Oreochromis mossambicus) and red tilapia (Oreochromis nilotica). Food Chem. 77, 81–84.

Jejurikar, A., Ting Seow, X., Lawrie, G., Martin, D., Jayakrishnan, A., Grøndahl, L., 2012. Degradable alginate hydrogels crosslinked by the macromolecular crosslinker alginate dialdehyde. J. Mater. Chem. 22, 9751–9758.

Jiang, Z., Cao, X., Li, Z., Guo, L., 2016. Rheological behaviors and secondary networks of polyacrylamide hydrogel filled with silica. J. Pet. Explor. Prod. Technol. 6, 93–99.

John, R., Dhillon, M.S., Syam, K., Prabhakar, S., Behera, P., Singh, H., 2016. Epidemiological profile of sports-related knee injuries in northern India: An observational study at a tertiary care centre. J. Clin. Orthop. Trauma 7, 207–211.

Johnson, D.L., Swenson, T.M., Livesay, G.A., Aizawa, H., Fu, F.H., Harner, C.D., 1995. Insertion-site anatomy of the human menisci: gross, arthroscopic, and topographical anatomy as a basis for meniscal transplantation. Arthrosc. J. Arthrosc. Relat. Surg. Off. Publ. Arthrosc. Assoc. N. Am. Int. Arthrosc. Assoc. 11, 386–394.

Kalpakci, K.N., Kim, E.J., Athanasiou, K.A., 2011. Assessment of Growth Factor Treatment on Fibrochondrocyte and Chondrocyte Co-Cultures for TMJ Fibrocartilage Engineering. Acta Biomater. 7, 1710–1718.

Kamimura, T., Kimura, M., 2014. Meniscal Repair of Degenerative Horizontal Cleavage Tears Using Fibrin Clots: Clinical and Arthroscopic Outcomes in 10 Cases. Orthop. J. Sports Med. 2, 2325967114555678.

Kang, S.-W., Son, S.-M., Lee, J.-S., Lee, E.-S., Lee, K.-Y., Park, S.-G., Park, J.-H., Kim, B.-S., 2006. Regeneration of whole meniscus using meniscal cells and polymer scaffolds in a rabbit total meniscectomy model. J. Biomed. Mater. Res. A 77, 659–671.

Kanth, S.V., Ramaraj, A., Rao, J.R., Nair, B.U., 2009. Stabilization of type I collagen using dialdehyde cellulose. Process Biochem. 44, 869–874.

Kaplan, D.L., Mandal, B.B., 2013. Multilayered silk scaffolds for meniscus tissue engineering. US20130172999 A1.

Karimi-Soflou, R., Nejati, S., Karkhaneh, A., 2021. Electroactive and antioxidant injectable in-situ forming hydrogels with tunable properties by polyethylenimine and polyaniline for nerve tissue engineering. Colloids Surf. B Biointerfaces 199, 111565.

Kasibhatla, S., Amarante-Mendes, G., Finucane, D., Brunner, T., Bossy-Wetzel, E., Green, D., 2006. Acridine Orange/Ethidium Bromide (AO/EB) Staining to Detect Apoptosis. CSH Protoc. 2006.

Keira, S.M., Ferreira, L.M., Gragnani, A., Duarte, I. da S., Barbosa, J., 2004. Experimental model for collagen estimation in cell culture. Acta Cirúrgica Bras. 19, 17–22.

Kessler, L., Gehrke, S., Winnefeld, M., Huber, B., Hoch, E., Walter, T., Wyrwa, R., Schnabelrauch, M., Schmidt, M., Kueckelhaus, M., Lehnhardt, M., Hirsch, T., Jacobsen, F., 2017. Methacrylated gelatin/hyaluronan-based hydrogels for soft tissue engineering. J. Tissue Eng. 8, 1–14.

Khan, Y., 2019. Characterizing the Properties of Tissue Constructs for Regenerative Engineering. In: Narayan, R. (Ed.), Encyclopedia of Biomedical Engineering. Elsevier, Oxford, pp. 537–545.

Khorshidi, S., Karkhaneh, A., 2018. Particle-coated electrospun scaffold: A semi-conductive drug eluted scaffold with layered fiber/particle arrangement. J. Biomed. Mater. Res. A 106, 3248–3254.

Kim, S.-H., An, Y.-H., Kim, H.D., Kim, K., Lee, S.-H., Yim, H.-G., Kim, B.-G., Hwang, N.S., 2018. Enzyme-mediated tissue adhesive hydrogels for meniscus repair. Int. J. Biol. Macromol. 110, 479–487.

Kirchmajer, D.M., Watson, C.A., Ranson, M., Panhuis, M. in het, 2012. Gelapin, a degradable genipin cross-linked gelatin hydrogel. RSC Adv. 3, 1073–1081.

Klontzas, M.E., Reakasame, S., Silva, R., Morais, J.C.F., Vernardis, S., MacFarlane, R.J., Heliotis, M., Tsiridis, E., Panoskaltsis, N., Boccaccini, A.R., Mantalaris, A., 2019. Oxidized alginate hydrogels with the GHK peptide enhance cord blood mesenchymal stem cell osteogenesis: A paradigm for metabolomics-based evaluation of biomaterial design. Acta Biomater. 88, 224–240.

Kluczynski, M.A., Marzo, J.M., Rauh, M.A., Bernas, G.A., Bisson, L.J., 2015. Sex-Specific Predictors of Intra-articular Injuries Observed During Anterior Cruciate Ligament Reconstruction. Orthop. J. Sports Med. 3.

Kohn, D., Moreno, B., 1995. Meniscus insertion anatomy as a basis for meniscus replacement: a morphological cadaveric study. Arthrosc. J. Arthrosc. Relat. Surg. Off. Publ. Arthrosc. Assoc. N. Am. Int. Arthrosc. Assoc. 11, 96–103.

Kot, F.S., 2015. Chapter 1 - Boron in the Environment. In: Kabay, N., Bryjak, M., Hilal, N. (Eds.), Boron Separation Processes. Elsevier, Amsterdam, pp. 1–33.

Kowalski, G., Kijowska, K., Witczak, M., Kuterasiński, Ł., Łukasiewicz, M., 2019. Synthesis and Effect of Structure on Swelling Properties of Hydrogels Based on High Methylated Pectin and Acrylic Polymers. Polymers 11, 114.

Kramer, D.L., 2001. Gels for Photographic Emulsions. In: Buschow, K.H.J., Cahn, R.W., Flemings, M.C., Ilschner, B., Kramer, E.J., Mahajan, S., Veyssière, P. (Eds.), Encyclopedia of Materials: Science and Technology. Elsevier, Oxford, pp. 3495–3497.

Kretlow, J.D., Klouda, L., Mikos, A.G., 2007. Injectable matrices and scaffolds for drug delivery in tissue engineering. Adv. Drug Deliv. Rev. 59, 263–273.

Kristiansen, K.A., Potthast, A., Christensen, B.E., 2010. Periodate oxidation of polysaccharides for modification of chemical and physical properties. Carbohydr. Res., Special Issue: Selected Papers from the 15th European Carbohydrate Symposium, Vienna 2009 345, 1264–1271.

Kurowiak, J., Kaczmarek- Pawelska, A., Mackiewicz, A., Bedzinski, R., 2020. Analysis of the Degradation Process of Alginate-Based Hydrogels in Artificial Urine for Use as a Bioresorbable Material in the Treatment of Urethral Injuries. Processes 8.

Kwak, H.S., Nam, J., Lee, J.-H., Kim, H.J., Yoo, J.J., 2017. Meniscal repair in vivo using human chondrocyte-seeded PLGA mesh scaffold pretreated with platelet-rich plasma. J. Tissue Eng. Regen. Med. 11, 471–480.

Lee, K.Y., Mooney, D.J., 2012. Alginate: properties and biomedical applications. Prog. Polym. Sci. 37, 106–126.

Lee, S.J., Park, K., 1996. Synthesis and characterization of sol-gel phase-reversible hydrogels sensitive to glucose. J. Mol. Recognit. JMR 9, 549–557.

Leite, Á.J., Sarker, B., Zehnder, T., Silva, R., Mano, J.F., Boccaccini, A.R., 2016. Bioplotting of a bioactive alginate dialdehyde-gelatin composite hydrogel containing bioactive glass nanoparticles. Biofabrication 8, 035005.

Leonard, M., Rastello De Boisseson, M., Hubert, P., Dellacherie, E., 2004. Production of microspheres based on hydrophobically associating alginate derivatives by dispersion/gelation in aqueous sodium chloride solutions. J. Biomed. Mater. Res. A 68, 335–342.

Li, Q., Liu, C.-G., Huang, Z.-H., Xue, F.-F., 2011. Preparation and Characterization of Nanoparticles Based on Hydrophobic Alginate Derivative as Carriers for Sustained Release of Vitamin D3. J. Agric. Food Chem. 59, 1962–1967.

Li, Z., Liu, D., Dong, J., Gong, L., Wang, Y., Tang, P., Zhang, Y., 2016. Effects of Cold Irrigation on Early Results after Total Knee Arthroplasty. Medicine (Baltimore) 95.

Liang, W., Chen, J., Li, L., Li, M., Wei, X., Tan, B., Shang, Y., Fan, G., Wang, W., Liu, W., 2019. Conductive Hydrogen Sulfide-Releasing Hydrogel Encapsulating ADSCs for Myocardial Infarction Treatment. ACS Appl. Mater. Interfaces 11, 14619–14629.

Lien, S.-M., Ko, L.-Y., Huang, T.-J., 2009. Effect of pore size on ECM secretion and cell growth in gelatin scaffold for articular cartilage tissue engineering. Acta Biomater. 5, 670–679.

Linh, N.T., Paul, K., Kim, B., Lee, B.-T., 2016. Augmenting in vitro osteogenesis of a glycine-arginine-glycine-aspartic-conjugated oxidized alginate-gelatin-biphasic calcium phosphate hydrogel composite and in vivo bone biogenesis through stem cell delivery. J. Biomater. Appl. 31, 661–673.

Liu, F., Xu, H., Huang, H., 2019. A novel kartogenin-platelet-rich plasma gel enhances chondrogenesis of bone marrow mesenchymal stem cells in vitro and promotes wounded meniscus healing in vivo. Stem Cell Res. Ther. 10, 201.

Liu, K., Liu, P., Liu, R., Wu, X., 2015. Dual AO/EB Staining to Detect Apoptosis in Osteosarcoma Cells Compared with Flow Cytometry. Med. Sci. Monit. Basic Res. 21, 15–20.

Longo, U.G., Loppini, M., Forriol, F., Romeo, G., Maffulli, N., Denaro, V., 2011. Advances in Meniscal Tissue Engineering. Stem Cells Int. 2012, e420346.

Longo, U.G., Loppini, M., Romeo, G., Maffulli, N., Denaro, V., 2013. Histological scoring systems for tissue-engineered, ex vivo and degenerative meniscus. Knee Surg. Sports Traumatol. Arthrosc. Off. J. ESSKA 21, 1569–1576.

Ma, L., Cheng, C., Nie, C., He, C., Deng, J., Wang, L., Xia, Y., Zhao, C., 2016. Anticoagulant sodium alginate sulfates and their mussel-inspired heparin-mimetic coatings. J. Mater. Chem. B 4, 3203–3215.

Ma, L., Su, W., Ran, Y., Ma, X., Yi, Z., Chen, G., Chen, X., Deng, Z., Tong, Q., Wang, X., Li, X., 2020. Synthesis and characterization of injectable self-healing hydrogels based on oxidized alginate-hybrid-hydroxyapatite nanoparticles and carboxymethyl chitosan. Int. J. Biol. Macromol. 165, 1164–1174.

MacCONAILL, M.A., 1951. The movements of bones and joints; the mechanical structure of articulating cartilage. J. Bone Joint Surg. Br. 33B, 251–257.

Makris, E.A., Hadidi, P., Athanasiou, K.A., 2011. The knee meniscus: Structure–function, pathophysiology, current repair techniques, and prospects for regeneration. Biomaterials 32, 7411–7431.

Maltby, J.G., Primavesi, G.R., 1949. The estimation of aldehydes, ketones and acetals by means of the hydroxylamine hydrochloride method. Analyst 74, 498–502.

Mandal, B.B., Kundu, S.C., 2009. Cell proliferation and migration in silk fibroin 3D scaffolds. Biomaterials 30, 2956–2965.

Marcacci, M., Grassi, A., Muccioli, G.M.M., Nitri, M., Zaffagnini, S., 2015. Meniscus Reconstruction Using a New Collagen Meniscus Implant. In: Doral, M.N., Karlsson, J. (Eds.), Sports Injuries: Prevention, Diagnosis, Treatment and Rehabilitation. Springer, Berlin, Heidelberg, pp. 1211–1222.

Martínez, H., Brackmann, C., Enejder, A., Gatenholm, P., 2012. Mechanical stimulation of fibroblasts in micro-channeled bacterial cellulose scaffolds enhances production of oriented collagen fibers. J. Biomed. Mater. Res. A 100A, 948–957.

Masuelli, M., Illanes, C., 2014. Review of the characterization of sodium alginate by intrinsic viscosity measurements. Comparative analysis between conventional and single point methods 1, 1–11.

Masuelli, M.A., 2014. Mark-Houwink Parameters for Aqueous-Soluble Polymers and Biopolymers at Various Temperatures. J. Polym. Biopolym. Phys. Chem. 2, 37–43.

Maynard, R.L., Downes, N., 2019. Chapter 3 - Introduction to the Skeleton: Bone, Cartilage and Joints. In: Maynard, R.L., Downes, N. (Eds.), Anatomy and Histology of the Laboratory Rat in Toxicology and Biomedical Research. Academic Press, pp. 11–22.

McDermott, I.D., Sharifi, F., Bull, A.M.J., Gupte, C.M., Thomas, R.W., Amis, A.A., 2004. An anatomical study of meniscal allograft sizing. Knee Surg. Sports Traumatol. Arthrosc. Off. J. ESSKA 12, 130–135.

Mcdevitt, C.A., Webber, R.J., 1990. The Ultrastructure and Biochemistry of Meniscal Cartilage. Clin. Orthop. Relat. Res. 252, 8–18.

Metcalf, M.H., Barrett, G.R., 2004. Prospective evaluation of 1485 meniscal tear patterns in patients with stable knees. Am. J. Sports Med. 32, 675–680.

Mhanna, R., Becher, J., Schnabelrauch, M., Reis, R.L., Pashkuleva, I., 2017. Sulfated Alginate as a Mimic of Sulfated Glycosaminoglycans: Binding of Growth Factors and Effect on Stem Cell Behavior. Adv. Biosyst. 1, 1700043.

Mikkonen, K.S., Parikka, K., Suuronen, J.-P., Ghafar, A., Serimaa, R., Tenkanen, M., 2014. Enzymatic oxidation as a potential new route to produce polysaccharide aerogels. RSC Adv. 4, 11884–11892.

Moeinzadeh, S., Jabbari, E., 2015. Gelation characteristics, physico-mechanical properties and degradation kinetics of micellar hydrogels. Eur. Polym. J. 72, 566–576.

Mondal, A., Gebeyehu, A., Miranda, M., Bahadur, D., Patel, N., Ramakrishnan, S., Rishi, A.K., Singh, M., 2019. Characterization and printability of Sodium alginate -Gelatin hydrogel for bioprinting NSCLC co-culture. Sci. Rep. 9, 19914.

Monllau, J.C., 2013. Collagen Meniscal Implant (CMI). In: Verdonk, R., Espregueira Mendes, J., Monllau, J.C. (Eds.), Meniscal Transplantation. Springer, Berlin, Heidelberg, pp. 73–82.

Moran, C.J., Busilacchi, A., Lee, C.A., Athanasiou, K.A., Verdonk, P.C., 2015. Biological augmentation and tissue engineering approaches in meniscus surgery. Arthrosc. J. Arthrosc. Relat. Surg. Off. Publ. Arthrosc. Assoc. N. Am. Int. Arthrosc. Assoc. 31, 944–955.

Mordecai, S.C., Al-Hadithy, N., Ware, H.E., Gupte, C.M., 2014. Treatment of meniscal tears: An evidence based approach. World J. Orthop. 5, 233–241.

Mulder, E.L.W. de, Hannink, G., Verdonschot, N., Buma, P., 2013. Effect of polyurethane scaffold architecture on ingrowth speed and collagen orientation in a subcutaneous rat pocket model. Biomed. Mater. 8, 025004.

Muyonga, J.H., Cole, C.G.B., Duodu, K.G., 2004. Fourier transform infrared (FTIR) spectroscopic study of acid soluble collagen and gelatin from skins and bones of young and adult Nile perch (Lates niloticus). Food Chem. 86, 325–332.

Naghizadeh, Z., Karkhaneh, A., Khojasteh, A., 2018. Self-crosslinking effect of chitosan and gelatin on alginate based hydrogels: Injectable in situ forming scaffolds. Mater. Sci. Eng. C Mater. Biol. Appl. 89, 256–264.

Nakano, T., Dodd, C.M., Scott, P.G., 1997. Glycosaminoglycans and proteoglycans from different zones of the porcine knee meniscus. J. Orthop. Res. Off. Publ. Orthop. Res. Soc. 15, 213–220.

Nguyen, T.-P., Lee, B.-T., 2012. Fabrication of oxidized alginate-gelatin-BCP hydrogels and evaluation of the microstructure, material properties and biocompatibility for bone tissue regeneration. J. Biomater. Appl. 27, 311–321.

Oda, S., Otsuki, S., Kurokawa, Y., Hoshiyama, Y., Nakajima, M., Neo, M., 2015. A new method for meniscus repair using type I collagen scaffold and infrapatellar fat pad. J. Biomater. Appl. 29, 1439–1448.

Otero-Espinar, F.J., Fernández-Ferreiro, A., González-Barcia, M., Blanco-Méndez, J., Luzardo, A., 2018. Chapter 6 - Stimuli sensitive ocular drug delivery systems. In: Grumezescu, A.M. (Ed.), Drug Targeting and Stimuli Sensitive Drug Delivery Systems. William Andrew Publishing, pp. 211–270.

Padhi, J.R., Nayak, D., Nanda, A., Rauta, P.R., Ashe, S., Nayak, B., 2016. Development of highly biocompatible Gelatin & i-Carrageenan based composite hydrogels: In depth physiochemical analysis for biomedical applications. Carbohydr. Polym. 153, 292–301.

Painter, T., Larsen, B., 1973. further illustration of nearest-neighbour auto-inhibitory effects in the oxidation of alginate by periodate ion. Acta Chem. Scand. 6, 1957–1962.

Painter, T.J., 1988. Control of depolymerisation during the preparation of reduced dialdehyde cellulose. Carbohydr. Res. 179, 259–268.

Palmroth, A., Pitkänen, S., Hannula, M., Paakinaho, K., Hyttinen, J., Miettinen, S., Kellomäki, M., 2020. Evaluation of scaffold microstructure and comparison of cell seeding methods using micro-computed tomography-based tools. J. R. Soc. Interface 17, 20200102.

Pangborn, C.A., Athanasiou, K.A., 2005. Effects of growth factors on meniscal fibrochondrocytes. Tissue Eng. 11, 1141–1148.

Park, J., Nam, J., Yun, H., Jin, H.-J., Kwak, H.W., 2021. Aquatic polymer-based edible films of fish gelatin crosslinked with alginate dialdehyde having enhanced physicochemical properties. Carbohydr. Polym. 254, 117317.

Pavlovic, V., Ciric, M., Jovanovic, V., Stojanovic, P., 2016. Platelet Rich Plasma: a short overview of certain bioactive components. Open Med. 11, 242–247.

Pawar, S.N., Edgar, K.J., 2013. Alginate esters via chemoselective carboxyl group modification. Carbohydr. Polym. 98, 1288–1296.

Pereira, H., Frias, A.M., Oliveira, J.M., Espregueira-Mendes, J., Reis, R.L., 2011. Tissue Engineering and Regenerative Medicine Strategies in Meniscus Lesions. Arthrosc. J. Arthrosc. Relat. Surg. 27, 1706–1719.

Pereira, L., Sousa, A., Coelho, H., Amado, A.M., Ribeiro-Claro, P.J.A., 2003. Use of FTIR, FT-Raman and 13C-NMR spectroscopy for identification of some seaweed phycocolloids. Biomol. Eng. 20, 223–228.

Peretti, G.M., Gill, T.J., Xu, J.-W., Randolph, M.A., Morse, K.R., Zaleske, D.J., 2004. Cell-based therapy for meniscal repair: a large animal study. Am. J. Sports Med. 32, 146–158.

Petersen, W., Tillmann, B., 1998. Collagenous fibril texture of the human knee joint menisci. Anat. Embryol. (Berl.) 197, 317–324.

Petrungaro, P.S., 2001. Using platelet-rich plasma to accelerate soft tissue maturation in esthetic periodontal surgery. Compend. Contin. Educ. Dent. Jamesburg NJ 1995 22, 729–732, 734, 736 passim; quiz 746.

Pier, G.B., Coleman, F., Grout, M., Franklin, M., Ohman, D.E., 2001. Role of alginate O acetylation in resistance of mucoid Pseudomonas aeruginosa to opsonic phagocytosis. Infect. Immun. 69, 1895–1901.

Polito, U., Peretti, G.M., Di Giancamillo, M., Boschetti, F., Carnevale, L., Veronesi, M.C., Sconfienza, L.M., Agnoletto, M., Mangiavini, L., Modina, S.C., Di Giancamillo, A., 2020. Meniscus Matrix Remodeling in Response to Compressive Forces in Dogs. Cells 9, 265.

Poursamar, S.A., Lehner, A.N., Azami, M., Ebrahimi-Barough, S., Samadikuchaksaraei, A., Antunes, A.P.M., 2016. The effects of crosslinkers on physical, mechanical, and cytotoxic properties of gelatin sponge prepared via in-situ gas foaming method as a tissue engineering scaffold. Mater. Sci. Eng. C 63, 1–9.

Proctor, C.S., Schmidt, M.B., Whipple, R.R., Kelly, M.A., Mow, V.C., 1989. Material properties of the normal medial bovine meniscus. J. Orthop. Res. 7, 771–782.

Pujol, N., Salle De Chou, E., Boisrenoult, P., Beaufils, P., 2015. Platelet-rich plasma for open meniscal repair in young patients: any benefit? Knee Surg. Sports Traumatol. Arthrosc. Off. J. ESSKA 23, 51–58.

Qadir, M., Hossan, J., Gafur, M., Karim, M., 2014. Preparation and Characterization of Gelatin-Hydroxyapatite Composite for Bone Tissue Engineering. Int. J. Eng. Technol. Sci. 14, 24.

Qiu, M., Chen, D., Shen, C., Shen, J., Zhao, H., He, Y., 2016. Platelet-Rich Plasma-Loaded Poly(d,l-lactide)-Poly(ethylene glycol)-Poly(d,l-lactide) Hydrogel Dressing Promotes Full-Thickness Skin Wound Healing in a Rodent Model. Int. J. Mol. Sci. 17.

Rajalekshmi, R., Kaladevi Shaji, A., Joseph, R., Bhatt, A., 2021. Scaffold for liver tissue engineering: Exploring the potential of fibrin incorporated alginate dialdehyde–gelatin hydrogel. Int. J. Biol. Macromol. 166, 999–1008.

Rampersad, S.N., 2012. Multiple Applications of Alamar Blue as an Indicator of Metabolic Function and Cellular Health in Cell Viability Bioassays. Sensors 12, 12347–12360.

Ravichandran, V., Jayakrishnan, A., 2018. Synthesis and evaluation of anti-fungal activities of sodium alginate-amphotericin B conjugates. Int. J. Biol. Macromol. 108, 1101–1109.

Reakasame, S., Boccaccini, A.R., 2018. Oxidized Alginate-Based Hydrogels for Tissue Engineering Applications: A Review. Biomacromolecules 19, 3–21.

Reakasame, S., Jin, A., Zheng, K., Qu, M., Boccaccini, A.R., 2020. Biofabrication and Characterization of Alginate Dialdehyde-Gelatin Microcapsules Incorporating Bioactive Glass for Cell Delivery Application. Macromol. Biosci. 20, 2000138.

Resmi, R., Parvathy, J., John, A., Joseph, R., 2020. Injectable self-crosslinking hydrogels for meniscal repair: A study with oxidized alginate and gelatin. Carbohydr. Polym. 234, 115902.

Ridley, T.J., McCarthy, M.A., Bollier, M.J., Wolf, B.R., Amendola, A., 2017. Age Differences in the Prevalence of Isolated Medial and Lateral Meniscal Tears in Surgically Treated Patients. Iowa Orthop. J. 37, 91–94.

Rodeo, S.A., Seneviratne, A., Suzuki, K., Felker, K., Wickiewicz, T.L., Warren, R.F., 2000a. Histological analysis of human meniscal allografts. A preliminary report. J. Bone Joint Surg. Am. 82-A, 1071–1082.

Rodeo, S.A., Seneviratne, A., Suzuki, K., Felker, K., Wickiewicz, T.L., Warren, R.F., 2000b. Histological analysis of human meniscal allografts. A preliminary report. J. Bone Joint Surg. Am. 82, 1071–1082.

Rosso, F., Bisicchia, S., Bonasia, D.E., Amendola, A., 2015. Meniscal allograft transplantation: a systematic review. Am. J. Sports Med. 43, 998–1007.

Rottensteiner-Brandl, U., Detsch, R., Sarker, B., Lingens, L., Köhn, K., Kneser, U., Bosserhoff, A.K., Horch, R.E., Boccaccini, A.R., Arkudas, A., 2018. Encapsulation of Rat Bone Marrow Derived Mesenchymal Stem Cells in Alginate Dialdehyde/Gelatin Microbeads with and without Nanoscaled Bioactive Glass for In Vivo Bone Tissue Engineering. Mater. Basel Switz. 11.

Sachan, N., Pushkar, S., Jha, A., Bhattcharya, A., 2009. Sodium alginate: The wonder polymer for controlled drug delivery. J. Pharm. Res. 2.

Sahin, F., USTAOGLU, Z., DEMIRCI, S., DEMIR, O., ASUTAY, A.B., 2016. Antimicrobial and antiviral hygienic products. WO2016085434A1.

Sahoo, D.R., Biswal, T., 2021. Alginate and its application to tissue engineering. SN Appl. Sci. 3, 30.

Saidoff, D.C., McDonough, A.L., 2004. Critical Pathways in Therapeutic Intervention, Extremities and Spine. J. Sport Rehabil. 13, 96–97.

Salomonsen, T., Jensen, H.M., Stenbæk, D., Engelsen, S.B., 2008. Chemometric prediction of alginate monomer composition: A comparative spectroscopic study using IR, Raman, NIR and NMR. Carbohydr. Polym. 72, 730–739.

Sarika, P.R., Cinthya, K., Jayakrishnan, A., Anilkumar, P.R., James, N.R., 2014. Modified gum arabic cross-linked gelatin scaffold for biomedical applications. Mater. Sci. Eng. C 43, 272–279.

Sarker, B., Li, W., Zheng, K., Detsch, R., Boccaccini, A.R., 2016. Designing Porous Bone Tissue Engineering Scaffolds with Enhanced Mechanical Properties from Composite Hydrogels Composed of Modified Alginate, Gelatin, and Bioactive Glass. ACS Biomater. Sci. Eng. 2, 2240–2254.

Sarker, B., Zehnder, T., Rath, S.N., Horch, R.E., Kneser, U., Detsch, R., Boccaccini, A.R., 2017. Oxidized Alginate-Gelatin Hydrogel: A Favorable Matrix for Growth and Osteogenic Differentiation of Adipose-Derived Stem Cells in 3D. ACS Biomater. Sci. Eng. 3, 1730–1737.

Sasaki, H., Rothrauff, B.B., Alexander, P.G., Lin, H., Gottardi, R., Fu, F.H., Tuan, R.S., 2018. In Vitro Repair of Meniscal Radial Tear With Hydrogels Seeded With Adipose Stem Cells and TGF-β3. Am. J. Sports Med. 46, 2402–2413.

Schmid, R., Schmidt, S.K., Hazur, J., Detsch, R., Maurer, E., Boccaccini, A.R., Hauptstein, J., Teßmar, J., Blunk, T., Schrüfer, S., Schubert, D.W., Horch, R.E., Bosserhoff, A.K., Arkudas, A., Kengelbach-Weigand, A., 2020. Comparison of Hydrogels for the Development of Well-Defined 3D Cancer Models of Breast Cancer and Melanoma. Cancers 12.

Schmid, T., Messmer, A., Yeo, B.-S., Zhang, W., Zenobi, R., 2008. Towards chemical analysis of nanostructures in biofilms II: Tip-enhanced Raman spectroscopy of alginates. Anal. Bioanal. Chem. 391, 1907–16.

Schrieber, R., Gareis, H., 2007. Gelatine Handbook: Theory and Industrial Practice I–XII.

Schwarz, S., Kuth, S., Distler, T., Gögele, C., Stölzel, K., Detsch, R., Boccaccini, A.R., Schulze-Tanzil, G., 2020. 3D printing and characterization of human nasoseptal chondrocytes laden dual crosslinked oxidized alginate-gelatin hydrogels for cartilage repair approaches. Mater. Sci. Eng. C 116, 111189.

Shahriari, D., Koffler, J., Lynam, D.A., Tuszynski, M.H., Sakamoto, J.S., 2016. Characterizing the degradation of alginate hydrogel for use in multilumen scaffolds for spinal cord repair. J. Biomed. Mater. Res. A 104, 611–619.

Shinjo, H., Nakata, K., Shino, K., Hamada, M., Nakamura, N., Mae, T., Miyama, T., Horibe, S., Yoshikawa, H., Ochi, T., 2002. Effect of irrigation solutions for arthroscopic surgery on intraarticular tissue: comparison in human meniscus-derived primary cell culture between lactate Ringer's solution and saline solution. J. Orthop. Res. Off. Publ. Orthop. Res. Soc. 20, 1305–1310.

Singh, R., Wieser, A., Reakasame, S., Detsch, R., Dietel, B., Alexiou, C., Boccaccini, A.R., Cicha, I., 2017. Cell specificity of magnetic cell seeding approach to hydrogel colonization. J. Biomed. Mater. Res. A 105, 2948–2957.

Slaughter, B.V., Khurshid, S.S., Fisher, O.Z., Khademhosseini, A., Peppas, N.A., 2009. Hydrogels in Regenerative Medicine. Adv. Mater. Deerfield Beach Fla 21, 3307–3329.

Solandt, O.M., 1941. Some Observations Upon Sodium Alginate. Q. J. Exp. Physiol. Cogn. Med. Sci. 31, 25–30.

Soltan, N., Ning, L., Mohabatpour, F., Papagerakis, P., Chen, X., 2019. Printability and Cell Viability in Bioprinting Alginate Dialdehyde-Gelatin Scaffolds. ACS Biomater. Sci. Eng. 5.

Steiner, D., Lingens, L., Fischer, L., Köhn, K., Detsch, R., Boccaccini, A.R., Fey, T., Greil, P., Weis, C., Beier, J.P., Horch, R.E., Arkudas, A., 2018. Encapsulation of Mesenchymal Stem Cells Improves Vascularization of Alginate-Based Scaffolds. Tissue Eng. Part A.

Sun, J., Tan, H., 2013. Alginate-Based Biomaterials for Regenerative Medicine Applications. Mater. Basel Switz. 6, 1285–1309.

Svensson, A., Nicklasson, E., Harrah, T., Panilaitis, B., Kaplan, D.L., Brittberg, M., Gatenholm, P., 2005. Bacterial cellulose as a potential scaffold for tissue engineering of cartilage. Biomaterials 26, 419–431.

Szekalska, M., Puciłowska, A., Szymańska, E., Ciosek, P., Winnicka, K., 2016. Alginate: Current Use and Future Perspectives in Pharmaceutical and Biomedical Applications. Int. J. Polym. Sci. 2016, e7697031.

T. Somasekharan, L., Kasoju, N., Raju, R., Bhatt, A., 2020. Formulation and Characterization of Alginate Dialdehyde, Gelatin, and Platelet-Rich Plasma-Based Bioink for Bioprinting Applications. Bioengineering 7, 108.

Tariverdian, T., Navaei, T., Milan, P.B., Samadikuchaksaraei, A., Mozafari, M., 2019. Chapter 16 - Functionalized polymers for tissue engineering and regenerative medicines. In: Mozafari, M., Singh Chauhan, N.P. (Eds.), Advanced Functional Polymers for Biomedical Applications. Elsevier, pp. 323–357.

Taubner, T., Čopíková, J., Havelka, P., Synytsya, A., 2013. Preparation of amidated derivatives of monocarboxy cellulose. Cellulose 20, 2045–2055.

Temenoff, J.S., Mikos, A.G., 2000. Review: tissue engineering for regeneration of articular cartilage. Biomaterials 21, 431–440.

Thompson, W.O., Thaete, F.L., Fu, F.H., Dye, S.F., 1991. Tibial meniscal dynamics using three-dimensional reconstruction of magnetic resonance images. Am. J. Sports Med. 19, 210–215; discussion 215-216.

Tian, M., Chen, X., Li, H., Ma, L., Gu, Z., Qi, X., Li, X., Tan, H., You, C., 2016. Long-term and oxidative-responsive alginate–deferoxamine conjugates with a low toxicity for iron overload. RSC Adv. 6, 32471–32479.

Tormos, C.J., Abraham, C., Madihally, S.V., 2015. Improving the stability of chitosan-gelatin-based hydrogels for cell delivery using transglutaminase and controlled release of doxycycline. Drug Deliv. Transl. Res. 5, 575–584.

Tucker, B., Khan, W., Al-Rashid, M., Al-Khateeb, H., 2012. Tissue Engineering for the Meniscus: A Review of the Literature. Open Orthop. J. 6, 348–351.

Uhthoff, H.K., Kumagai, J., 1992. Embryology of Human Meniscus. In: M.D, K.H., M.D, K.M., M.D, T.M. (Eds.), Trends in Research and Treatment of Joint Diseases. Springer Japan, pp. 135–141.

Unnikrishnan, M., Umashankar, P.R., Viswanathan, S., Savlania, A., Joseph, R., Muraleedharan, C.V., Agrawal, V., Shenoy, S.J., Krishnan, L.K., Mohanan, P.V., Sabareeswaran, A., 2017. Preclinical evaluation of hydrogel sealed fluropassivated indigenous vascular prosthesis. Indian J. Med. Res. 146, 646–653.

Veelaert, S., de Wit, D., Tournois, H., 1994. An improved kinetic model for the periodate oxidation of starch. Polymer 35, 5091–5097.

Verdonk, P.C.M., Forsyth, R.G., Wang, J., Almqvist, K.F., Verdonk, R., Veys, E.M., Verbruggen, G., 2005. Characterisation of human knee meniscus cell phenotype. Osteoarthritis Cartilage 13, 548–560.

Verdonk, R., Kohn, D., 1999. Harvest and conservation of meniscal allografts. Scand. J. Med. Sci. Sports 9, 158–159.

Verdonk, Rene, 2013. Polyurethane Implant (ACTIFIT). In: Verdonk, René, Espregueira Mendes, J., Monllau, J.C. (Eds.), Meniscal Transplantation. Springer, Berlin, Heidelberg, pp. 83–97.

Vundelinckx, B., Vanlauwe, J., Bellemans, J., 2014. Long-term Subjective, Clinical, and Radiographic Outcome Evaluation of Meniscal Allograft Transplantation in the Knee. Am. J. Sports Med. 42, 1592–1599.

Wang, H.-L., Avila, G., 2007. Platelet Rich Plasma: Myth or Reality? Eur. J. Dent. 1, 192–194.

Wang, J., Fu, W., Zhang, D., Yu, X., Li, J., Wan, C., 2010. Evaluation of novel alginate dialdehyde cross-linked chitosan/calcium polyphosphate composite scaffolds for meniscus tissue engineering. Carbohydr. Polym. 79, 705–710.

Wang, J., Zhao, L., Zhang, A., Huang, Y., Tavakoli, J., Tang, Y., 2018. Novel Bacterial Cellulose/Gelatin Hydrogels as 3D Scaffolds for Tumor Cell Culture. Polymers 10, 581.

Wang, L., Deng, F., Wang, W., Li, A., Lu, C., Chen, H., Wu, G., Nan, K., Li, L., 2018. Construction of Injectable Self-Healing Macroporous Hydrogels via a Template-Free

Method for Tissue Engineering and Drug Delivery. ACS Appl. Mater. Interfaces 10, 36721–36732.

Wang, L., Hou, Y., Zhong, X., Hu, J., Shi, F., Mi, H., 2019. Preparation and catalytic performance of alginate-based Schiff Base. Carbohydr. Polym. 208, 42–49.

Wang, Qian, He, W., Huang, J., Liu, S., Wu, G., Teng, W., Wang, Qinmei, Dong, Y., 2011. Synthesis of Water Soluble, Biodegradable, and Electroactive Polysaccharide Crosslinker with Aldehyde and Carboxylic Groups for Biomedical Applications. Macromol. Biosci. 11, 362–372.

Wang, S., Wang, X., Neufurth, M., Tolba, E., Schepler, H., Xiao, S., Schröder, H.C., Müller, W.E.G., 2020. Biomimetic Alginate/Gelatin Cross-Linked Hydrogels Supplemented with Polyphosphate for Wound Healing Applications. Molecules 25, 5210.

Wang, W., Wang, A., 2010. Nanocomposite of carboxymethyl cellulose and attapulgite as a novel pH-sensitive superabsorbent: Synthesis, characterization and properties. Carbohydr. Polym. 82, 83–91.

Wei, S.-M., Pei, M.-Y., Pan, W.-L., Thissen, H., Tsai, S.-W., 2020. Gelatin Hydrogels Reinforced by Absorbable Nanoparticles and Fibrils Cured In Situ by Visible Light for Tissue Adhesive Applications. Polymers 12.

Wei, X., Chen, K., Cai, B., Rao, L., Wang, Z., Sun, Y., Yu, M., Liu, W., Guo, S., Zhao, X.-Z., 2019. An Acoustic Droplet-Induced Enzyme Responsive Platform for the Capture and On-Demand Release of Single Circulating Tumor Cells. ACS Appl. Mater. Interfaces 11, 41118–41126.

Weizel, A., Distler, T., Schneidereit, D., Friedrich, O., Bräuer, L., Paulsen, F., Detsch, R., Boccaccini, A.R., Budday, S., Seitz, H., 2020. Complex mechanical behavior of human articular cartilage and hydrogels for cartilage repair. Acta Biomater. 118, 113–128.

Weng, L., Chen, X., Chen, W., 2007. Rheological Characterization of in situ Crosslinkable Hydrogels Formulated from Oxidized Dextran and N-Carboxyethyl Chitosan. Biomacromolecules 8, 1109–1115.

Wirth, C.J., Peters, G., Milachowski, K.A., Weismeier, K.G., Kohn, D., 2002. Long-term results of meniscal allograft transplantation. Am. J. Sports Med. 30, 174–181.

Wolf, M.T., Daly, K.A., Brennan-Pierce, E.P., Johnson, S.A., Carruthers, C.A., D'Amore, A., Nagarkar, S.P., Velankar, S.S., Badylak, S.F., 2012. A hydrogel derived from decellularized dermal extracellular matrix. Biomaterials 33, 7028–7038.

Wu, J., Ding, Q., Dutta, A., Wang, Y., Huang, Y.-H., Weng, H., Tang, L., Hong, Y., 2015. An injectable extracellular matrix derived hydrogel for meniscus repair and regeneration. Acta Biomater. 16, 49–59.

Xiao, D., Yan, H., Wang, Q., Lv, X., Zhang, M., Zhao, Y., Zhou, Z., Xu, J., Sun, Q., Sun, K., Li, W., Lu, M., 2017. Trilayer Three-Dimensional Hydrogel Composite Scaffold Containing Encapsulated Adipose-Derived Stem Cells Promotes Bladder Reconstruction via SDF-1α/CXCR4 Pathway. ACS Appl. Mater. Interfaces 9, 38230–38241.

Xiao, T., Guo, W., Chen, M., Hao, C., Gao, S., Huang, J., Yuan, Z., Zhang, Y., Wang, M., Li, P., Peng, J., Wang, A., Wang, Y., Sui, X., Zhang, L., Xu, W., Lu, S., Yin, H., Yang, J., Liu, S., Guo, Q., 2017. Fabrication and In Vitro Study of Tissue-Engineered Cartilage

Scaffold Derived from Wharton's Jelly Extracellular Matrix. BioMed Res. Int. 2017, e5839071.

Yaacob, N., Talip, N., Mahmud, M., Mat, S., Akma, S., Ahmad, F., 2013. Determination of viscosity-average molecular weight of chitosan using intrinsic viscosity measurement. J. Nucl. Relat. Technol. 10, 39–44.

Yan, W., Xu, X., Xu, Q., Sun, Z., Jiang, Q., Shi, D., 2020. Platelet-rich plasma combined with injectable hyaluronic acid hydrogel for porcine cartilage regeneration: a 6-month follow-up. Regen. Biomater. 7, 77–90.

Yang, G., Xiao, Z., Long, H., Ma, K., Zhang, Junpeng, Ren, X., Zhang, Jiang, 2018. Assessment of the characteristics and biocompatibility of gelatin sponge scaffolds prepared by various crosslinking methods. Sci. Rep. 8, 1616.

Yang, G., Xiao, Z., Ren, X., Long, H., Qian, H., Ma, K., Guo, Y., 2016. Enzymatically crosslinked gelatin hydrogel promotes the proliferation of adipose tissue-derived stromal cells. PeerJ 4.

Yang, J.S., Ren, H.B., Xie, Y.J., 2011. Synthesis of amidic alginate derivatives and their application in microencapsulation of λ-cyhalothrin. Biomacromolecules 12, 2982–2987.

Yang, J.-S., Xie, Y.-J., He, W., 2011. Research progress on chemical modification of alginate: A review. Carbohydr. Polym. 84, 33–39.

Yuan, Z., Liu, S., Hao, C., Guo, W., Gao, S., Wang, M., Chen, M., Sun, Z., Xu, Y., Wang, Y., Peng, J., Yuan, M., Guo, Q.-Y., 2016. AMECM/DCB scaffold prompts successful total meniscus reconstruction in a rabbit total meniscectomy model. Biomaterials 111, 13–26.

Zaleskas, J.M., Kinner, B., Freyman, T.M., Yannas, I.V., Gibson, L.J., Spector, M., 2001. Growth Factor Regulation of Smooth Muscle Actin Expression and Contraction of Human Articular Chondrocytes and Meniscal Cells in a Collagen–GAG Matrix. Exp. Cell Res. 270, 21–31.

Zehnder, T., Boccaccini, A.R., Detsch, R., 2017. Biofabrication of a co-culture system in an osteoid-like hydrogel matrix. Biofabrication 9, 025016.

Zellner, J., Hierl, K., Mueller, M., Pfeifer, C., Berner, A., Dienstknecht, T., Krutsch, W., Geis, S., Gehmert, S., Kujat, R., Dendorfer, S., Prantl, L., Nerlich, M., Angele, P., 2013. Stem cell-based tissue-engineering for treatment of meniscal tears in the avascular zone. J. Biomed. Mater. Res. B Appl. Biomater. 101, 1133–1142.

Zellner, J., Pattappa, G., Koch, M., Lang, S., Weber, J., Pfeifer, C.G., Mueller, M.B., Kujat, R., Nerlich, M., Angele, P., 2017. Autologous mesenchymal stem cells or meniscal cells: what is the best cell source for regenerative meniscus treatment in an early osteoarthritis situation? Stem Cell Res. Ther. 8, 225.

Zhu, G., Zhu, X., Fan, Q., Wan, X., 2011. Raman spectra of amino acids and their aqueous solutions. Spectrochim. Acta. A. Mol. Biomol. Spectrosc. 78, 1187–1195.

Zhu, J., Marchant, R.E., 2011. Design properties of hydrogel tissue-engineering scaffolds. Expert Rev. Med. Devices 8, 607–626.

Ziegler-Borowska, M., Wegrzynowska-Drzymalska, K., Chelminiak-Dudkiewicz, D., Kowalonek, J., Kaczmarek, H., 2018. Photochemical Reactions in Dialdehyde Starch. Mol. Basel Switz. 23, E3358.

ZORZI, C., RIGOTTI, S., SCREPIS, D., GIORDAN, N., PIOVAN, G., 2016. A new hydrogel for the conservative treatment of meniscal lesions: a randomized controlled study. Joints 3, 136–145.

LIST OF PUBLICATIONS

1. Rajalekshmi Resmi, Jayasree Parvathy, Annie John, and Roy Joseph. Injectable Self-Crosslinking Hydrogels for Meniscal Repair: A Study with Oxidized Alginate and Gelatin. **Carbohydrate Polymers 2020, 234, 115902**. https://doi.org/10.1016/j.carbpol.2020.115902.

2. Rajalekshmi Resmi, Anusree Kaladevi Shaji, Roy Joseph, and Anugya Bhatt. "Scaffold for Liver Tissue Engineering: Exploring the Potential of Fibrin Incorporated Alginate Dialdehyde–Gelatin Hydrogel. **International Journal of Biological Macromolecules 2021,166: 999–1008.** https://doi.org/10.1016/j.ijbiomac.2020.10.256.

Rajalekshmi Resmi, Jayasree Parvathy, Ramakrishna Perumal Saravana, Gijo Raj, and Roy Joseph. Biosynthesized Nanosilver from Alginate Dialdehyde: An *In Vitro* Evaluation. **Chemistry Select. 2021;6(43):12007 17**. https://doi.org/10.1002/slct.202103220.

3. Anitha Radhakrishnan, Sreekanth Sreekumaran, Sudha Anjali, Rajalekshmi Resmi, Ramakrishna Perumal Saravana. Chapter 20 - Emerging Strategies in Bone Tissue Engineering. **Tissue Engineering. 2022; 469-492**. https://doi.org/10.1016/B978-0-12-824064-9.00013-7.

4. Surendranath Medha, Rajalekshmi Resmi, Rekha M Ramesan, Prakash Nair and Ramesh Parameswaran. UV Crosslinked Electrospun Zein/PEO Fibroporous Membranes for Wound Dressing. Accepted for publication in **ACS Applied Bio Materials**.

ANNEXURE

1. Estimation of the degree of oxidation of ADA

5ml of ADA solution before dialysis was taken in an iodometric flask. To this add 10 ml of 10% $NaHCO_3$ and 5 ml of 10 % KI. The colour of the solution turns brown when KI was added. This solution was kept in dark for 15 min. After 15 min, this was titrated against 0.1 N $Na_2SO_3.5H_2O$ until the colour of the solution turns yellow. At this point, 2 ml of the starch indicator was added. The colour changes from yellow to blackish blue. The titration was continued until the colour becomes off-white. Burette readings were recorded.

1.1. Calculations

1) **Normality of $Na_2SO_3.5H_2O$** =

   (Volume of KIO_3 x Normality of KIO_3) / Volume of $Na_2SO_3.5H_2O$

2) **Normality of $NaIO_4$** =

   (Volume of $Na_2SO_3.5H_2O$ x Normality of $Na_2SO_3.5H_2O$) / $Volume\ of\ ADA\ taken\ (5\ ml)$

3) ***Weight equivalent of* $NaIO_4$ *remaining in the reaction mixture*** =

   (Normality of $NaIO_4$ x $M.wt\ of\ NaIO_4(213.89g)$ x $total\ volume\ of\ reaction$)/1000

4) ***Weight of* $NaIO_4$ *used up in the reaction*** = $Weight\ of\ NaIO_4\ taken -$

   $Weight\ of\ NaIO_4\ remaining$

5) **Number of moles of $NaIO_4$ consumed** =

   $Weight\ of\ NaIO_4\ used\ up$ / $M.wt\ of\ NaIO_4(213.89g)$

6) **Number of moles of alginate consumed** =

   $Weight\ of\ alginate\ taken\ for\ the\ reaction/Weight\ of\ the\ single\ ring\ of\ alginate\ chain$ (198)

7) **Oxidation in** % =

   $\{Number\ of\ moles\ of\ NaIO_4\ consumed|Number\ of\ moles\ of\ alginate\ consumed\}x$ 100

2. Papain composition

Name of chemical	Quantity (g)
Disodium hydrogen phosphate	1.78
Papain	0.0125
EDTA sodium salt	0.186
L-cysteine	0.079
Volume of distilled water	100 ml

3. RNA Isolation and cDNA synthesis

The cell seeded hydrogels were washed with sterile PBS and 1ml of trizol reagent was added to the 100 mg sample and homogenized until it formed a fine paste. The contents were then transferred to a fresh sterile tube. 200 µl of chloroform was added and shaking was done vigorously for 15 sec and incubated for 2-3 min at room temperature, followed by centrifugation at 14000 rpm for 15 min at 4°C. The aqueous layer was collected and 500 µl of 100 % isopropanol was added. It was incubated for 10 minutes at room temperature and then centrifuged at 14000 rpm for 15 min at 4°C. Supernatant was discarded and the pellet thus obtained was washed with 200 µl of 75% of ethanol. It was then centrifuged at 14000 rpm for 5 min at 4°C. The pellet was air-dried and added with 50 µl of RNAse free water and incubated at 55°C for 10 min.

cDNA was synthesized by reverse transcriptase PCR in a thermal cycler.1µg RNA was used in a 20 µl of reaction mix with Superscript III reverse transcriptase. The reaction mix was incubated at 25°C for 10 min and the reverse transcriptase step for 30 min at 50°C. The final incubation at 85ºC for 5 min was given to inactivate the reverse transcriptase enzyme. The synthesized cDNA was stored at -20ºC until use.

The cDNA was amplified by using the Roche light cycler Real-Time PCR system using the KAPA SYBR Fast qPCR master mix. The cycling conditions for the reaction was given below.

Steps	Time required	Temperature
Initial activation step	2 min	95^{o}C
Denaturation	10 sec	94^{o}C
Annealing	1 min	55^{o}C
Extension	1 min/kb	72^{o}C
Number of cycles	40 cycles	68^{o}C

4. Staining

4.1. Safranin O-fast green

Solutions and Reagents

1. Weigert's Iron Haematoxylin Solution

1.1. Stock Solution A

Haematoxylin ---------- 1 g

95% Alcohol ---------- 100 ml

1.2. Stock Solution B

29% Ferric chloride in water ---------- 4 ml

Distilled water ---------- 95 ml

Conc. Hydrochloric ---------- 1ml

1.3. Weigert's Iron Haematoxylin Working Solution

Mix equal parts of stock solution A and B. This working solution is stable for about 4 weeks.

2. 0.05 % Fast Green (FCF) Solution

Fast green, FCF, C.I. 42053 ---------- 0.05 g

Distilled water ---------- 100 ml

3. 1 % Acetic Acid Solution

Acetic acid, glacial ---------- 1 ml

Distilled water ---------- 99 ml

4. 0.1 % Safranin O Solution

Safranin O ---------- 0.1 g

Distilled water ---------- 100 ml

After deparaffinization and rehydration of slides follow the protocol given below.

Reagents	**Time**
Weigert's Iron Haematoxylin Working Solution----------	1.5 min
Running tap water----------	5 min
Destain with acid alcohol----------	1 dip
Running tap water----------	5 min
Fast green----------	5 min
Acetic acid----------	5 min
Safranin O----------	20 min
Running tap water----------	5 min
Dehydration	
1. 90 % IPA----------	5 min
2. 100 % IPA----------	5 min
3. 100% IPA----------	5 min
Xylene I----------	5 min
Xylene II----------	15 min
Xylene II----------	15 min

After staining, slides were air-dried and mounted with Cytoseal TM 60 (Electron Microscopic Sciences, USA) and coverslipped.

4.2. Alcian blue staining

Solutions and Reagents

1. 3% Acetic Acid Solution

Glacial acetic acid ---------- 3 ml

Distilled water ---------- 97 ml

2. Alcian Blue Solution (pH 2.5)

Alcian blue, 8GX ---------- 1 g

Acetic acid, 3% solution ---------- 100 ml

Mix well and adjust pH to 2.5 using acetic acid.

After deparaffinization and rehydration of slides follow the protocol given below.

Reagents	**Time**
Weigert's Iron Haematoxylin Working Solution----------	1.5 min
Running tap water----------	5 min
Destain with acid alcohol----------	1 dip
Running tap water----------	5 min
Alcian blue----------	30 min
Running tap water----------	5 min
Dehydration	
1. 90 % IPA----------	5 min
2. 100 % IPA----------	5 min
3. 100% IPA----------	5 min
Xylene I----------	5 min
Xylene II----------	15 min
Xylene II----------	15 min

After staining, slides were air-dried and mounted with Cytoseal TM 60 (Electron Microscopic Sciences, USA) and coverslipped.

4.3. Masson's trichrome staining

Solutions and Reagents

1. Bouin's Solution

Picric acid (saturated) ---------- 75 ml

Formaldehyde (37-40%) ---------- 25 ml

Glacial acetic acid ---------- 5 ml

After deparaffinization and rehydration of slides follow the protocol given below.

1. Place slides in preheated Bounin's solution at 56ºC for 15 min or at room temperature overnight.
2. Cool slides in tap water (18-26ºC) by adding water to one side of the slides without touching the sections.
3. Wash in running tap water to remove the yellow color from sections.
4. Weigert's Iron Hematoxylin Working Solution---------- 5 min
5. Running tap water---------- 5 min
6. Masson's Trichrome LG solution---------- 5 min
7. Running tap water---------- 5 min
8. 0.5 % Acetic acid---------- 1 min
9. Running tap water---------- 5 min
10. Dehydration
    a. 90 % IPA---------- 5 min
    b. 100 % IPA---------- 5 min
    c. 100% IPA---------- 5 min
11. Xylene I---------- 5 min
12. Xylene II---------- 15 min
13. Xylene II---------- 15 min

After staining, slides were air-dried and mounted with Cytoseal TM 60 (Electron Microscopic Sciences, USA) and coverslipped.